

University of Nevada, Reno

Structural Controls of the Tuscarora Geothermal Field, Elko County, Nevada

A thesis submitted in partial fulfillment of the
requirements for the degree of Master in Science in Geology

by

Gregory M. Dering

Dr. James E. Faulds/Thesis Advisor

May, 2013

UMI Number: 1540175

All rights reserved

INFORMATION TO ALL USERS

The quality of this reproduction is dependent upon the quality of the copy submitted.

In the unlikely event that the author did not send a complete manuscript and there are missing pages, these will be noted. Also, if material had to be removed, a note will indicate the deletion.



UMI 1540175

Published by ProQuest LLC (2013). Copyright in the Dissertation held by the Author.

Microform Edition © ProQuest LLC.

All rights reserved. This work is protected against unauthorized copying under Title 17, United States Code



ProQuest LLC.
789 East Eisenhower Parkway
P.O. Box 1346
Ann Arbor, MI 48106 - 1346



University of Nevada, Reno
Statewide • Worldwide

THE GRADUATE SCHOOL

We recommend that the thesis
prepared under our supervision by

GREGORY M. DERING

entitled

Structural Controls of the Tuscarora Geothermal Field, Elko County, Nevada

be accepted in partial fulfillment of the
requirements for the degree of

MASTER OF SCIENCE

James E. Faulds, Ph.D., Advisor

Steven G. Wesnousky, Ph.D., Committee Member

Mae S. Gustin, Ph.D., Graduate School Representative

Marsha H. Read, Ph. D., Dean, Graduate School

May, 2013

Abstract

Detailed geologic mapping, structural analysis, and well data have been integrated to elucidate the stratigraphic framework and structural setting of the Tuscarora geothermal area. Tuscarora is an amagmatic geothermal system that lies in the northern part of the Basin and Range province, ~15 km southeast of the Snake River Plain and ~90 km northwest of Elko, Nevada. The Tuscarora area is dominated by late Eocene to middle Miocene volcanic and sedimentary rocks, all overlying Paleozoic metasedimentary rocks. A geothermal power plant was constructed in 2011 and currently produces 18 MWe from an ~170°C reservoir in metasedimentary rocks at a depth of ~1430 m. Analysis of drill core reveals that the subsurface geology is dominated to depths of ~700-1000 m by intracaldera deposits of the Eocene Big Cottonwood Canyon caldera, including blocks of basement-derived megabreccia. Furthermore, the Tertiary-Paleozoic nonconformity within the geothermal field has been recognized as the margin of this Eocene caldera. Structural relations combined with geochronologic data from previous studies indicate that Tuscarora has undergone extension since the late Eocene, with significant extension in the late Miocene-Pliocene to early Pleistocene. Kinematic analysis of fault slip data reveal an east-west-trending least principal paleostress direction, which probably reflects an earlier episode of Miocene extension.

Two distinct structural settings at different scales appear to control the geothermal field. The regional structural setting is a 10-km wide complexly faulted left step or relay ramp in the west-dipping range-bounding Independence-Bull Run Mountains normal fault system. Geothermal activity occurs within the step-over where sets of east- and west-dipping normal faults overlap in a northerly trending accommodation zone. The

distribution of hot wells and hydrothermal surface features, including boiling springs, fumaroles, and siliceous sinter, indicate that the geothermal system is restricted to the narrow (< 1 km) axial part of the accommodation zone, where permeability is maintained at depth around complex fault intersections. Shallow up-flow appears to be focused along several closely spaced steeply west-dipping north-northeast-striking normal faults within the axial part of the accommodation zone. These faults are favorably oriented for extension and fluid flow under the present-day northwest-trending regional extension direction indicated by previous studies of GPS geodetic data, earthquake focal mechanisms, and kinematic data from late Quaternary faults.

The recognition of the axial part of an accommodation zone as a favorable structural setting for geothermal activity may be a useful exploration tool for development of drilling targets in extensional terranes, as well as for developing geologic models of known geothermal fields. Preliminary analysis of broad step-overs similar to Tuscarora reveals that geothermal activity occurs in a variety of subsidiary structural settings within these regions. In addition, the presence of several high-temperature systems in northeastern Nevada demonstrates the viability of electrical-grade geothermal activity in this region despite low present-day strain rates as indicated by GPS geodetic data. Geothermal exploration potential in northeastern Nevada may therefore be higher than previously recognized.

Acknowledgments

This study builds on a decade of research by Dr. James Faulds and others at the Nevada Bureau of Mines and Geology to better understand the structural controls of geothermal activity in the Great Basin. I am grateful to Dr. Faulds for his encouragement and fairness, demand for clarity and solid reasoning, and, above all, patience. Many discussions with Nick Hinz helped to place my observations at Tuscarora in the context of other geothermal systems. I thank Peter Drakos of Ormat Technologies, Inc. for sharing well logs, geophysical data, drill core and cuttings, and providing work space for analyses and field accommodations. Nevada Bureau of Mines and Geology faculty Chris Henry and John Bell contributed helpful observations of the volcanic stratigraphy and Quaternary deposits, respectively. Matthew Richardson and Jennifer Mauldin guided the cartographic compilation of the geologic map. Thanks also to my committee members Drs. Mae Gustin and Steve Wesnousky for their time and thorough reviews. This study was primarily supported by a Department of Energy-ARRA (American Recovery and Reinvestment Act) grant awarded to Dr. Faulds (grant number DE-EE0002748), as well as through scholarships from ExxonMobil, the Nevada Petroleum and Geothermal Society, and American Association of Petroleum Geologists. This work is dedicated to my mother, who patched my field vest, and father, who taught me to read a topographic map. My deepest gratitude goes to Stacia Gordon for her constant love and tolerance of all my rambling about the upper crust.

Table of Contents

1. Introduction	1
2. Geologic Setting	6
TERTIARY TECTONIC-MAGMATIC HISTORY	6
NEOTECTONIC SETTING	8
TUSCARORA GEOTHERMAL SYSTEM	9
3. Stratigraphic Framework	15
SUBSURFACE CONSTRAINTS	23
4. Structural Framework	29
GEOMETRY OF FAULTING	31
FAULT KINEMATICS	37
TIMING OF DEFORMATION	40
5. Discussion	43
STRUCTURAL CONTROLS ON GEOTHERMAL ACTIVITY	41
STRUCTURAL PERMEABILITY IN ACCOMMODATION ZONES	46
CALDERA MARGIN STRUCTURES AND IMPLICATIONS FOR PERMEABILITY	49
GEOTHERMAL ACTIVITY IN BROAD STEP-OVERS	50
IMPLICATIONS FOR GEOTHERMAL EXPLORATION IN NORTHEAST NEVADA	54
6. Conclusions	55
References	58
Appendix A: Description of map units	67
Appendix B: Geologic logs of diamond drill holes	75
Plate 1: Geologic map	81
Plate 2: Cross-sections	82

List of Figures

1. Introduction

- Figure 1.1 Strain rates and geothermal systems in the Great Basin region 2
- Figure 1.2 Common structural settings of Great Basin geothermal systems 4

2. Geologic Setting

- Figure 2.1 Geothermal systems in the Humboldt geothermal belt 10
- Figure 2.2 Aerial image of the study area 11
- Figure 2.3 Oblique aerial view of Tuscarora geothermal area 13
- Figure 2.4 Isotopic composition of spring water from the Tuscarora 14

3. Stratigraphic Framework

- Figure 3.1 Generalized geologic map of study area 16
- Figure 3.2 Stratigraphic column 18
- Figure 3.3 Simplified map of the Big Cottonwood Canyon caldera 20
- Figure 3.4 Geothermal surface features 22
- Figure 3.5 Map of well field 24
- Figure 3.6 Compaction foliation in drill core 25
- Figure 3.7 Breccia textures in drill core 26
- Figure 3.8 Basement-derived megabreccia in drill holes 28

4. Structural Framework

- Figure 4.1 Major Neogene and Quaternary faults in the Tuscarora region 32
- Figure 4.2 Rose diagram of fault plane strike azimuths 33
- Figure 4.3 Fault map of study area 34
- Figure 4.4 Geologic cross sections 36
- Figure 4.5 Stereographic projections of kinematic data 39

Figure 4.6 Stereonets and dip rose diagrams of bedding and layering	41
---	----

5. Discussion

Figure 5.1 Block diagram of an accommodation zone within a relay ramp	44
---	----

Figure 5.2 Alternating activity of oppositely dipping normal faults	47
---	----

Figure 5.3 Conceptual model of Tuscarora geothermal reservoir	48
---	----

Figure 5.4 Geothermal activity in broad step-overs	51
--	----

1. Introduction

Geothermal activity is observed in a wide variety of tectonic settings, including continental rifts, oceanic spreading centers, magmatic arcs, and intraplate hot spots. Within all of these tectonic environments, faults commonly control fluid flow in the brittle crust and are therefore critical to the exploration of both fossil and active hydrothermal systems. An additional factor that impacts fluid flow is the internal architecture of individual fault zones (i.e. the development of gouge versus breccia). Faults may localize fluid flow along high permeability breccia-dominated pathways or inhibit fluid flow across a relatively impermeable fault core consisting of clay gouge (Caine et al., 1996). Although faults play a critical role in controlling fluid flow within the crust, the structural settings conducive to geothermal activity are generally not well characterized.

Characterizing the favorable structural settings of geothermal activity is particularly important in the Basin and Range province of western North America. The Basin and Range is a broad region of extension and transtension that accommodates diffuse deformation between the Pacific and North American plates (Figure 1.1) (Wernicke, 1992). Quaternary volcanism, which is commonly associated with geothermal systems worldwide, is mainly restricted to the eastern and western margins of the Basin and Range (Best et al., 1989; Glazner and Ussler, 1989; Lipman, 1992). The majority of the 431 known geothermal systems in the Basin and Range are not spatially associated with recent magmatism and thus are considered to be amagmatic (Faulds et al., 2004, 2006). In the absence of a magmatic heat source, faults are the most critical element controlling geothermal activity. Four interrelated aspects of Basin and Range tectonics

contribute to the abundance and distribution of geothermal activity across the province:

- 1) high rates of dilatant crustal strain (Blewitt et al., 2003; Coolbaugh et al., 2005; Faulds et al., 2012);
- 2) transfer of dextral shear from the Walker Lane to extension in the

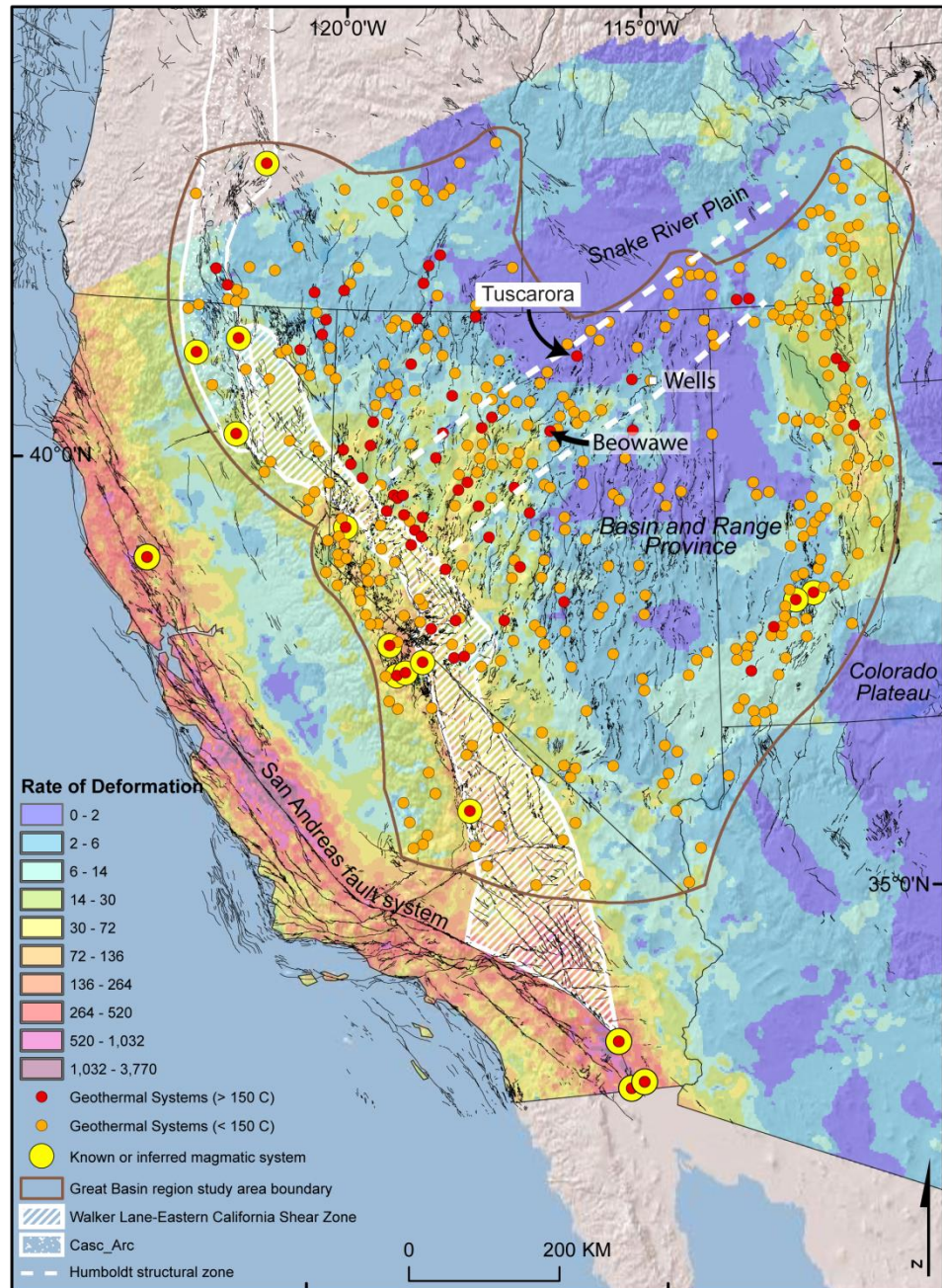


Figure 1.1. Map of strain rates and geothermal systems in the Great Basin and adjacent regions (slightly modified from Faulds et al., 2012, with original strain map from Kreemer et al., 2012). Tuscarora lies in a region of comparatively low strain rates, unlike the geothermal systems clustered in the northwestern Great Basin. Strain rates reflect the second invariant strain rate tensor $10^{-9}/\text{yr}$.

northwestern Great Basin (Faulds et al., 2004; Faulds and Henry, 2008); 3) elevated crustal heat flow of $\sim 75 \pm 5 \text{ mWm}^{-2}$ (Blackwell, 1983; Blackwell and Richards, 2004); and 4) Quaternary extensional and transtensional faulting (Bell and Ramelli, 2007). In amagmatic systems, meteoric water travels downward to depths of 1-3 km along steeply dipping active faults, where it comes into contact with fractured rock heated by the anomalously high geothermal gradient.

Despite the plethora of Quaternary normal faults and widespread high heat flow, known geothermal activity in the Basin and Range province is spatially restricted and favors specific structural settings. Steeply-dipping, breccia-dominated normal faults oriented approximately orthogonal to the least principal stress direction host most of the high temperature geothermal systems (Faulds et al., 2004, 2006, 2011). Favorable fault geometries include sites of strain arrest, where stress is elevated and fracture density is high, but displacement is relatively minor compared to the mid-segment of the fault system (Curewitz and Karson, 1997; Micklethwaite and Cox, 2004; Faulds et al., 2006). The most favorable structural settings for geothermal activity in the Basin and Range (Faulds et al., 2011) are: 1) step-overs (or relay ramps) linking normal faults, 2) terminations of normal faults where an individual fault breaks into multiple interacting fault splays, 3) fault intersections, 4) displacement transfer zones between strike-slip faults and normal faults, and 5) accommodation zones, where belts of oppositely dipping normal faults intermesh (Figure 1.2). Notably, many high temperature geothermal systems in the Great Basin are characterized by more than one favorable structural setting.

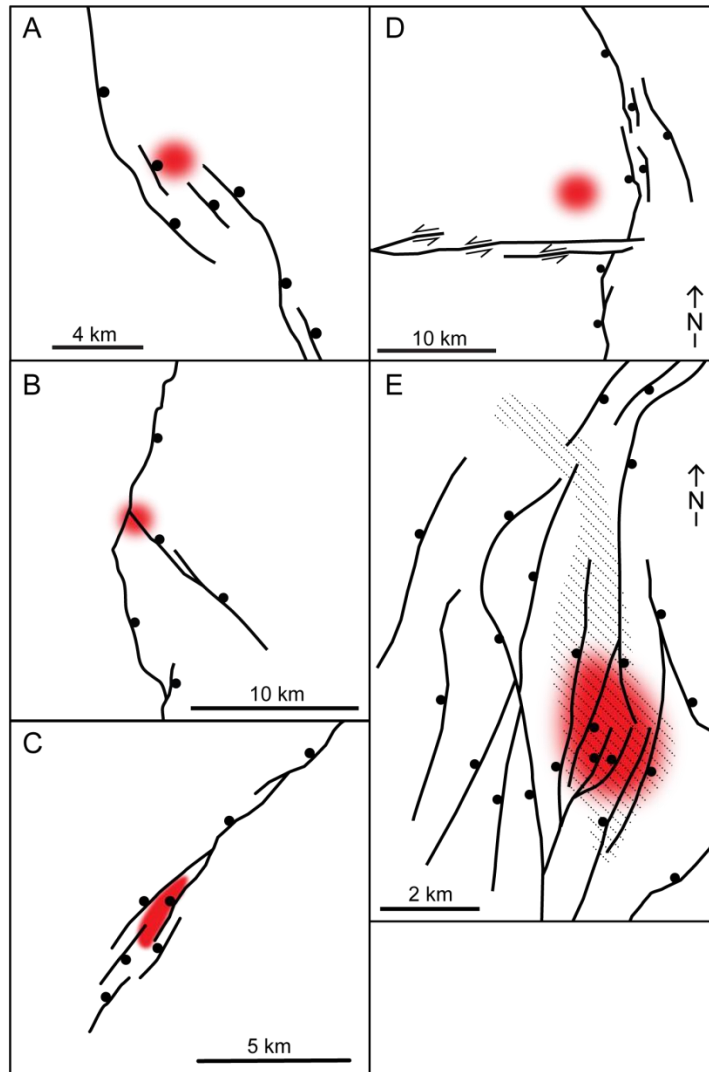


Figure 1.2. Examples of the five most common structural settings for geothermal activity found in the Great Basin. Red indicates area of geothermal upwelling (e.g. hot spring or subsurface temperature anomaly). **A.** Step-over where strain is transferred between two subparallel synthetically-dipping normal faults. The two continuous fault segments shown here overlap along strike, forming a relay ramp occupied by two smaller faults. However, strain may also be transferred between underlapping and/or hard-linked fault segments. **B.** Fault intersection. **C.** Termination of a discrete normal fault, where displacement is diffused into several smaller overlapping fault splays. **D.** Displacement transfer zone, where strain is accommodated by different modes of faulting. Shown here, sinistral slip on E-striking faults is transferred into down-to-the-west displacement in a northerly striking normal fault zone. **E.** Belts of overlapping normal faults that terminate in an accommodation zone. In this example, simplified from detailed mapping by Hinz et al. (2011a), an array of easterly dipping normal faults partially overlap with westerly dipping normal faults. The stippled area indicates the zone of fault interaction at the surface.

The purpose of this paper is to assess the structural setting of the Tuscarora geothermal field in northeastern Nevada, where Ormat Technologies, Inc. recently constructed an 18 MWe capacity geothermal power plant. Although several robust geothermal systems are present in northeastern Nevada (Figure 1.1), the structural controls on geothermal activity in this relatively low-strain region are poorly understood. Thus, this study provides critical data to evaluate whether structural controls within the Basin and Range differ between tectonically distinct subregions of the province and are perhaps partly dependent on strain rates and directions. For example, a marked contrast exists between the tectonic setting of northeastern Nevada compared to the western and eastern parts of the Great Basin. Lower GPS geodetic strain rates, as recorded in the past ~20 years, and less historical seismicity characterize northeastern Nevada (Bennett et al., 2003; Anderson, 2011). However, a M6.0 earthquake severely damaged the town of Wells in 2008 (dePolo et al., 2011), and the highest temperature amagmatic geothermal system in the Basin and Range resides at Beowawe (Figure 1.1).

The structural setting of the Tuscarora geothermal system is described here in terms of the geometry, kinematics, and dynamics of faulting encompassing the geothermal field and adjacent areas. This study integrated detailed geologic mapping with well data and kinematic analyses of faults to elucidate the structural setting of the geothermal system. Geologic mapping at 1:24,000 scale of ~110 km² of the northeastern-most portion of the Tuscarora Mountains and northernmost Independence Valley was used to define the stratigraphy and structural framework (Plate 1). Stratigraphic units were further defined by petrographic analysis of thin sections. Kinematic analyses of fault surfaces to discern slip data was used to estimate the orientation of mean principal

stresses in the study area. Detailed logging of lithology, structure, and alteration in drill core and well cuttings from the geothermal field constrained interpretations of the subsurface geology. Surface mapping and subsurface geology were integrated in five interpretive cross-sections to better understand the structural setting of the geothermal system. In addition, the geologic map, spring localities, and structural data were compiled in an ArcGIS geodatabase.

2. Geologic Setting

TERTIARY TECTONIC-MAGMATIC HISTORY

Cenozoic extension in northeastern Nevada began earlier than elsewhere in the Great Basin region (Figure 1.1), overprinting a series of contractional episodes from the latest Paleozoic to late Mesozoic. Episodes of crustal extension in northeastern Nevada are well documented from ca. 40-38 Ma (Smith and Ketner, 1976), ca. 16-17 Ma (Zoback et al., 1994), and during the Quaternary (Wesnousky et al., 2005). In addition to these pulses, recent geochronologic analyses and geologic mapping in the Copper Basin, ~60 km northeast of Tuscarora, suggest an episode of extension in the early Oligocene (Henry et al., 2011).

Major episodes of Cenozoic magmatism in northeastern Nevada occurred in the Eocene to early Oligocene and the middle to late Miocene, approximately coinciding with periods of extension. Magmatism from ca. 45 to 36 Ma migrated across the northeastern Great Basin, with the eruption of calc-alkaline volcanic rocks and emplacement of shallow intrusions. This activity was part of a larger regional episode of dominantly silicic magmatism that began in southern British Columbia and swept

southward across western Montana, Idaho, western Utah and Nevada from the early Eocene to late Oligocene (Christiansen and Yeats, 1992). The Tuscarora volcanic field is the largest of these Eocene volcanic centers in northeastern Nevada and is dominated by andesitic and dacitic lavas with lesser rhyolite and ash-flow tuff, all erupted between ca. 40.0 and 39.3 Ma (Henry et al., 1999). Magmatism persisted in northeastern Nevada until approximately 36 Ma.

Widespread magmatism resumed with bimodal volcanism ca 16.7 Ma associated with the inception of the Yellowstone hot spot in the Oregon-Idaho-Nevada border area (Pierce and Morgan, 1992; Brueseke et al., 2008). Rhyolitic caldera complexes erupted between 16.7 and 15.0 Ma in northwestern Nevada and southeastern Oregon (Castor and Henry, 2000; Coble and Mahood, 2012). Coeval rhyolite flows erupted from widely distributed vents across north-central Nevada and southern Idaho (Brueseke et al., 2008). Middle Miocene silicic volcanism was contemporaneous with renewed extension in the northern Basin and Range province as well as with the eruption of the Steens and Columbia River flood basalts (Christiansen and Yeats, 1992) and the basalts in the northern Nevada rift (Zoback et al., 1994). Volcanism advanced toward the northeast at approximately 14-11 Ma, forming the southernmost central Snake River Plain (Pierce and Morgan, 1992). In the Oregon-Idaho-Nevada border area, basaltic volcanism persisted from ca. 11 to 5 Ma forming the bulk of the Owyhee Plateau. Basalt flows at the southernmost edge of the Owyhee Plateau lie ~25 km northwest of the geothermal field. Whole rock analysis of these basalts yielded K/Ar ages of 9.3 ± 0.68 Ma and $8.9 \text{ Ma} \pm 0.63$ Ma (Hart et al., 1984), and thus are the youngest volcanic rocks in the Tuscarora region.

Magmatism in the late Eocene-early Oligocene and middle to late Miocene approximately corresponds with periods of extension in the northern Basin and Range province. However, there is no correlation between the locations of particular magmatic centers and regions of focused extensional strain (Wernicke, 1992). Therefore, the relationship between magmatism and extension is broad, applicable at the scale of the Basin and Range province but not individual basins.

NEOTECTONIC SETTING

Areas of largest magnitude extensional strain have, in a general sense, shifted from the center of the northern Basin and Range province to the margins since the Miocene (Wernicke, 1992). At present, the north-central Basin and Range is a tectonically distinct part of the Basin and Range province characterized by low internal strain rates (Hammond et al., 2011) and sparse historic seismicity (Ramelli and dePolo, 2011). However, the region is actively extending, as evidenced by the 6.0 M February 28, 2008, Wells earthquake on a north-northeast-striking blind normal fault (Smith et al., 2011). Other normal faults shown to be active in the Holocene in the north-central Basin and Range province include the Crescent fault (Friedrich et al., 2004), Dry Hills fault (Wesnousky et al., 2005), and system of faults bounding the west side of the Ruby-East Humboldt Range (Wesnousky and Willoughby, 2003).

Analysis of long GPS time series (>10 yrs) from northeastern Nevada and westernmost Utah yields a maximum extension direction of N59°W at a rate of 4.6 ± 0.8 nanostrain/year, which is equivalent to 0.46 ± 0.08 mm/year of extension across 100 km (Hammond et al., 2011). These findings are roughly consistent with the extension direction in the western Basin and Range, suggesting that this region is an active part of

the Pacific/North American plate boundary system. However, the majority of present-day deformation within the Basin and Range is concentrated at the margins of the province. At the western margin is the Walker Lane, a zone of transtensional shear that accommodates approximately 1 cm/year of dextral motion between the Sierra Nevada microplate and central Basin and Range (Figure 1.1) (Bennett et al., 2003; Hammond and Thatcher, 2004). The eastern Basin and Range province (east of 114°W) accommodates 2.8 ± 0.2 mm/yr of approximately east-west-oriented extension, with the most rapid strain concentrated along the Wasatch fault zone (Bennett et al., 2003).

Despite the relative quiescence of northeastern Nevada, Quaternary faults define the present-day topography. North-trending ranges are bound on at least one side by widely spaced, steeply dipping Quaternary normal faults that cut shallower dipping Tertiary normal faults (Henry and Colgan, 2011). The pattern of northerly trending structures is disrupted in northern Nevada by a series of east-northeast-striking discontinuous sinistral-normal faults and physiographic lineaments. This 150-200 km wide region, known as the Humboldt structural zone, extends more than 800 km from the Carson Sink in west-central Nevada to southeast Idaho (Figure 1.1) (Rowan and Wetlaufer, 1981; Faulds et al., 2004). The Humboldt geothermal belt is an east-northeast-trending belt within the Humboldt structural zone of moderate to high temperature geothermal systems (Figure 2.1), which includes the Tuscarora and Beowawe systems in northeast Nevada.

TUSCARORA GEOTHERMAL SYSTEM

The Tuscarora geothermal field lies in the Hot Creek drainage ~1.5 km northwest of the northern Independence Valley in the northeastern Tuscarora Mountains (Figure

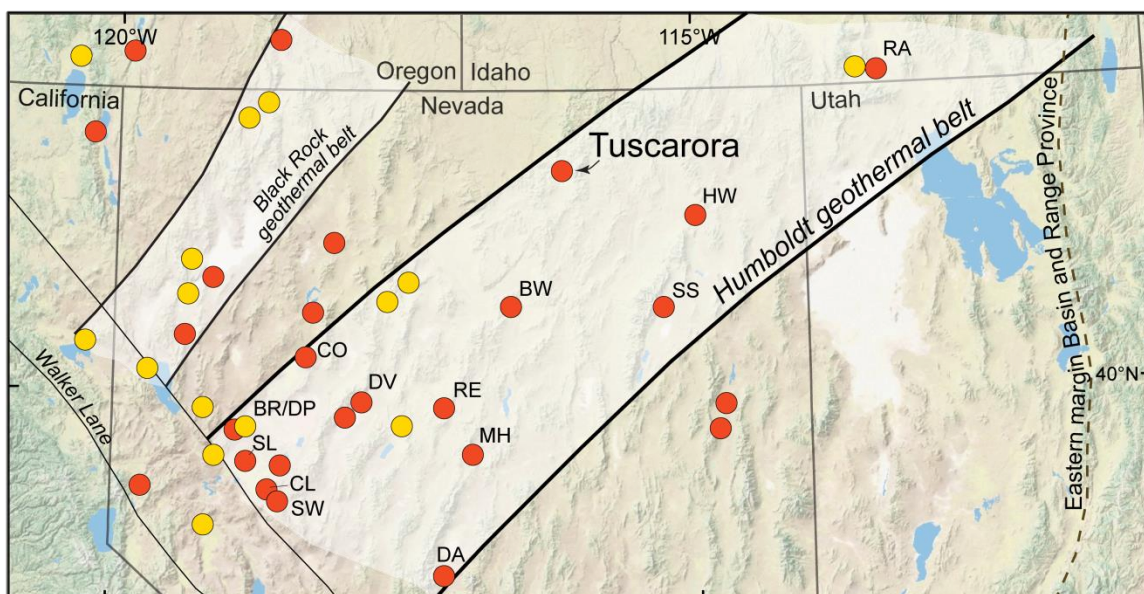


Figure 2.1. Shaded relief map of the Basin and Range province in northern Nevada and neighboring states, showing known geothermal systems. Red circles denote geothermal systems with temperatures greater than 150°C. Yellow circles denote geothermal systems with temperatures greater than 99°C and less than 150°C. Faults et al. (2004) recognized that geothermal systems cluster in northeast-trending belts, including the informally named Humboldt and Black Rock geothermal belts. High temperature geothermal systems within the Humboldt geothermal belt include: BR/DP, Bradys/Desert Peak; BW, Beowawe; CL, Carson Lake; CO, Colado; DA, Darrough's; DV, Dixie Valley; HW, Humboldt Wells; MH, McGinniss Hills; RA, Raft River; RE, Reese River; SL, Soda Lake; SS, Sulphur Springs; SW, Salt Wells.

2.2). Hot springs, abundant sinter, and silica-cemented alluvium occur along Hot Creek.

The most prominent geothermal surface feature is a broad silica sinter terrace ~700 m long and ~260 m wide. The sinter terrace is inactive and perched ~10 m above the Hot Creek drainage (Figure 2.3). A tight cluster of >15 boiling springs and fumaroles actively precipitate travertine, sinter, and sulfur (Sibbett, 1982) and lie ~400 m north-northeast of the inactive sinter terrace. Minor hydrous silica veining and veinlets cut Miocene lava flows proximal to the hot springs. Isolated silica-cemented alluvium is observed in patches subparallel to the Hot Creek drainage.

The thermal anomaly is confined to the area of surface alteration and hot spring activity within the Hot Creek drainage. Extensive exploration of the geothermal system from 1978-1981 included the drilling of 32 temperature gradient holes peripheral to and

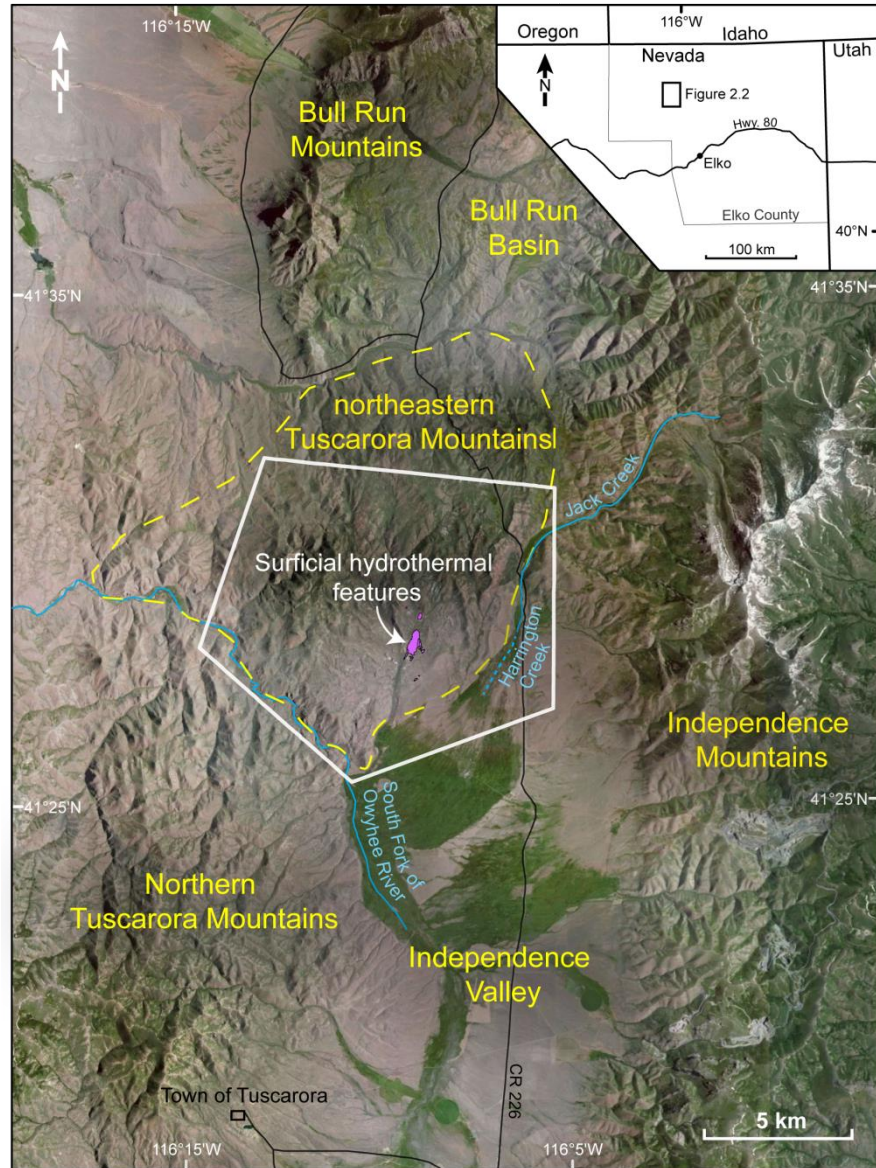


Figure 2.2. Aerial image showing the study area outlined in white, approximate extent of the northeastern Tuscarora Mountains outlined by the dashed yellow line, surficial hydrothermal alteration of the geothermal system, and major physiographic features.

within the known thermal anomaly. Warm ($\sim 40^{\circ}\text{C}$) water encountered in several gradient holes in northern Independence Valley appears to be outflow from the Tuscarora geothermal field (Pilkington, 1981). Silica-cemented alluvium mapped to the southeast of the sinter terrace also suggests that shallow outflow from the geothermal system has migrated toward Independence Valley. Exploration drilling has identified no other

thermal anomalies in the northeastern Tuscarora Mountains or northern Independence Valley.

Construction of an 18 MWe gross capacity geothermal power plant at Tuscarora was completed by Ormat Technologies, Inc. in 2011. The power plant and four closely spaced geothermal production wells are located at the south end of the ancient sinter terrace (Figure 2.3). A maximum temperature of 170 °C at a depth of 899 m (2950 ft) was reported from a test well at the south end of the sinter terrace (Goranson, 2005). At present, geothermal production is from fractured Paleozoic siliciclastic rocks and dolomite at ~1430 m depth.

The geologic setting and geochemical data show no evidence of a shallow magmatic heat source at Tuscarora. The most recent volcanism in the region is late Miocene (Coats, 1987; Shoemaker, 2004) and thus is not a heat source for the active geothermal system. Similarly, the geochemistry of geothermal fluid points to a meteoric origin rather than a magmatic origin. $\delta D - \delta^{18}O$ results for hot and cold springs in the Tuscarora area plot near the meteoric water line (Figure 2.4), consistent with values for such water in northern Nevada (Bowman and Cole, 1982). Slight deviations in δD and $\delta^{18}O$ values for hot spring water away from the meteoric water line are explained by evaporation and/or low temperature isotopic exchange with carbonate rocks in the basement. A comparison of δD and $\delta^{18}O$ values from hot and cold springs in the Tuscarora area shows that geothermal fluids correlate with cold springs to the west and southeast of the geothermal area and not with springs to the north (Bowman and Cole, 1982). Thus, recharge was inferred to be either from the Independence Mountains to the southeast or from the Tuscarora Mountains to the west of the geothermal area. It is

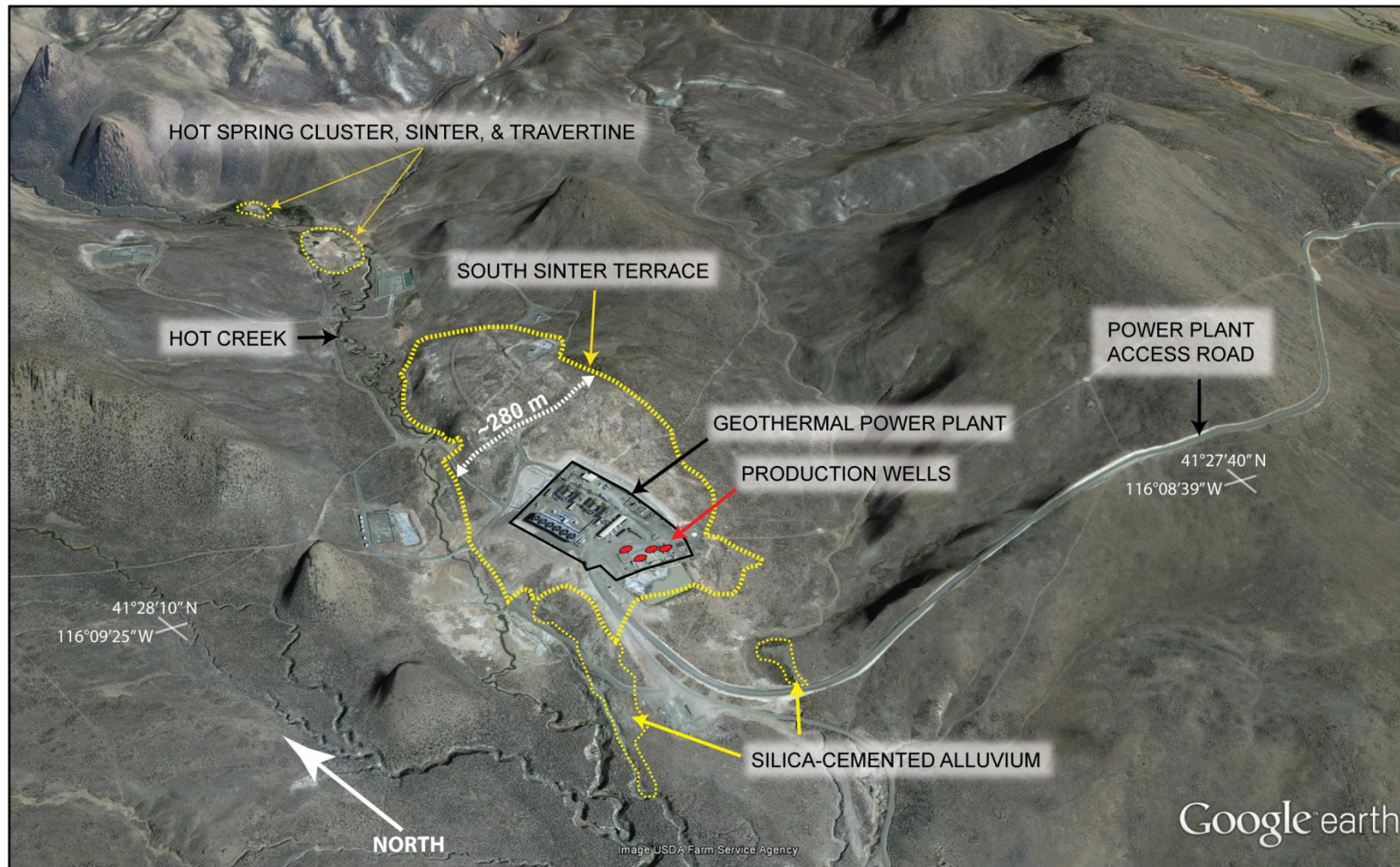


Figure 2.3. Oblique aerial view of the Tuscarora geothermal area with major surface features highlighted and labeled. Relief is shown with three times vertical exaggeration to emphasize the elevation contrast between the south sinter terrace and present Hot Creek drainage.

important to note that stable isotopic data cannot delineate a definitive geothermal heat source. However, the data from Tuscarora do not indicate a magmatic contribution to the geothermal fluid.

Trace element geochemistry can, in some cases, be used to distinguish amagmatic from magmatic geothermal systems in the Great Basin. However, the existing data from Tuscarora do not clearly demonstrate either a magmatic or amagmatic signature. For geothermal systems with Cl concentrations of 10^2 – 10^3 ppm, ratios of Li-Cl and B-Cl show distinguishable divergent trends for amagmatic and magmatic systems (Arehart et al., 2003). At Tuscarora reported Cl concentrations of geothermal fluids range from 6–26 ppm (Bowman and Cole, 1982) and are therefore too low to fit a meaningful trend. The combined geologic, isotopic, and trace element data provide no evidence for a magmatic heat source driving the Tuscarora geothermal system.

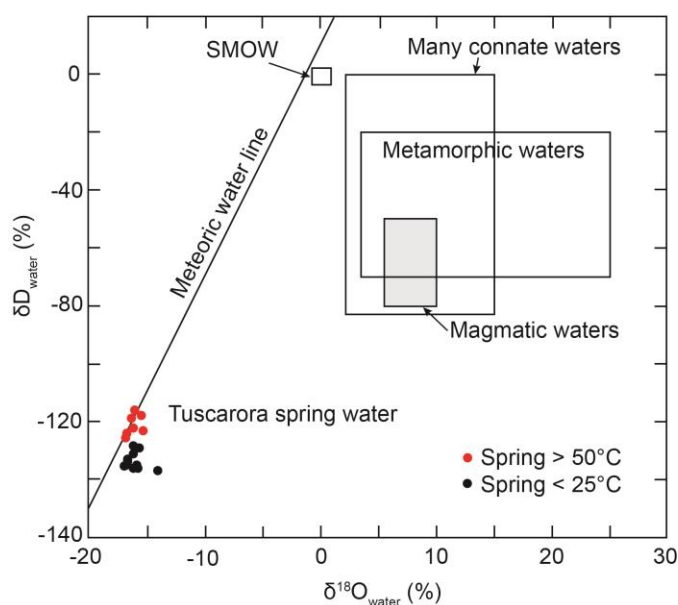


Figure 2.4. δD_{water} versus $\delta^{18}O_{\text{water}}$ values for hot and cold springs from the Tuscarora study area, reported by Bowman and Cole (1982), are compared with the isotopic fields for ocean waters, magmatic waters, metamorphic waters, and some connate waters. The connate and metamorphic water fields are from Hoefs (2009). The magmatic water field is after Sheppard (1986).

3. Stratigraphic Framework

The northeastern Tuscarora Mountains and adjacent northern Independence Valley are composed of Paleozoic metasedimentary basement, Eocene to Miocene volcanic and sedimentary rocks, late Miocene-Pliocene to Quaternary alluvium, and Quaternary geothermal deposits (Figures 3.1 & 3.2; Plate 1) (Appendix A). Basement in the northeastern Tuscarora Mountains is concealed by Eocene and younger strata. However, siliciclastic and carbonate rocks intercepted in geothermal drill holes correlate with Paleozoic units of the Independence and Bull Run Mountains.

The Independence and Bull Run Mountains are dominantly composed of Paleozoic and minor Proterozoic metasedimentary rocks of the Golconda and Roberts Mountains allochthons (Miller et al., 1984; Ehman and Clark, 1986; Coats, 1987). The Roberts Mountains allochthon in the northern Independence Mountains consists of chert and limestone of the Ordovician Snow Canyon Formation and the massive Ordovician McAfee Quartzite, regionally correlated with the Valmy Formation (Muntean and Henry, 2006). The only exposure of these rocks within the study area is isoclinally folded bedded chert of the Snow Canyon Formation east of Harrington Creek (Plate 1). These units were emplaced onto the edge of the North American continental shelf during the late Devonian-early Mississippian Antler orogeny along the Roberts Mountains thrust (Johnson and Pendergast, 1981). Following the Antler orogeny, the Roberts Mountains allochthon was partially eroded, shedding sediments westward onto the continental margin from the Devonian to early Permian. Regional contraction resumed with the late Permian-early Triassic Sonoma orogeny, which thrust shelf- and slope-facies sedimentary rocks of the Golconda allochthon southeast and east, over Devonian and older rocks of the

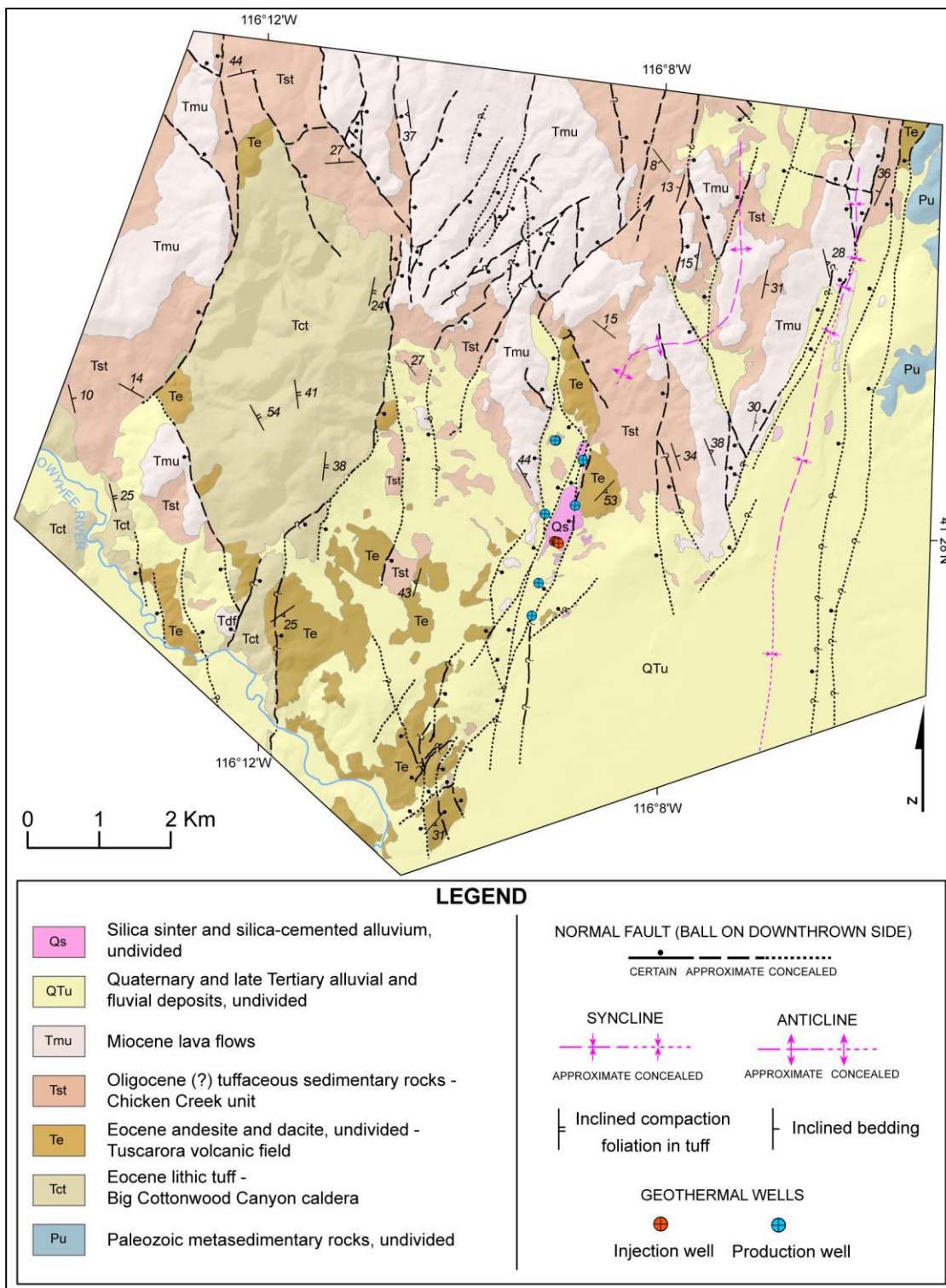


Figure 3.1. Generalized geologic map of the Tuscarora geothermal area, showing major groups of stratigraphic units (simplified from Plate 1).

Roberts Mountains allochthon. In the northern Independence Mountains, the Golconda allochthon consists of highly deformed and thrust-bounded sequences of siltstone, argillite, calcareous sandstone, and metabasalt of the late Devonian to early Permian Schoonover Formation (Fagan, 1968; Miller et al., 1984). Shale subcrop of the Schoonover Formation is identified in the northeastern-most part of the Tuscarora area.

Eocene to early Miocene volcanic and sedimentary rocks dominate the Tuscarora area. Most of the Tertiary section is composed of Eocene rocks derived from the Tuscarora volcanic field, erupted during a brief period of intense andesitic to rhyolitic volcanism from 40.0–39.3 Ma (Berger et al., 1991; Henry et al., 1999). The northern Tuscarora volcanic field is dominated by rhyolitic lithic tuff of the late Eocene Big Cottonwood Canyon caldera (Figures 3.2 and 3.3). This intracaldera tuff crops out in the western half of the map area and is encountered in wells within the geothermal field. Within the intracaldera tuff, intervals of hetero-lithic, largely basement-derived breccia >300 m thick encountered in drill holes HSS-2 and HSS-3 ~750 m beneath the hot springs (Plate 1) are interpreted to be intracaldera collapse breccia, deposited proximal to the inner caldera margin. Intracaldera mesobreccias consist of andesite, dacite, and basement-derived metasedimentary clasts ranging from millimeters to several meters in diameter in a quartz-rich fine-grained clastic matrix. The proportion of basement-derived metasedimentary rocks in these breccia deposits ranges from 5–95%. In addition to these hetero-lithic mesobreccia deposits, blocks of megabreccia, consisting entirely of Paleozoic metasedimentary rocks up to 73 m in diameter, have been penetrated by wells. Andesite and dacite flows and domes overlie the intracaldera tuff, though the thickness

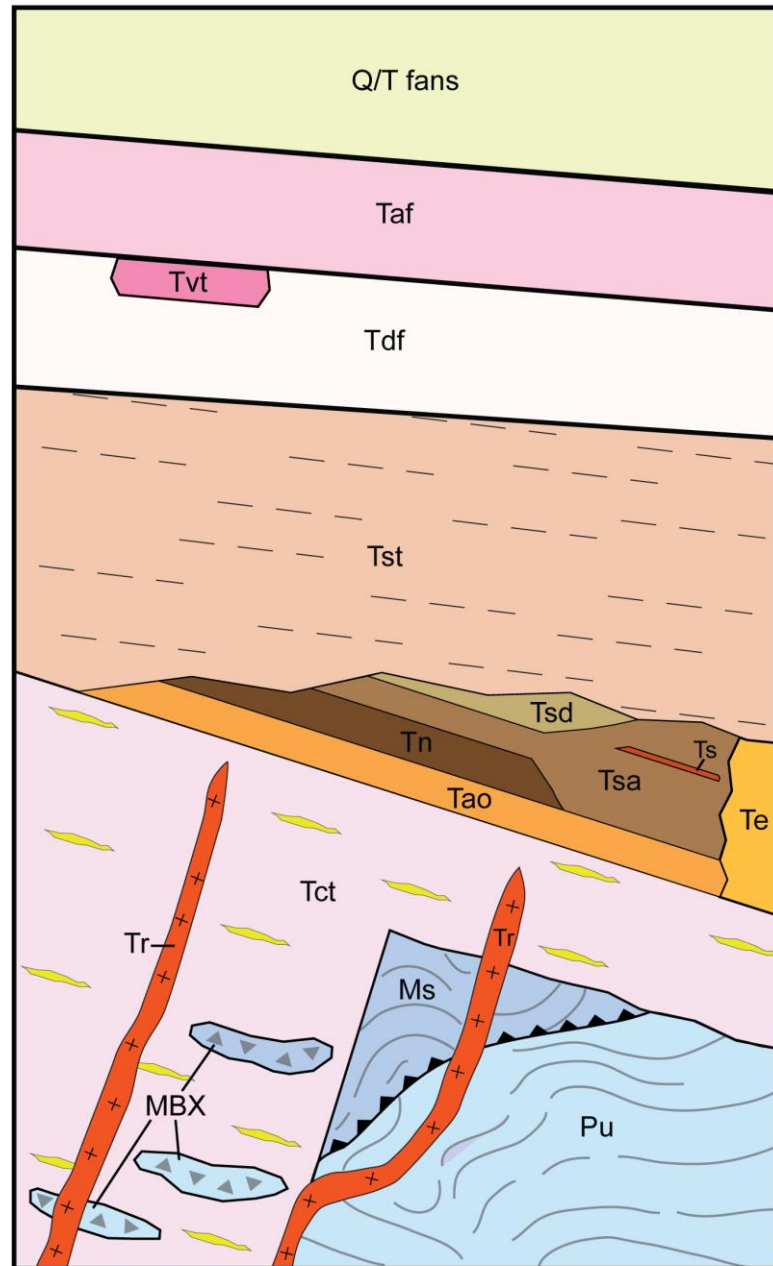


Figure 3.2. Generalized stratigraphic column of the northeastern Tuscarora Mountains illustrating cross-cutting relationships, angular unconformities, and approximate degrees of tilting. Lithologic units in ascending order: Pu-undivided Paleozoic metasedimentary rocks; Ms-Schoonover Formation; MBX-basement-derived lenses of intracaldera megabreccia. Tct-tuff of Big Cottonwood Canyon caldera; Te-undivided dacite and andesite of the Tuscarora volcanic field; Tao-porphyrritic andesite; Tn-porphyrritic andesite; Tsa-porphyrritic andesite; Ts-intercalated siltstone; Tsd-porphyrritic dacite; Tr-undivided porphyritic andesite, dacite, and rhyolite intrusions; Tst-tuffaceous sedimentary rocks of Chicken Creek; Tdf-porphyrritic rhyolite, correlative with the Jarbidge Rhyolite (Henry et al., 2011); Tvt-glassy porphyritic dacite flows; Taf-glassy sparsely porphyritic dacite; Q/T fans-unconsolidated alluvial fans and basin-fill deposits undivided.

and lateral extent of these lavas is highly variable and poorly constrained. Porphyritic dacite and rhyolite intrusions ≤ 150 m thick cross-cut the lithic tuff, hetero-lithic breccias, and metasedimentary basement.

Overlying the igneous rocks of the Tuscarora volcanic field in slight (5° - 15°) angular unconformity is a 300 m thick section of poorly to moderately indurated tuffaceous siltstone and sandstone containing sparse lenses of poorly sorted sand-pebble conglomerate, informally referred to in this study as the Chicken Creek unit (Figure 3.2). Where andesite and dacite flows and domes are absent, the Chicken Creek unit lies directly on the tuff of Big Cottonwood Canyon caldera. Overlying and underlying volcanic strata bracket the age of this sedimentary section to >16.15 Ma and <39.3 Ma.

Middle Miocene rhyolite and dacite flows overlie the sedimentary section. A distinct package of sheet-like rhyolite flows ~ 120 m thick is widespread over the study area and is correlated with the Jarbidge Rhyolite (Figure 3.2). This rhyolite is grayish-pink and coarsely porphyritic, containing 2-5% sanidine phenocrysts up to 8 mm in diameter. Sanidine from this unit in the western portion of the study area yielded an $^{40}\text{Ar}/^{39}\text{Ar}$ age of 16.15 ± 0.02 Ma (Henry et al., 2011) (Plate 1, sample NV-0190). The Jarbidge Rhyolite is widespread over northern Elko County and associated with regional bimodal volcanism related to the inception of the Yellowstone mantle plume in the Oregon-Idaho-Nevada border area (Brueseke et al., 2008; Coble and Mahood, 2012). The rhyolite is overlain by erosional remnants of glassy dacite flows.

Quaternary and possibly late Tertiary alluvium and fluvial deposits overlie the Eocene to Miocene strata (Figure 3.2). Coarse unconsolidated deposits dominated by well-rounded quartzite cobbles and boulders form broad surfaces of Quaternary or

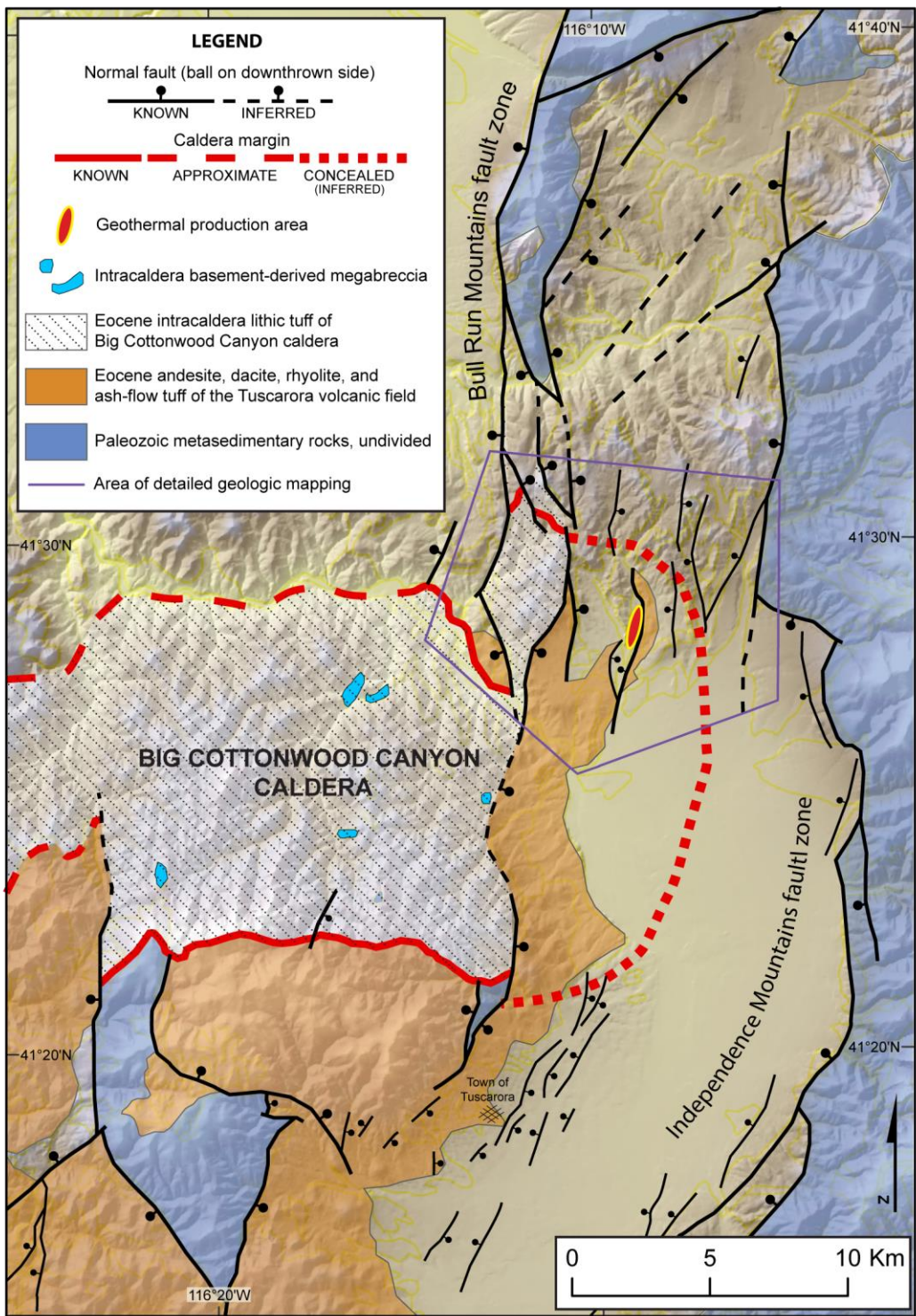


Figure 3.3. Generalized geologic map of the Tuscarora volcanic field overlain on a colored shaded relief map, emphasizing the extent of the Big Cottonwood Canyon caldera. The northeastern caldera margin is inferred from well data within the geothermal area. Compiled from Coats (1987), Henry et al. (1999), Adams and Sawyer (1999), and this study.

possibly late Miocene-Pliocene age. These surfaces are gently tilted and do not conform to the present drainage pattern. Quartzite clasts may be derived from the McAfee Quartzite, which is exposed over tens of square kilometers in the northern Independence Mountains. Well-rounded quartzite cobbles and boulders are reworked into younger Quaternary alluvial fans around the northern edge of Independence Valley. Small alluvial fans flank narrow (<400 m) drainages within Tertiary bedrock of the northeastern Tuscarora Mountains. The northern Independence Valley is covered entirely by an active alluvial fan which originates at the mouth of Harrington Creek and widens toward the South Fork of the Owyhee River.

Within the geothermal area, silica sinter deposits mantle Quaternary alluvium and siltstone of the Chicken Creek unit. Southeast of the power plant, an older inactive sinter deposit is overlain by late Pleistocene alluvium, indicating prolonged geothermal activity in the area. The inactive south sinter terrace covers a gently west-facing slope above Hot Creek (Figure 2.3). Where undisturbed, the surface is moderately to densely vegetated. The terrace is dominantly chalcedonic sinter with isolated opaline sinter at the upper- and eastern-most part of the deposit. Maximum thickness of the deposit is ~10 m. A cluster of >15 hot springs, located ~400 m north-northeast of the older sinter terrace, precipitate silica sinter in a low relief mound. This younger shield-shaped deposit is ~150 m in diameter, at least 3 m thick and overlies fluvial deposits of Hot Creek and Quaternary alluvium (Figure 3.4). In addition to these large surface deposits, an apron of travertine ~3 m in diameter is actively precipitated from an isolated warm spring, located 700 m southwest of the older sinter terrace.

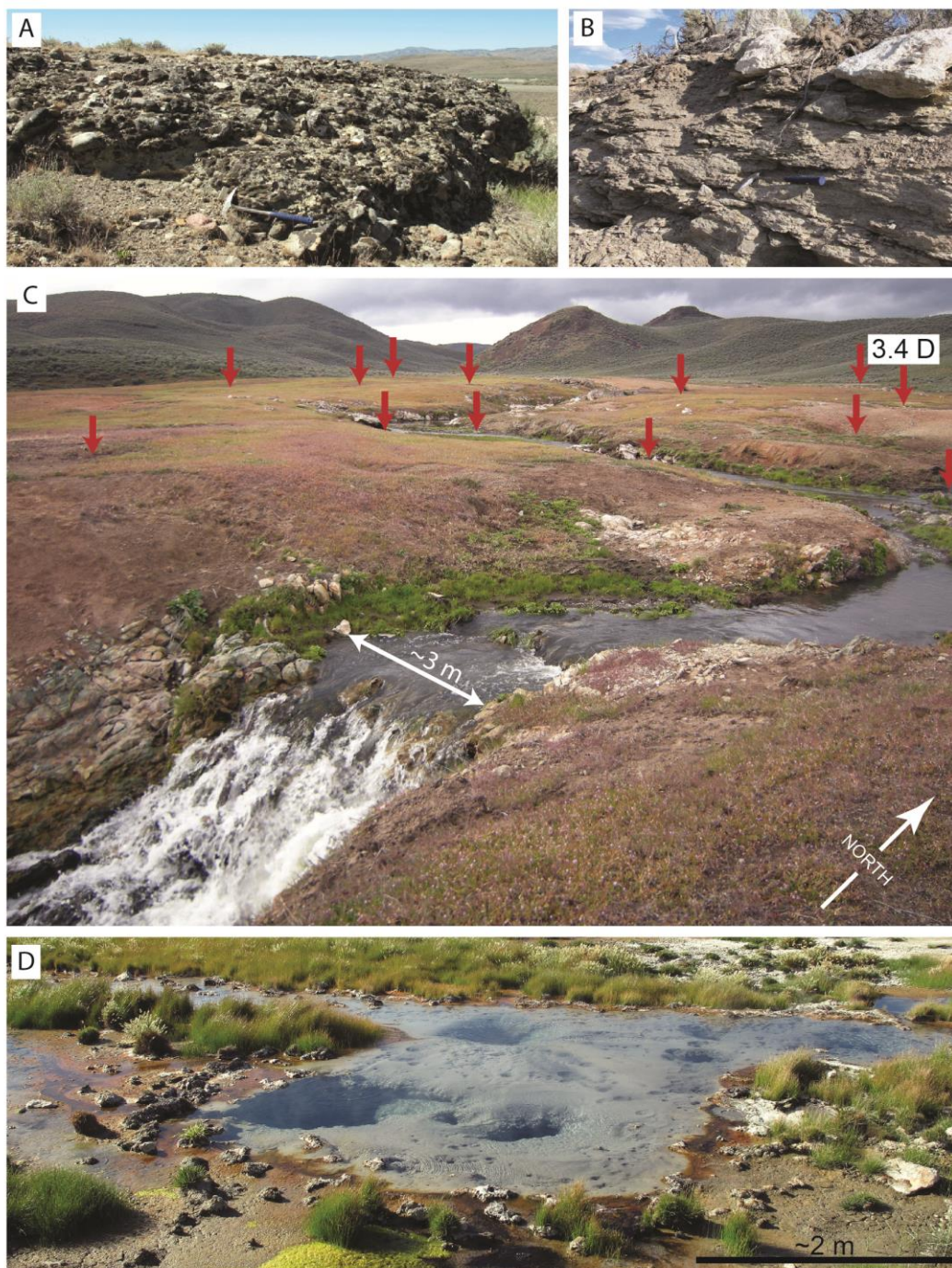


Figure 3.4. Photographs of geothermal surface features **A.** Silica-cemented alluvium. **B.** Weathered chalcedonic sinter, typical of the older and inactive south sinter terrace. **C.** Silica sinter ~3 m thick, exposed where Hot Creek erodes the southern margin of the active sinter mound. The extent of sinter is demarcated by the sparse reddish vegetation. Red arrows indicate active hot springs and fumaroles. **D.** Hot springs (96°C) emanating from the younger sinter mound.

SUBSURFACE CONSTRAINTS

Detailed geologic logging of core and cuttings from drill holes were integrated with geologic mapping to elucidate the subsurface distribution of strata and faults, as well as produce cross sections through the geothermal field (Plate 2). Well data were used to determine: 1) thickness of stratigraphic units, 2) dip maxima (in core), 3) composition of Eocene intracaldera deposits, and 4) depth to basement. Within the geothermal field, drill cuttings and core provide critical information about the Tertiary and Paleozoic bedrock, which is mainly concealed by alluvium and channel deposits of Hot Creek.

Lithologic data from drill holes were projected onto cross sections C-C', D-D', and E-E' (Figure 3.5) to constrain unit thickness and magnitude of tilting within fault blocks. Core samples yielded dip information from bedding in the Chicken Creek unit and compaction foliation in welded tuff. In core hole HSS-1, the sandstone of Chicken Creek dips 20°–30°. In core holes HSS-2 and HSS-3, fiamme in welded tuff dip 24°–65° (Figure 3.6). These dips are consistent with observations from surface mapping. Because drill core provides no azimuthal control, dip azimuths from nearby outcrops at the margins of the geothermal field were used to estimate the dip direction of strata encountered in drilling. Dip azimuths measured in outcrop to the east and west of the geothermal field range from east-northeast to east-southeast. Therefore, strata penetrated by wells in this area were presumed to dip easterly.

Breccia textures and lithologic contacts revealed by drill core suggest that rocks of the Eocene Tuscarora volcanic field are intracaldera deposits of the Big Cottonwood Canyon caldera. A heterogeneous interval composed of lithic tuff, dacite, andesite, poly-lithic breccia, and basement-derived metasedimentary rocks is encountered beneath an

undivided interval of Eocene dacite and andesite in all drill holes. This heterogeneous package of rocks lacks internal stratigraphy that can be correlated between drill holes, though it is consistently present beneath unit Te and the overlying Paleozoic basement. Core hole HSS-2 contains a 250 m interval of poly-lithic breccia, consisting of subangular clasts of porphyritic andesite and dacite, tuff, and basement clasts of weakly metamorphosed siltstone, argillite, and sandy limestone (Figure 3.7). Breccia clasts

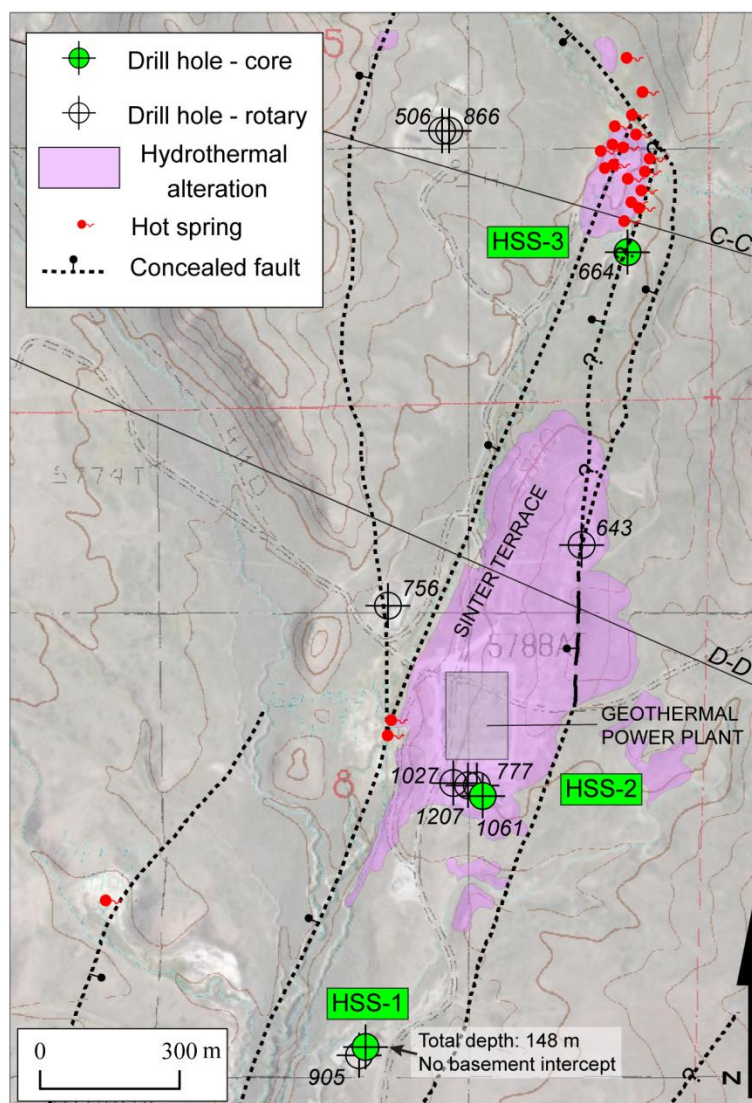


Figure 3.5. Map of the geothermal well field highlighting the location of core holes in green and rotary drill holes in black outline. Drill holes are annotated with depth to basement shown in meters.

generally range in size from 1 mm to 1 m, with rare clasts > 1 m in diameter (as penetrated by drill holes 51-09, 53-08, 66-05, HSS-2, and HSS-3). The ratio of volcanic clasts to basement-derived metasedimentary clasts varies from 10:1 to 1:10. The mesobreccia is well-cemented by a fine-grained clastic matrix and shows no evidence for greater primary permeability (e.g. hydrothermal alteration) than the overlying volcanic units.

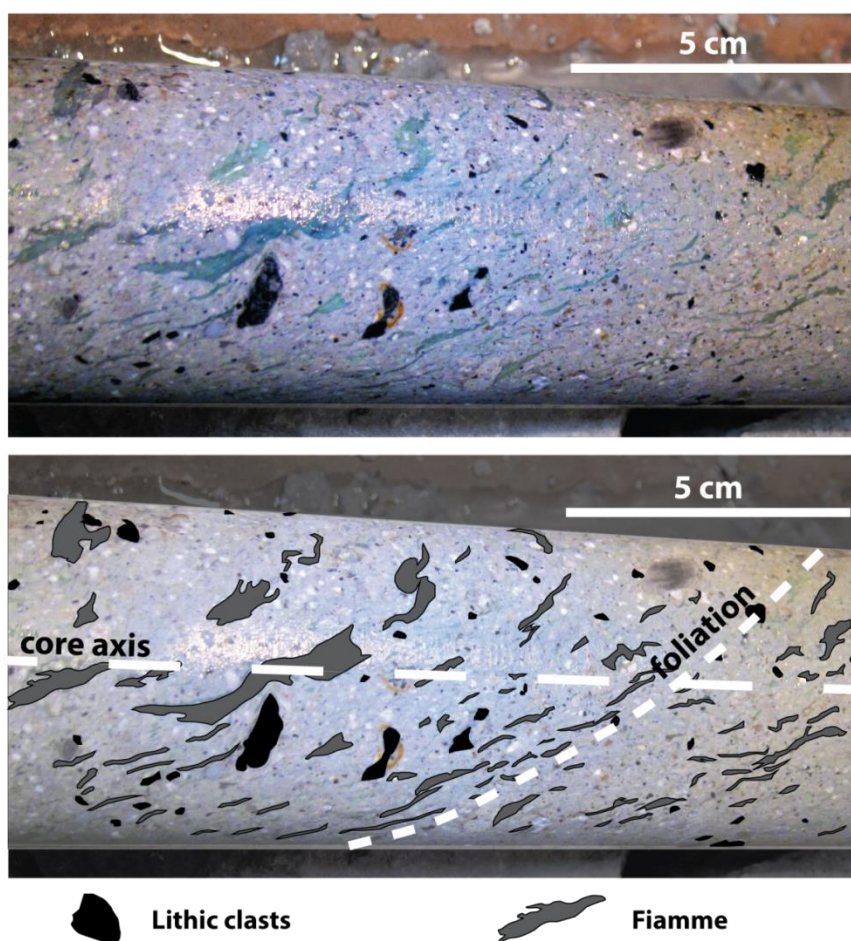


Figure 3.6. Photo of core from drill hole HSS-2 at a depth of 645.5 m showing compaction foliation in welded lithic tuff of the Big Cottonwood Canyon caldera. Measurement of the angle of compaction foliation relative to the core axis is a proxy for the maximum tilt of unit Tct within this fault block.

In addition to mesobreccia containing a significant proportion of basement-derived metasedimentary clasts, blocks of basement-derived megabreccia are

encountered in four drill holes (Figure 3.8). Intervals of coherent Paleozoic sedimentary rocks range from 2 – 73 m in thickness and concordantly overlie Eocene welded tuff. Based on the relationships observed in core, the mesobreccia and megabreccia are interpreted to be intracaldera deposits, related to the eruption and collapse of the Big Cottonwood Canyon caldera ca 40.0 Ma. During eruption or possibly shortly after eruption, portions of the over-steepened caldera walls probably collapsed inwards, breaking apart and mixing with volcanic debris. Basement-derived blocks of megabreccia

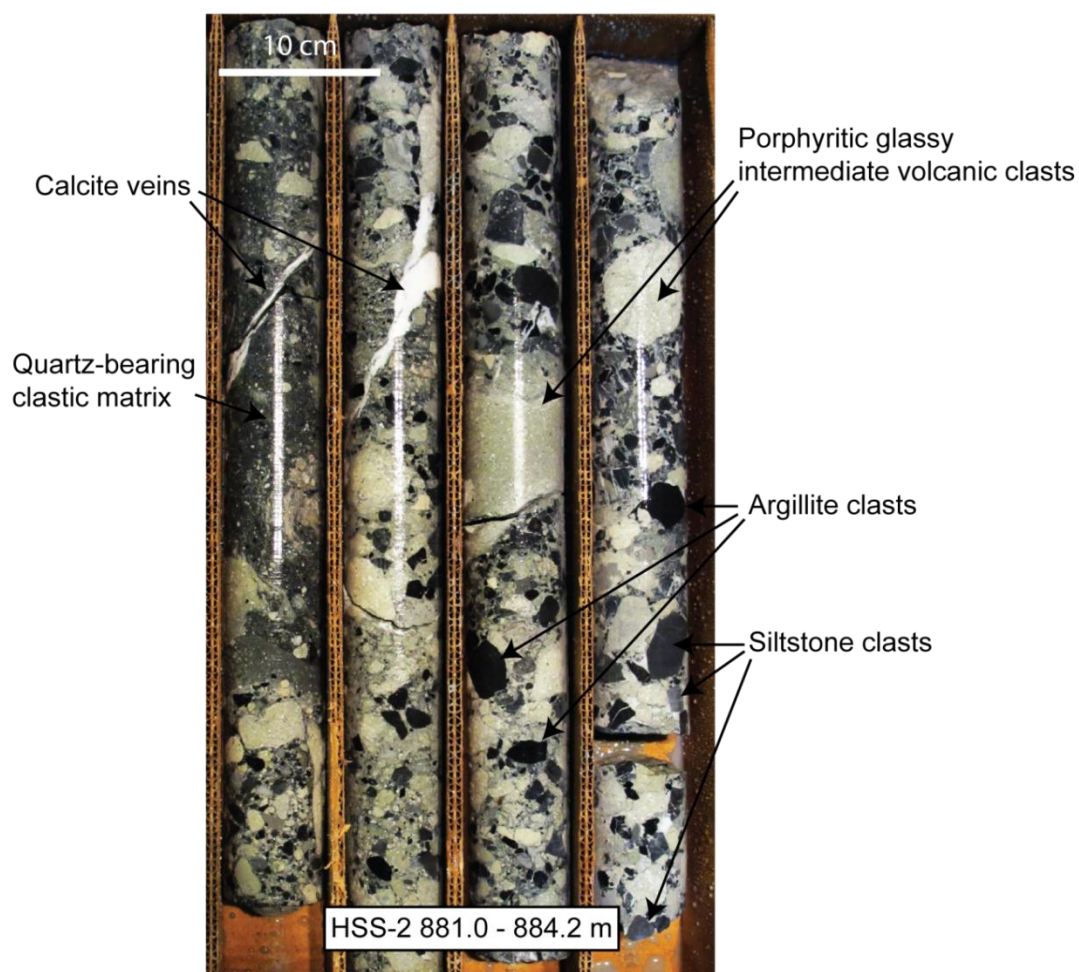


Figure 3.7. Photo of core from drill hole HSS-2 showing clast-supported heterolithic mesobreccia. Interval contains ~70% clasts of porphyritic intermediate volcanic rocks, ~20% basement-derived fine-grained metasedimentary rocks, and ~10% fine grained clastic matrix. Breccia is interpreted as an Eocene-age intracaldera collapse deposit of the Big Cottonwood Canyon caldera.

are observed elsewhere within the Big Cottonwood Canyon caldera. Geologic mapping within the Tuscarora volcanic field southwest of the geothermal area reveals megabreccia blocks >100 m in diameter composed of Paleozoic metasedimentary rocks at the southern margin of the Big Cottonwood Canyon caldera (Figure 3.3) (Coats, 1987; Henry et al., 1999).

The depth at which drill holes intersect Paleozoic metasedimentary basement and encounter no extrusive igneous rocks at greater depth varies from 505 to 1207 m in the vicinity of the geothermal field (Figure 3.5). Factors that contribute to variability in depth to basement include paleotopography on the Paleozoic-Tertiary nonconformity and Cenozoic normal faulting. The presence of intracaldera deposits within the geothermal field suggests that the Paleozoic-Tertiary nonconformity encountered beneath these deposits is the gently dipping inner wall or floor of the Big Cottonwood Canyon caldera. The caldera in this area has been tilted eastward toward westerly-dipping normal faults, covered by younger lava flows and sedimentary rocks, and then cut by at least one generation of normal faults. Therefore, the Paleozoic-Tertiary nonconformity within the study area is complex. The intracaldera deposits of the Big Cottonwood Canyon caldera are mapped only to the west and southwest of the geothermal area (Figure 3.1). Consequently, the depth to Paleozoic basement within the study area is interpreted to be greater to the west, where intracaldera fill is probably much thicker.

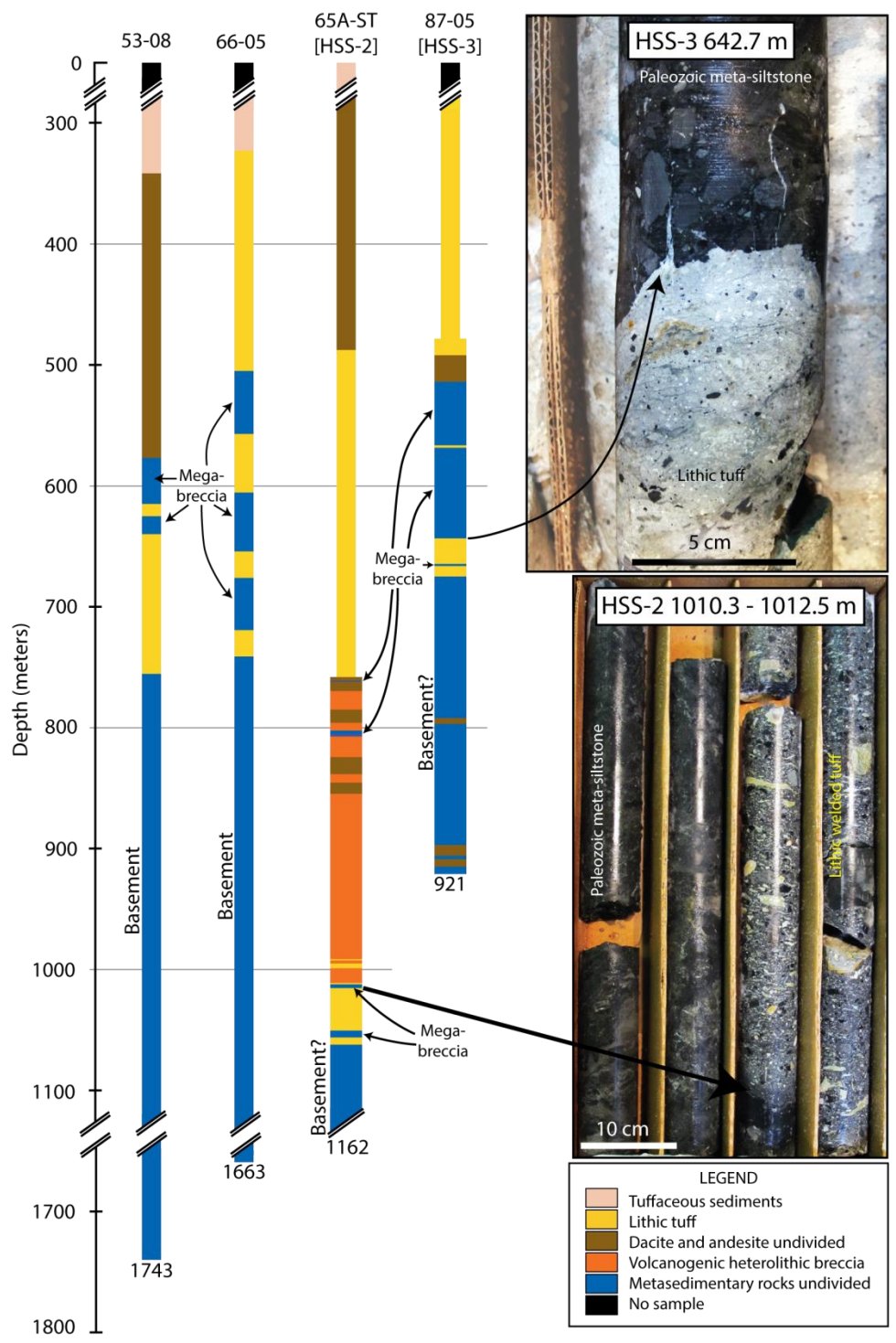


Figure 3.8. Simplified down-hole lithologic logs of four boreholes that contain intervals of allochthonous Paleozoic metasedimentary basement within the Tertiary volcanic section. Photographs of core samples show Paleozoic rocks in concordant contact with lithic welded tuff. Thin drill-hole logs indicate rotary samples. Thick drill logs indicate core samples. Total depth in meters is at the bottom of each log.

4. Structural Framework

With respect to Neogene extension, the major structural components of the study area include 1) an east-tilted half graben that comprises much of Independence Valley, 2) the west-dipping Independence and Bull Run Mountains range-front fault zones, and 3) in the vicinity of the geothermal system, several gently to moderately east- and west-tilted fault blocks that are bound by primarily northerly striking normal faults and essentially link the Independence and Bull Run Mountains fault zones (Figure 4.1). Independence Valley is an east-tilted north-northeast-trending half-graben filled with sediments derived from the Tuscarora and Independence Mountains. This basin is bounded to the east by the west-dipping Independence Mountains fault zone, where scarps in Pleistocene alluvial fans indicate recent tectonism. Regional gravity data suggest that the basin is approximately 1500 m deep at the center (Erwin, 1988). On the southwest side of Independence Valley a dense array of north-northeast-striking, east- and west-dipping faults in Pleistocene alluvial fan deposits is well defined near the town of Tuscarora (Figure 3.3) (Coats, 1968; Dohrenwend and Moring, 1991). The westernmost of these faults dip east, whereas the easternmost faults near the center of Independence Valley dip west (Henry et al., 1999).

At the latitude of the geothermal system, the Independence Mountains fault zone juxtaposes east-tilted Miocene strata of the northeastern Tuscarora Mountains against complexly deformed Paleozoic basement of the Independence Mountains. Minimum offset on this segment of the fault is ~2000 m. Cumulative displacement across the Independence Mountains fault zone diminishes to the north, terminating in the Bull Run basin ~14 km east-northeast of the geothermal field.

The Bull Run Mountains range-front fault zone also dips west and juxtaposes Miocene lavas and Quaternary alluvium in the hanging wall against pre-Tertiary basement in the footwall. Offset across this major range-bounding fault zone is probably several thousand meters along the west flank of the Bull Run Mountains. At the southern tip of the Bull Run Mountains, the Bull Run fault zone breaks into a series of smaller east- and west-dipping faults with diminishing offset and topographic relief toward the south (Figure 4.1).

A broad (~10 km wide) step-over or relay ramp (cf., Larsen, 1988) lies between the overlapping ends of the west-dipping Bull Run and Independence Mountains fault zones and is dominated by small northerly striking faults (Figures 3.3 and 4.1). Subsidiary faults within the step-over subparallel the major bounding faults, and thus do not mechanically link the Bull Run and Independence Mountains fault zones, at least at the surface. Northeast-striking faults also occupy the relay ramp and are expressed mainly in pre-Miocene rocks (Ehman and Clark, 1986; Coats, 1987). These northeast-striking faults may be an expression of the Humboldt structural zone (Figure 1.1) and appear to mainly predate the northerly-striking range-bounding fault system. The Tuscarora geothermal system resides in a zone of closely spaced northerly trending normal faults in the southern portion of the step-over. The Bull Run Mountains fault zone terminates southward ~5 km to the west of the Tuscarora geothermal area, whereas the Independence Mountains fault zone lies ~5 km to the east and dies out northward.

Within the step-over, the geothermal system occupies a small accommodation zone (cf., Faulds and Varga, 1998), as evidenced by both east- and west-tilted fault blocks bounded by sets of oppositely dipping normal faults. Accommodation zones are

belts of overlapping normal faults. They may contain intermeshing, oppositely dipping fault sets or overlapping synthetic faults. The change in fault polarity across an accommodation zone is commonly accompanied by a reversal of fault-block tilts, resulting in an extensional fold, with extensional anticlines developing where inward-dipping fault systems overlap (e.g. Faulds, 1996; Faulds and Varga, 1998). In the Tuscarora geothermal area, overlapping northerly striking, east- and west-dipping faults form an accommodation zone. In the vicinity of the sinter, hot springs, and production wells, however, all fault blocks are tilted gently to moderately east. Directly west and north of the geothermal activity, however, fault blocks form an extensional anticline, with west- and east-dipping normal faults bounding east- and west-tilted blocks, respectively (Figure 3.1; Plates 1 and 2). The following sections describe in greater detail the geometry, kinematics, and timing of faulting within the accommodation zone that hosts the geothermal system.

GEOMETRY OF FAULTING

As introduced above, the Tuscarora geothermal area lies within an ~10 km wide zone of structural overlap between two major northerly striking range-bounding fault zones, including the northward-terminating Independence Mountains fault zone to the east and southward-terminating Bull Run Mountains fault system to the west (Figure 4.1). Directly west of the geothermal area, oppositely dipping fault splays of the Bull Run Mountains fault system form a prominent horst block, exposing the tuff of the Big Cottonwood Canyon caldera (Figure 3.1 and Plate 1). The east side of the horst block is bounded by a northerly striking steeply east-dipping normal fault, informally referred to here as the Cottonwood Peak fault. A prominent west-dipping splay of the Bull Run

Mountains fault zone, informally named the Skull Creek fault, bounds the west side of the fault block.

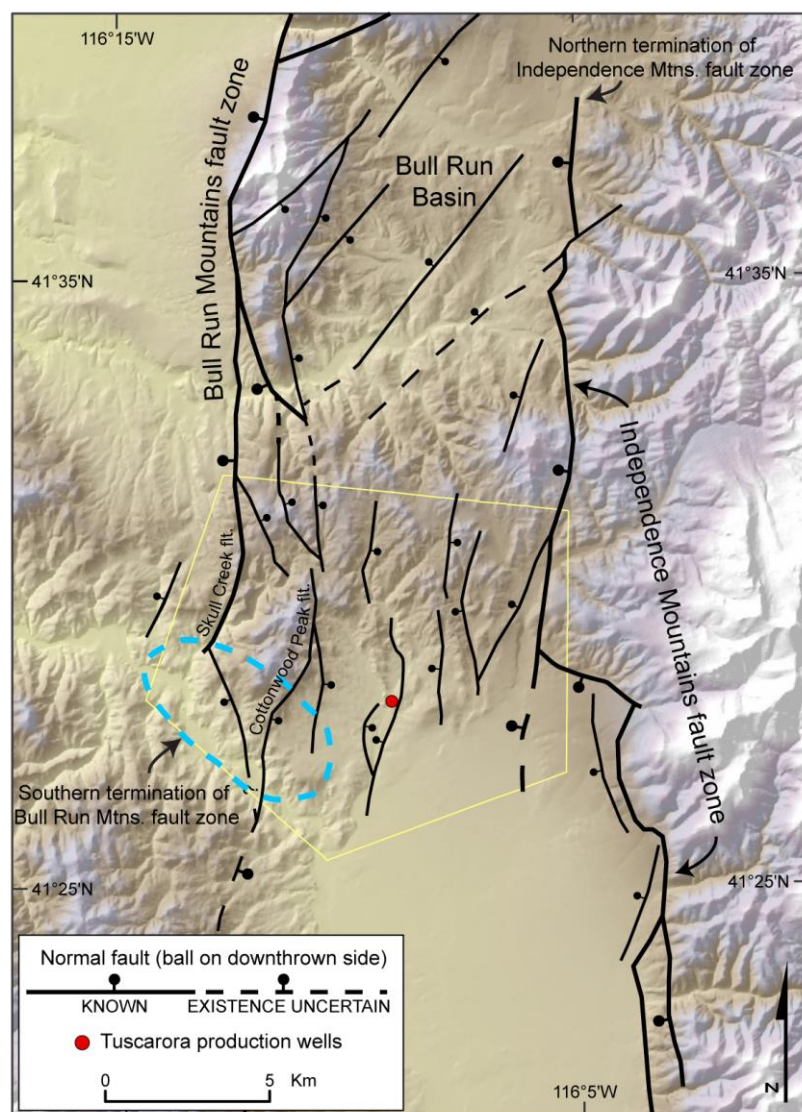


Figure 4.1. Shaded relief map of major faults involving Eocene and younger rocks near the Tuscarora geothermal field. Yellow line denotes the Tuscarora study area boundary. Faults are approximately located from Ehman and Clark (1986), Coats (1987), Adams and Sawyer (1999), and this study.

Between the Cottonwood Peak fault and Independence Mountains fault zone, an array of closely-spaced small-offset faults strikes north-northwest to north-northeast (Figures 3.1 and 4.2) and dip both east and west. These oppositely dipping faults define

the northerly trending accommodation zone. Individual faults within this area are mostly < 3 km long and have maximum offsets of < 350 m. To the west of the primary surface expressions of the geothermal system (e.g., sinter terrace and hot springs), these small faults mainly dip east and southeast. To the east of the geothermal area, small normal faults mainly dip west and northwest. Thus, the geothermal area occupies the axial part of the northerly trending accommodation zone, where these east- and west-dipping fault sets overlap (Figure 4.3).

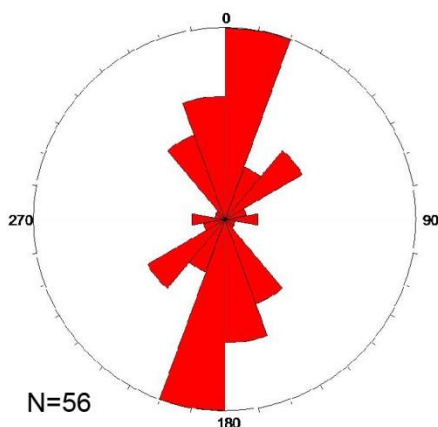


Figure 4.2. Rose diagram of all fault plane strike directions measured within the study area, showing that faults mainly strike northerly. Largest petal represents 30% of the total dataset.

The accommodation zone is essentially bounded to the west by the east-dipping Cottonwood Peak fault and to the east by the west-dipping Independence Mountains fault zone, whereas its extent to the north and south is less well defined. Inward-dipping northerly striking normal fault sets persist several kilometers beyond the northern boundary of the study area but not as far as the Bull Run basin (Ehman and Clark, 1986) (Figure 4.1), suggesting that the accommodation zone dies out in the northernmost part of the northeastern Tuscarora Mountains. Faults in the southeastern portion of the study area are concealed by Holocene alluvial fans of Harrington Creek and the Independence

Mountains, and thus the geometry and extent of the accommodation zone here are not precisely known.

The axial part of the accommodation zone is segmented at abrupt lateral steps where short faults of opposite polarity terminate in the same area, with strain stepping over to an adjacent set. The accommodation zone can be further described in terms of the position of the axial part, with respect to the bounding faults, and fault-block tilt domains. The northern portion of the study area is characterized by fault-blocks tilted approximately $\sim 9^{\circ}$ – 31° away from the hinge zone in an extensional anticline (Figures 3.1 and 4.4).

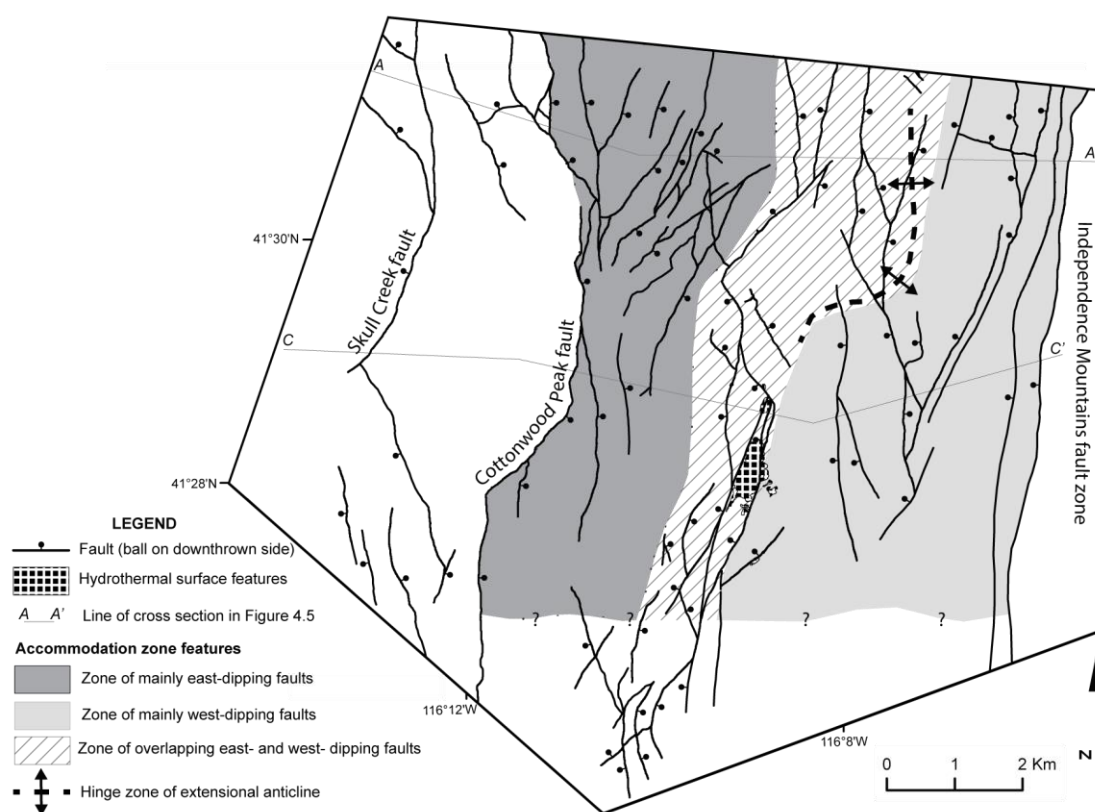


Figure 4.3. Fault map of the study area, with hatched area denoting the change in fault polarity from east- to west-dipping faults. The hinge line of an extensional anticline (heavy dashed line) is developed in the northern part of the accommodation zone. Quaternary valley fill conceals faults in the southeastern portion of the study area, thereby preventing projection of the accommodation zone to the south.

East-dipping normal faults dominate the northern part of the accommodation zone such that the hinge zone lies near the Independence Mountains fault zone (Figure 4.3). In the area of geothermal activity, geologic cross sections (Plate 2) reveal a pattern of oppositely dipping overlapping fault sets similar to the northern segment of the accommodation zone. However, fault-blocks at the latitude of the geothermal field are all tilted easterly from $\sim 10^{\circ}$ – 37° (Figure 4.4). At the eastern margin of the accommodation zone, a syncline has developed where strata within east-tilted fault blocks dip moderately ($\sim 30^{\circ}$) west as a result of drag along the Independence Mountains fault zone.

Within the geothermal field, two steeply west-dipping normal faults on the east side of Hot Creek localize geothermal upflow near the surface (Figure 3.5) (Plate 1). The older south sinter terrace is bounded upslope to the east by one of these west-dipping normal faults. The absence of sinter upslope of this fault trace suggests that hot water flowed out along this fault, precipitating subaerial silica sinter in the hanging wall down slope from the fault. At the north end of the geothermal field, two west-dipping, north-northeast-striking normal faults intersect a north-northwest-striking, west-dipping normal fault. Boiling springs, fumaroles, and sinter occur in the mutual hanging wall of these intersecting faults. Geothermal features occur along the apparent traces of the north-northeast-striking faults but are not observed along the trace of the north-northwest-striking fault beyond the fault intersection area.

FAULT KINEMATICS

Kinematic analysis of fault slip data was undertaken to distinguish slip directions and infer both orientations of principal strain and stress axes. Kinematic indicators, including slickenlines and Riedel shears (e.g. Petit, 1987), were used to determine slip sense on 30 fault surfaces from 25 localities (Figure 4.5a). The data show that the steeply dipping normal faults and a smaller population of dextral-normal faults characterize the Tuscarora geothermal area. The mapped extent of dextral-normal faults is limited due to poor exposure. It appears that the dextral-normal faults involve only rocks older than 16.5 Ma.

The kinematic data were then used to quantitatively determine the principal axes of extension and shortening, employing the method of Marrett and Allmendinger (1990). The orientation of fault planes and kinematic indicators together constitute a fault slip datum, which is converted to kinematic axes (P-shortening, T-extension, B-intermediate) (Figure 4.6b). Calculations of kinematic axes and mean principal strain axes for the entire dataset were performed using TectonicsFP 1.75, which calculates a linked Bingham distribution that essentially determines a best fit orientation for all fault slip data (Ortner et al., 2002).

The kinematic data were inverted to determine the mean paleostress tensor by the Numerical Dynamic Analysis (NDA) method (Spang, 1972). The homogeneity of the dataset is tested by measuring the angular deviation of the calculated maximum shear stress from the observed slip lineation. The fluctuation histogram summarizing deviation from the calculated maximum shear stress for the entire Tuscarora fault population shows

that the angular deviation of some of the fault data is greater than the maximum 20° expected in a fault population activated in the same stress field (Figure 4.5b) (Ortner et al., 2002). Sorting of this heterogeneous dataset yields a homogenous subgroup of 15 faults for which all kinematic data are within 20° of the mean maximum shear stress (Figures 4.5d and 4.5e). The remaining PTB data are heterogeneous, and kinematic analyses suggest they do not represent a coherent fault population formed in a single stress field. The heterogeneity may be explained by a combination of the following factors: 1) pre-Miocene reorientation of some fault planes; 2) a change in the local stress field during the Eocene related to collapse and/or resurgence of the Big Cottonwood Canyon caldera; and 3) the subgroup of data is not large enough for recognition of multiple fault populations.

The calculated mean principal stresses for the statistically coherent subgroup of 15 faults are $\sigma_1 = 312^\circ/85^\circ$, $\sigma_2 = 175^\circ/04^\circ$, $\sigma_3 = 085^\circ/03^\circ$ (Figure 4.5f). The computed orientations of σ_1 and σ_3 lie close to vertical and horizontal planes, respectively, in good agreement with the Cenozoic extensional stress regime. However, the trend of σ_3 (085°) differs considerably from the Holocene northwest-trending least principal stress direction indicated by earthquake focal mechanism solutions (Smith et al., 2011), geodetic data (Hammond et al., 2011), and kinematic data (Zoback, 1989). The age of most fault slip data within the study area is constrained to < 16.1 Ma and, in a few cases, only constrained to < 40 Ma. Therefore, the stress inversion calculated from these data reflects a paleostress state averaged since the middle Miocene, which may not represent the Holocene stress field. Clockwise rotation of the least principal stress direction in northern

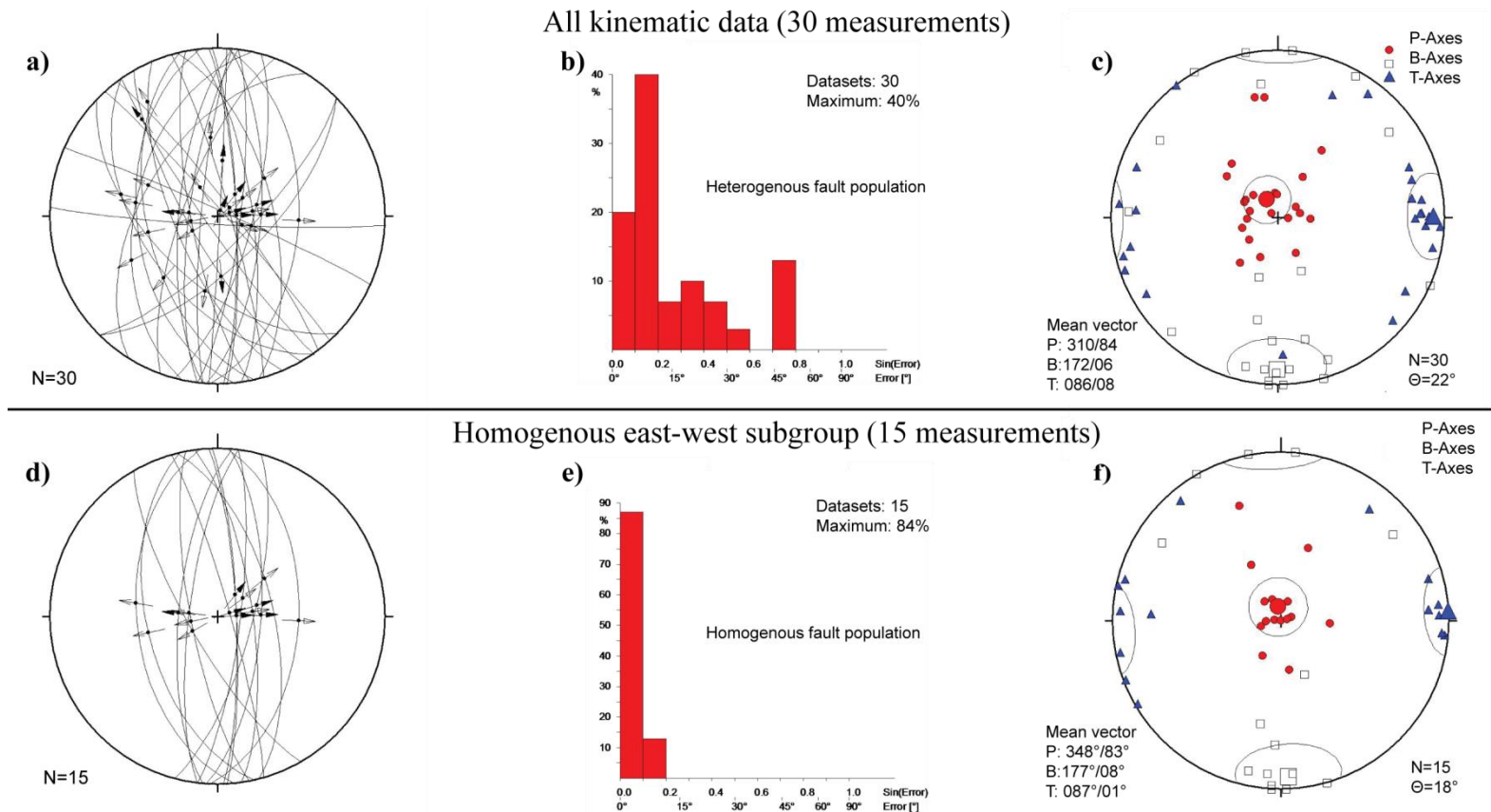


Figure 4.5. Kinematic data sorted into a statistically homogenous subgroup, following the method of Ortner et al. (2002). (a) Plot of all fault slip data (Angelier, 1994) with arrows indicating hanging wall slip direction. (b) Fluctuation histogram of all fault slip data showing calculated error between the measured shear stress vector and calculated mean resolved shear stress vector. Larger x-axis values indicate greater discrepancy between the measured lineation and the calculated mean shear stress vector. (c) Principal strain axes calculated for all fault slip data using a θ value of 24° , which is the angle between the fault plane and σ_1 . Red circle=P-axis=shortening. White square=B-axes=intermediate. Blue triangle=T-axis=extension. Larger symbols indicate calculated best fit principal strain axes for all 30 measurements of fault slip data. (d) Plot of fault surfaces showing hanging wall slip direction for a subpopulation of 15 faults identified based on the similarity of their kinematic axes. (e) Fluctuation histogram of shear stress vectors, demonstrating the statistical homogeneity of slip vectors used to define this homogenous fault subpopulation. (f) Principal strain axes calculated using a θ angle of 18° for this kinematically homogenous fault subpopulation.

Nevada from west-southwest to northwest has occurred since the middle Miocene (Zoback and Thompson, 1978). The approximately east-west least principal paleostress direction at Tuscarora lies between the middle Miocene and Holocene least principal stress directions and may reflect a transitional stress regime.

TIMING OF DEFORMATION

An angular unconformity between Eocene rocks of the Tuscarora volcanic field and the overlying Chicken Creek unit suggests an episode of extension after ~40 Ma and before deposition of the Chicken Creek unit, no later than ~16 Ma. Within the study area, the tuff of the Big Cottonwood Canyon caldera is tilted an average of 43°, whereas the average dip of the overlying Chicken Creek unit is 25° and are mostly < 37° (Figure 4.6a). Several dips greater than 37° were recorded in the Chicken Creek unit near faults, where local drag appears to have contributed to steepening of strata. The 18° discrepancy between the average dips of these units is interpreted to represent extension and tilting that predate deposition of the Chicken Creek unit. A period of extension and basin formation post-dating Eocene volcanism and pre-dating mid-Miocene volcanism has also been recognized at Copper Basin (Henry et al., 2011) but is not widely documented elsewhere in northeastern Nevada. Similar to the tuff of Big Cottonwood Canyon, lavas of the Tuscarora volcanic field dip more steeply on average than the Chicken Creek unit, though attitude data from flows are more widely scattered than data from welded tuff. The wide range of flow orientations observed in the lavas of the Tuscarora volcanic field is in part attributed to deposition-related variability in primary flow orientation. Flow fronts and margins, the flanks of domes, and lavas deposited on irregular

paleotopography could produce moderate to steeply dipping flow foliations unrelated to any tectonic tilting.

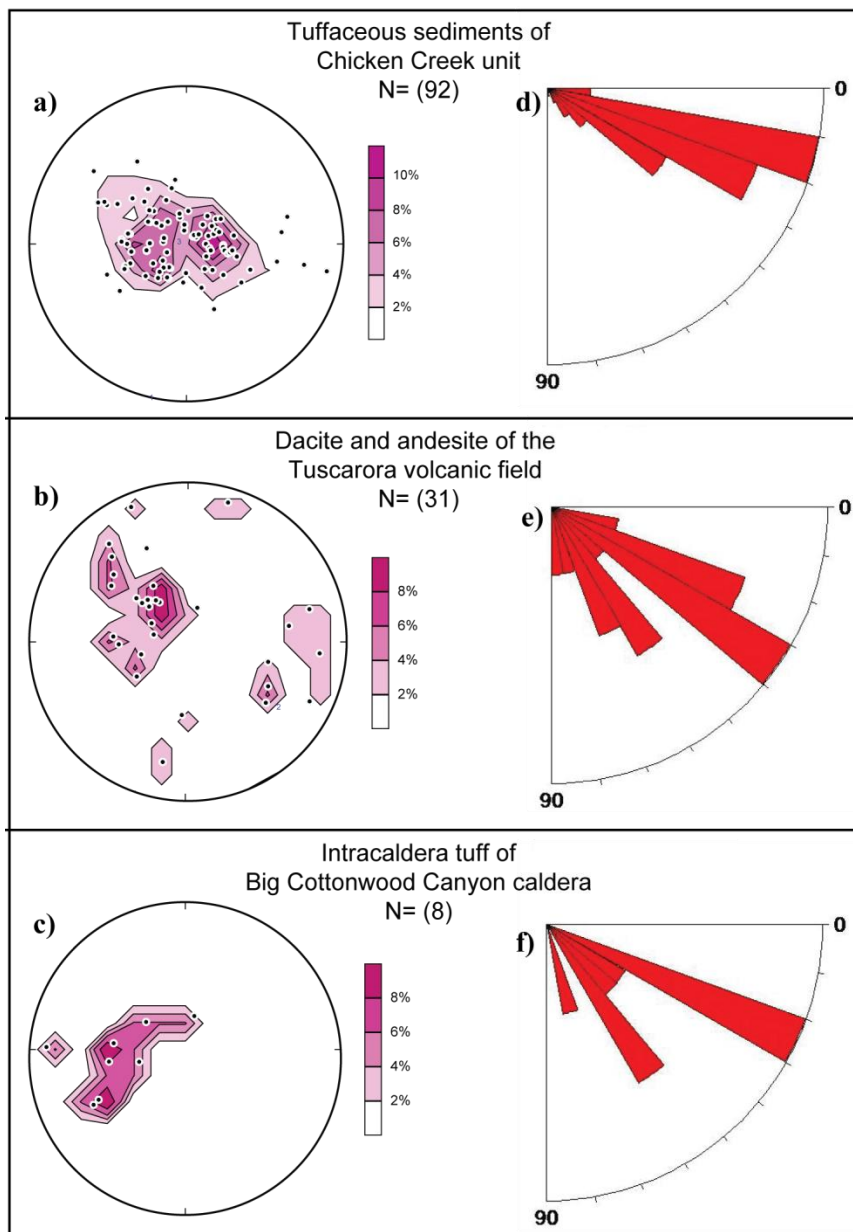


Figure 4.6. Left column shows poles to bedding and layering, respectively, for sedimentary and volcanic units plotted on lower hemisphere equal-area projections. (a) Poles to bedding in Oligocene (?) sedimentary rocks of the Chicken Creek unit (Tst in Plate 1); (b) Poles to flow foliation in Eocene dacite and andesite flows (Te, Tsa, Tsd, Tao, Tn, and Ti in Plate 1); (c) Poles to compaction foliation in 40.0 Ma welded tuff of Big Cottonwood Canyon caldera (Tct in Plate 1). Shaded contour intervals at 2, 4, 6, 8, and 12% of data per 1% area. Data points are shown as black dots. Right column shows dip values displayed as rose plots in 10° increments from 0° (horizontal) to 90° (vertical). For both the stereonet and rose diagrams, the number of measurements is shown in parentheses.

The accommodation zone is defined mainly by steeply dipping ($>60^\circ$) normal faults that have been active since ~ 16 Ma, though structural relations described above combined with $^{40}\text{Ar}/^{39}\text{Ar}$ geochronologic data (Henry et al., 1999; Henry et al., 2011) indicate that Tuscarora has undergone extension since the late Eocene. Flows of the Jarbidge Rhyolite are tilted up to $\sim 37^\circ$ east, indicating significant extension since ~ 16 Ma. Late Miocene-Pliocene to early Pleistocene fan deposits are tilted $\sim 10^\circ$, suggesting that much of this extension occurred between the middle Miocene and Pliocene but also that some extension has continued since the latest Tertiary. Evidence of on-going Quaternary deformation is abundant in the region (e.g. Independence Valley and Bull Run Mountains) but sparse in the northeastern Tuscarora Mountains. Within the study area a single probable north-northeast-trending Quaternary scarp was recognized adjacent to Hot Creek ~ 2 km south of the geothermal field. This study does not resolve whether Cenozoic extension has been continuous or episodic. Observations from Tuscarora are compatible, however, with studies elsewhere in northern Nevada that document several pulses of extension from Eocene to present (e.g. Colgan and Henry, 2009).

5. Discussion

STRUCTURAL CONTROLS ON GEOTHERMAL ACTIVITY

This study employed geologic mapping, structural analysis, and well data to better understand the geometry and kinematics of deformation in and around the Tuscarora geothermal field of northeastern Nevada. Two distinct settings at different scales appear to control the Tuscarora geothermal system. The regional structural setting is a 10 km-wide complexly faulted left step or relay ramp (c.f., Larsen, 1988) in a range-bounding fault system. The Bull Run Mountains and Independence Mountains fault zones are the major fault segments that together form a semi-continuous system of west-dipping normal faults, kinematically linked by the broad step-over and relay ramp. Within the step-over, sets of east- and west-dipping normal faults overlap in a northerly trending accommodation zone (Figure 5.1). The distribution of hot wells at Tuscarora indicates that the geothermal system is restricted to the narrow (<1 km) axial part of the accommodation zone. Thus, the local structural control on geothermal activity is the accommodation zone, whereas the regional setting is characterized by the broad step-over and relay ramp. Previous work has shown that at least several other high temperature geothermal systems in the Great Basin are also characterized by more than one structural setting, including Brady's, Reese River, Salt Wells, and possibly Steamboat (Faulds et al., 2011; Hinz et al., 2011b).

Within the axial part of the accommodation zone, hot spring activity is most robust in the area with the greatest density of fault intersections. Boiling springs and active fumaroles are concentrated at the north end of the geothermal field, where three steeply dipping north-northeast-striking normal faults intersect a northwest-striking fault.

All four fault segments dip westerly, resulting in a complex southwest-plunging fault intersection that appears to localize outflow but may not control deeper upwelling in the geothermal system.

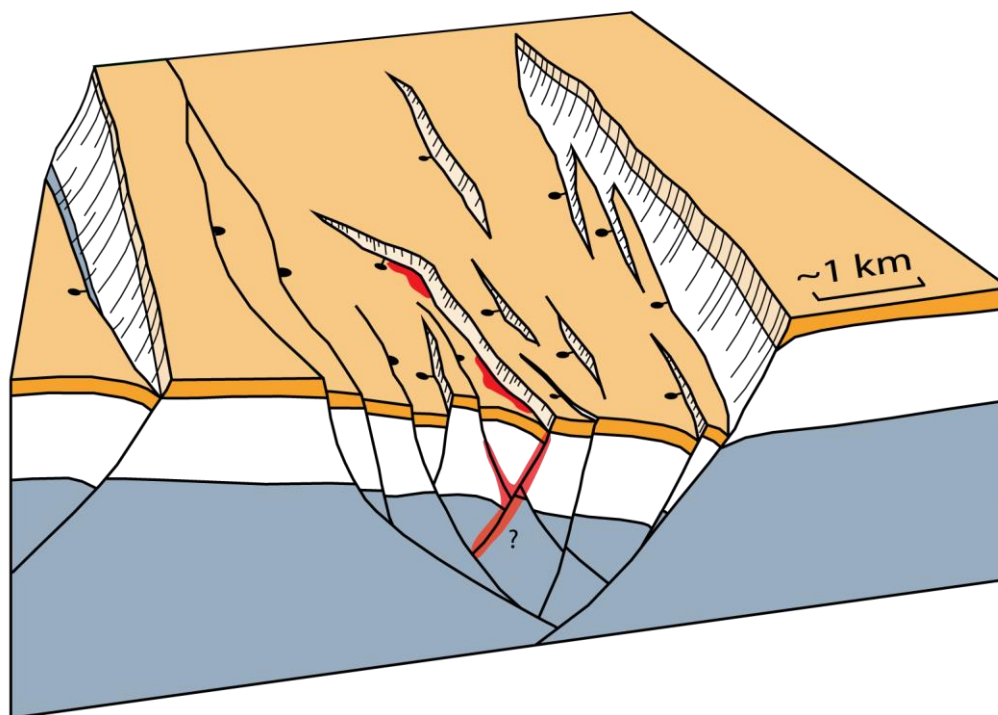


Figure 5.1. Block diagram depicting an antithetic accommodation zone developed within a portion of a relay ramp between large synthetic normal faults. The antithetic accommodation zone is defined here by domains of oppositely-dipping faults and not the orientation of fault blocks. Red shading depicts structurally controlled pathways of geothermal up flow and outflow within the hinge zone of the accommodation zone. For clarity, oppositely dipping faults show only one generation of offset.

Though surface out flow is greatest near this southwest-plunging fault intersection, geothermal production wells exploit an area dominated by north-northeast-striking normal faults ~1.4 km to the south. The distribution of hot wells and hydrothermal alteration suggest that ascending fluids are focused along these north-northeast-striking normal faults. Previous studies have shown that hydraulically conductive faults and fractures are commonly oriented approximately orthogonal to the

least principal stress direction (e.g. Barton et al., 1995; Faulds et al., 2006; Moeck et al., 2009). Geodetic data, earthquake focal mechanism solutions, and kinematic data indicate approximately northwest-southeast-directed extension in northeastern Nevada at present (Zoback, 1989; Hammond et al., 2011; Smith et al., 2011). Assuming a direct relationship between the regional extension direction and the orientation of least principal stress within the geothermal field, steeply dipping northeast-striking faults are most favorably oriented for extension in the regional stress regime. Faults in the geothermal area strike north-northeast to northwest. Within this range of existing fault orientations, north-northeast-striking faults are most favorably oriented for reactivation and dilation in the present stress regime. Accordingly, such faults host most of the geothermal activity, as evidenced by the distribution of hot springs, sinter, and production wells. Geothermal activity is notably sparse along north- and north-northwest-striking faults within the geothermal field.

The absence of geothermal activity along large-offset faults within the Bull Run-Independence Mountains fault system and localization in the axial part of an accommodation zone may be attributable to differing fault zone architectures. Fault planes with large magnitude offsets typically develop a core consisting of clay gouge, whereas fault planes with small offsets tend to be breccia and fracture-dominated (Caine et al., 1996). Gouge zones act as barriers to fluid flow across a fault, whereas brecciated damage zones promote fluid flow. At Tuscarora, the oppositely dipping normal fault sets that locally control the geothermal upwelling have relatively small offsets (<350 m) and are likely breccia-dominated. In contrast, the adjacent range-bounding fault zones are the focus of large magnitude strain, with offsets of several kilometers, and thus are more

likely to be gouge-dominant and inhibit fluid flow. Additionally, overlapping faults within accommodation zones form a greater density of fault intersections as compared with the mid-segments of major normal faults.

STRUCTURAL PERMEABILITY IN ACCOMMODATION ZONES

Within the accommodation zone steeply east- and west-dipping normal faults form complex fault intersections and areas of both increased fracture density and bulk permeability parallel to σ_2 (e.g. Sibson, 2000; Ferrill et al., 2000). Alternating reactivation of crossing normal faults accommodates offsets of earlier fault segments and results in the formation of new fault intersections (Figure 5.2) (Horsfield, 1980; Ferrill et al., 2000). Existing fault segments tend to be reactivated because fault zones are weaker than the surrounding rock and thus fail under lower differential stress (Morris et al., 1996). Additionally, field examples of conjugate normal faults reveal that new fault intersections are generated where offset segments are reactivated and propagate back across the cross-cutting faults, leading to new fault segments (Ferrill et al., 2009). Permeability in this setting is maintained both by the reactivation of preexisting faults and stress concentrated near fault tip lines (Curewitz and Karson, 1997; Gupta and Scholz, 2000). In zones of low intrinsic permeability, such as metasedimentary basement rocks at Tuscarora, fluid flow may be enhanced in the σ_2 -direction, parallel to the intersection of faults and fractures (Sibson, 1996). Additionally, cross-fault fluid flow is enabled by interconnected fault damage zones and fracture networks.

Vertical permeability of the geothermal reservoir is probably maintained by abundant interconnected fault zones and fracture networks in the axial part of the accommodation zone, involving many inward-dipping faults.

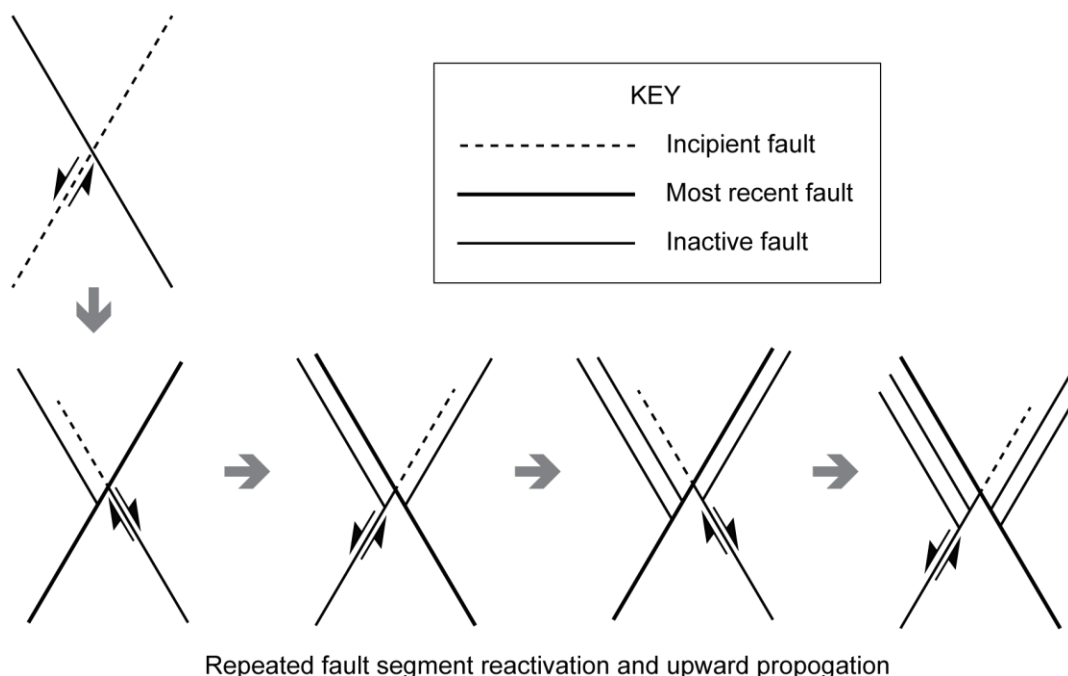


Figure 5.2. Alternating activity of oppositely dipping faults, showing the reactivation of shallow fault segments and formation of new fault segments. Repeated reactivation and fault propagation generates a high density of fault intersections in the vicinity of crossing faults (Adapted from Ferrill et al., 2000).

Here, fault intersections occur over a wide range ($< 1 - \sim 3$ km) of depths in a relatively narrow (< 2 km), steeply-plunging zone presumably characterized by dense fracture networks and complex fault damage zones (Figure 5.3). Thus, a steeply-plunging zone of structurally-maintained permeability may facilitate upwelling of hydrothermal fluids from relatively deep (~ 3 km) levels in the axial part of the accommodation zone.

Fluid flow to the surface, however, is focused along steeply-dipping normal faults, whereas geothermal production wells may exploit a more moderately-dipping fault near the uppermost part of the inferred high permeability zone. Steeply west-dipping normal faults that localize the geothermal surface expression are intersected by geothermal wells 87-05 and 65-08 within 50 m of the surface, or not at all (Figure 4.4; Plate 2). However, these wells may exploit hydraulically-conductive fractures in the

damage zone of a moderately ($\sim 55^\circ$) west-dipping normal fault that projects to the surface ~ 2 km to the east (Figure 5.3).

Alternatively, normal faults in the Hot Creek area may have very steep dips ($\sim 80^\circ$) such that the geothermal wells exploit dilatant fractures within a footwall breccia zone of these faults. Such dilatant footwall breccia zones were described by Caine et al. (2010) along the Stillwater normal fault in western Nevada and shown to host hydrothermal activity. Very steeply dipping normal faults within accommodation zones are interpreted in seismic reflection profiles from basins of the Malawi (Flannery and Rosendahl, 1990) and Rio Grande rifts (Russell and Snelson, 1994). However, further interpretation is hindered by the lack of precise knowledge of fault dips in the vicinity of the geothermal field.

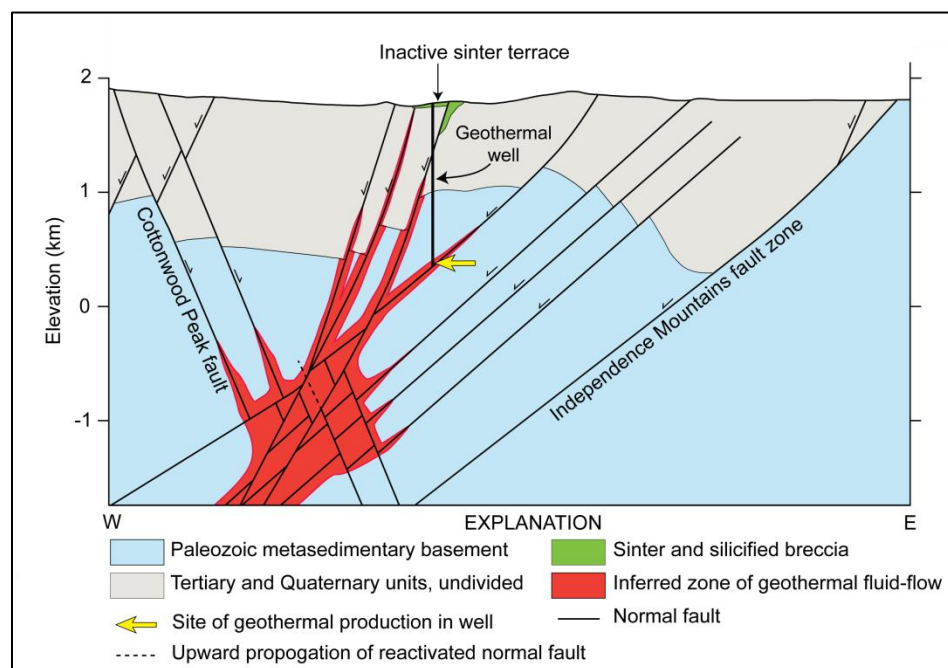


Figure 5.3. Conceptual model of the geothermal system shown in cross section. The geothermal reservoir lies within a zone of abundant fault intersections where inward-dipping sets of normal faults interact in the axial part of the accommodation zone. Away from the zone of abundant fault intersections, fluid-flow is restricted to discrete fault zones. Moderate argillic alteration along fault zones in Tertiary volcanic and tuffaceous sedimentary rocks is envisioned to further restrict up-flow paths.

Regardless of whether production wells currently exploit a moderately or steeply dipping fault zone, the down-dip projection of faults identified by this study suggests that the main geothermal reservoir lies to the west of the geothermal surface expression and at greater depth (Figure 5.3). The highest temperatures and greater permeability within the Tuscarora geothermal field are inferred to be ~1 km west of the geothermal surface expression along north-northeast-striking faults at 2 – 3 km depth. To further constrain the location of high-permeability fault intersections within the accommodation zone, future exploration efforts should seek to better constrain the orientations of both east- and west-dipping faults at the margins of the geothermal field.

Additional controls on the extent of the geothermal reservoir within the accommodation zone may include the depth and host-rock lithology of the fracture network. East- and west-dipping normal faults intersect beneath the geothermal production area in metasedimentary Paleozoic basement at depths of ~1.5 km to ~3 km (e.g. Figure 4.4) (Plate 2). However, shallower (<500 m) fault intersections occur in volcanic rocks ~1.5 km south of the production area but are not associated with geothermal activity.

CALDERA MARGIN STRUCTURES AND IMPLICATIONS FOR PERMEABILITY

Voluminous caldera collapse breccias encountered within the geothermal field coupled with geologic mapping of thick (>2.5 km) intracaldera tuff ~2 km west of the geothermal system strongly suggest that the northeastern margin of the Big Cottonwood Canyon caldera lies beneath younger sedimentary and volcanic strata in the northeastern Tuscarora Mountains (Figures 3.3 and 4.4). Though caldera margin structures (e.g. ring fault network) have not been delineated at Tuscarora, such features probably lie in the

vicinity of the geothermal field but may be covered by younger strata. A ring fracture zone may enhance permeability in the Paleozoic basement near the Paleozoic-Tertiary nonconformity within the geothermal field. Analog modeling of caldera collapse structures indicate that strain is focused in syncollapse fault networks at the margins of an evacuated magma chamber (Roche et al., 2000; Holohan et al., 2008). Modeled ring fault networks dip steeply ($>70^\circ$) and may be characterized by outward-dipping reverse faults and/or inward-dipping normal faults. These experimental results are compatible with field observations from the well exposed margins and ring fault networks of well studied calderas (e.g., John, 1995; Lipman, 1976). Fault breccia generated along ring faults during caldera subsidence would have enhanced permeability in Paleozoic basement rocks and may have in part localized hydrothermal fluid flow (e.g. Rytuba, 1994). The Big Cottonwood Canyon caldera is tilted $\sim 45^\circ$ east-northeast, and thus the inferred ring faults have probably been rotated to moderate westerly dips. Whether the inferred Eocene caldera ring fracture network actually enhances permeability within the geothermal reservoir at present is not easily resolved. It is notable, however, that geothermal activity appears to be restricted to the region where the inferred caldera margin intersects the axial part of the accommodation zone. Thus, the influence of Eocene structures on the Tuscarora geothermal system should not be ruled out.

GEOHERMAL ACTIVITY IN BROAD STEP-OVERS

Step-overs are the most common structural setting for geothermal activity in the Great Basin (Faulds et al. 2011), yet the details of most individual systems remain poorly understood. The geometry of three broad (>5 km) step-overs that host geothermal activity identified by Faulds et al. (2011) are examined here (Figure 5.4) and compared with the

fault system at Tuscarora. The three fault systems and attendant geothermal systems are: 1) Winter Rim fault zone/Summer Lake Hot Springs; 2) Steens Mountain fault zone/Alvord and Borax Lake Hot Springs; 3) Kawich-Hot Creek fault zone/Hot Creek Ranch springs. Like the Bull Run-Independence Mountains fault system, these three fault systems are defined by sub-parallel, synthetically-dipping major normal fault zones active in the Quaternary. The total length of each fault system is between 50 and 110 km (Sawyer and Anderson, 1998; Personious, 2002). Unlike the Bull Run-Independence Mountains fault system, major segments of both the Winter Rim and Kawich-Hot Creek systems are physically linked by smaller faults striking oblique or orthogonal to the greater fault system (Figures 5.4a and 5.4b). Minimal overlap is observed between major segments of the Winter Rim fault system, whereas segments of the Kawich-Hot Creek fault system appear to underlap. In contrast, major segments of the Steens Mountain fault system exhibit ~15 km of overlap, forming a south-tilted relay ramp, mirroring the Independence-Bull Run Mountains fault system. Unlike the Independence-Bull Run Mountains step-over, the Steens Mountain relay ramp is cut by a series of minor faults, which may provide hard linkage between major fault segments (Figure 5.4c). Quaternary faults are abundant near the southern termination of the eastern segment of the Steens Mountain fault system, whereas Quaternary faulting at Tuscarora is mainly documented at the major range fronts.

The location of geothermal activity is different within each of the broad step-overs described here but is consistently associated with Quaternary faults. Therefore, detailed characterization of subsidiary structures is necessary to explore effectively within this common structural setting. For example, hot springs at Summer Lake are

adjacent to small faults that strike orthogonal to and link major segments of the Winter Rim fault system. The springs lie in the middle of the step, approximately equidistant from the major fault segments. At Hot Creek Ranch, boiling springs emanate at the abrupt termination of several faults that together define the southern segment of the step-over in the Kawich-Hot Creek fault system. Alvord and Borax Lake Hot Springs both lie at the periphery of a broad step-over in the Steens Mountain fault system. A small (<1 km) step-over hosts the Alvord Hot Springs in the hanging wall of the eastern segment of the Steens Mountain fault system. Borax Lake Hot Springs occur along a series of small en echelon normal faults (Fairley and Hinds, 2004) that lie between the major fault segments of the broad right step in the Steens Mountain fault system. These examples demonstrate that geothermal activity within and adjacent to broad fault step-overs can be further characterized in terms of the geometry of the step-over (e.g. segment overlap and type of linkage) and subsidiary structural settings within each step-over (e.g. fault termination, small step-over).

The recognition of subsidiary structural settings within broad step-over regions or relay ramps, such as the northeastern Tuscarora Mountains, may help guide geothermal exploration in extended terranes. Broad step-overs in large normal fault systems are commonly easy to identify by bends or embayments in range fronts. However, geothermal activity typically occupies only a small portion of these broad step-over regions. Geologic mapping of bedrock and, in some cases, alluvial cover can be an effective method to characterize subsidiary structures that focus up-flow and optimize the placement of drill holes, particularly when integrated with methods such as shallow temperature probes, geophysical surveys, and slip and dilation tendency analysis.

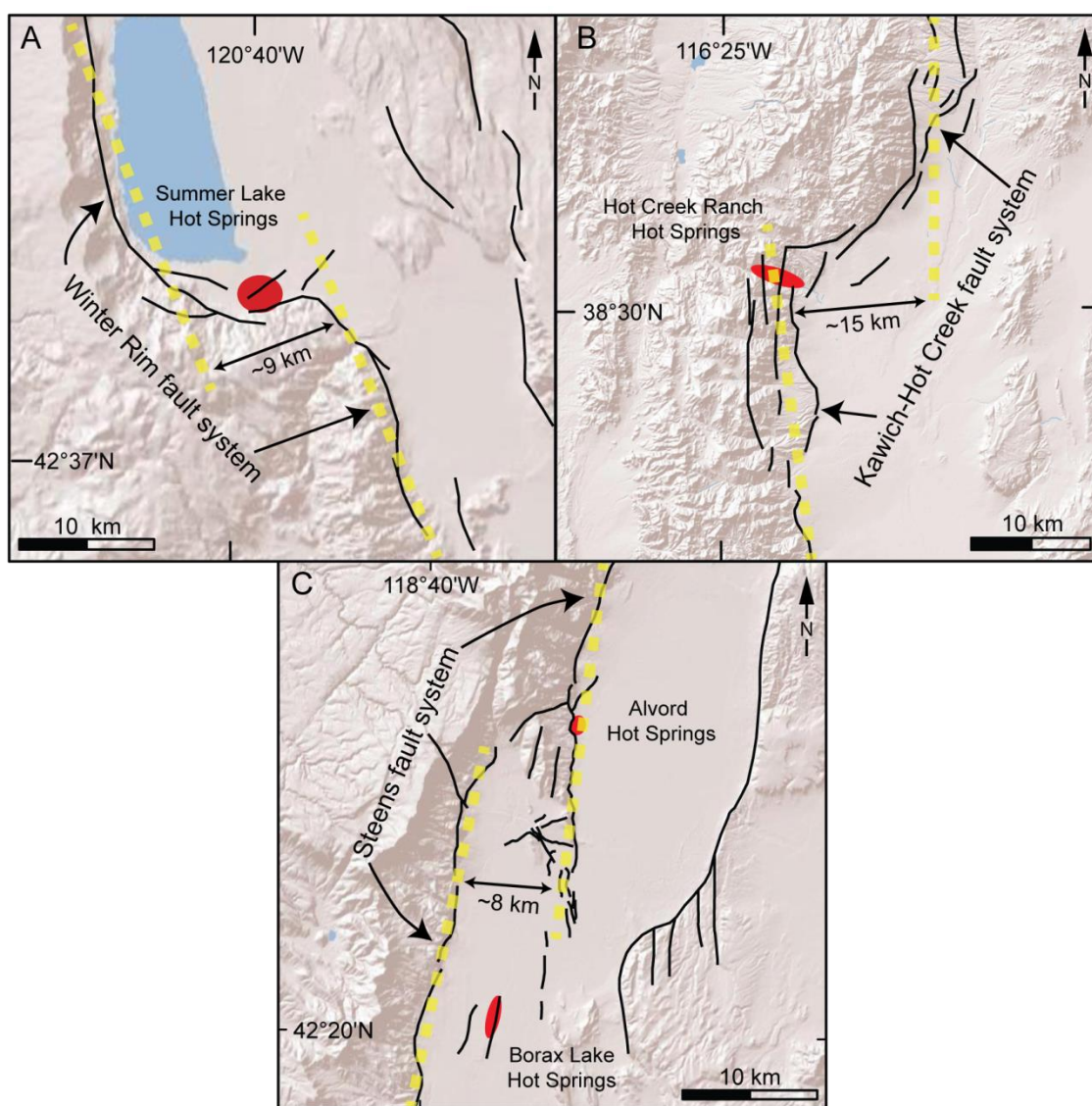


Figure 5.4. Shaded relief maps showing examples of geothermal systems (red shading) that lie within broad step-overs in major Quaternary normal fault systems (black lines). Dashed yellow lines show the approximate distance between major fault segments. **A.** Summer Lake Hot Springs lie within the zone of linkage between major normal fault segments where short, closely spaced faults strike perpendicular to the major fault segments. **B.** Hot springs at Hot Creek Ranch emanate at the northern termination of the southern segment of a right-stepping normal fault system. **C.** Alvord Hot Springs lie within a small (<1 km) left step-over formed by normal faults that define the eastern segment of a broad right step-over. Up flow at

Borax Lake Hot Springs occurs along a fault that lies between the major fault segments of the broad right step.

IMPLICATIONS FOR GEOTHERMAL EXPLORATION IN NORTHEAST NEVADA

Insights gained from detailed geologic mapping of the relatively well exposed relay ramp and accommodation zone in the northeastern Tuscarora Mountains may benefit geothermal exploration in areas of northeastern Nevada where bedrock and potential geothermal systems are concealed by basin fill. Broad step-overs in major northerly trending faults systems abound in northeastern Nevada and have been shown by this study and others (e.g. Faulds et al., 2011) to host geothermal activity. However, alluvial cover commonly prevents direct observation of the subsidiary structures (i.e. small faults and extensional folds) within these step-over regions. Where geophysical data permit interpretation of subsurface geology, exploration efforts in step-over regions should focus on areas with the highest density of fault interactions and target north-northeast-striking faults, which are optimally oriented for extension in the regional stress field.

Many high-temperature Great Basin geothermal systems have been shown to be associated with Quaternary faults (Koenig and McNitt, 1983; Bell and Ramelli, 2007). However, evidence for Quaternary faulting (e.g. scarps) is scarce in the vicinity of the Tuscarora geothermal system. Thus, compilations of Quaternary faults, commonly included in GIS-based studies of geothermal favorability (e.g. Coolbaugh et al., 2003; Zehner et al., 2009), do not include the Tuscarora geothermal area. High-temperature geothermal systems in northeastern Nevada, including Beowawe and Humboldt Wells,

are spatially associated with late Quaternary faults (Wesnousky et al., 2005; Henry and Colgan, 2011), but relations in the Tuscarora area indicate that regions lacking well-documented Quaternary deformation should still be considered prospective.

Furthermore, the presence of several high-temperature systems in northeastern Nevada, including Beowawe and Tuscarora, demonstrates the viability geothermal activity in this region despite low present-day strain rates as indicated by GPS data (Bennett et al., 2003; Kreemer et al., 2012). Therefore, extensional terranes, such as northeastern Nevada, undergoing relatively low rates of Holocene deformation but characterized by widespread Quaternary faulting should not be precluded from geothermal exploration. Northeastern Nevada may therefore have higher geothermal potential than suggested by previous studies.

6. Conclusions

The structural and stratigraphic framework of the Tuscarora geothermal area has been defined by detailed geologic mapping and structural analysis, integrated with well and regional geologic data. The northeastern Tuscarora Mountains consist mainly of metasedimentary Paleozoic basement nonconformably overlain by Eocene tuff, andesite, and dacite of the Tuscarora volcanic field, Oligocene-middle Miocene tuffaceous sedimentary rocks, and middle Miocene rhyolite and dacite lavas. Tertiary strata are exposed in gently to moderately east- and west-tilted fault blocks bounded by northerly-striking normal faults. The subsurface geology of the geothermal field is dominated by intracaldera deposits of the Big Cottonwood Canyon caldera to depths of 700-1000 m, including blocks of basement-derived megabreccia. Recognition of the Tertiary-

Paleozoic nonconformity at Tuscarora as a caldera margin has provided a new framework to interpret subsurface data and further develop a structural and stratigraphic model of the geothermal system.

Detailed geologic analyses reveal that the Tuscarora geothermal field is characterized by two structural settings: 1) a broad left step-over or relay ramp in a major normal fault system, and 2) an accommodation zone, which occupies part of the relay ramp formed by the step-over. Abundant fault intersections in Paleozoic basement formed by the alternating reactivation of crossing normal faults of opposite dip within the axial part of the accommodation zone likely promotes increased permeability and fluid circulation at depth. A ring fracture network related to subsidence of the Big Cottonwood Canyon caldera may also be present within the geothermal field and further enhance basement permeability. Steeply dipping north-northeast-striking normal faults provide a subvertical conduit for geothermal fluids and control the distribution of hydrothermal surface features.

GPS geodetic data, earthquake focal mechanism solutions, and kinematic data from Quaternary faults indicate a northwest-trending extension direction in northeastern Nevada (Zoback, 1989; Hammond et al., 2011; Smith et al., 2011). This is compatible with the observation that north-northeast-striking normal faults and associated fracture networks are the most hydraulically conductive within the geothermal field. Additionally, kinematic analysis of fault slip data and the results of a stress inversion at Tuscarora reveal an east-west-trending least principal paleostress direction, which probably reflects an earlier episode of Miocene extension.

This study has identified the axial part of an accommodation zone as the site most conducive to fluid up-flow. The recognition of this specific portion of an accommodation zone as a favorable structural setting for geothermal activity may be a useful exploration tool for development of drilling targets in extensional terranes, as well as for developing geologic models of known geothermal fields. Assessment of several other broad step-overs indicates that geothermal activity may occur in a variety of subsidiary structural settings, in addition to accommodation zones. In northeastern Nevada, broad step-overs are prospective regions for exploration of blind geothermal systems. Delineation of favorable structural settings within step-over regions analogous to Tuscarora, but lacking bedrock exposure may further benefit from the findings of this study. On the basis of GPS geodetic data, northeastern Nevada is characterized by low present-day strain rates but also hosts several high temperature geothermal systems, indicating that electrical-grade geothermal activity is viable in this tectonic setting. Ultimately, this information may help to reduce the risks of targeting successful geothermal wells in such settings.

REFERENCES

- Adams, K.K., and Sawyer, T.L., 1999, Fault number 1553a, eastern Independence Valley fault zone, northern section, Quaternary fault and fold database of the United States: <http://earthquakes.usgs.gov/hazards/qfaults> (November, 2012).
- Anderson, J.G., 2011, Seismicity and seismic hazard of northeastern Nevada earthquake *in* dePolo, C.M., and LaPointe, D.D., eds., The 21 February 2008 Mw 6.0 Wells, Nevada Earthquake: Nevada Bureau of Mines and Geology Special Publication 36, p. 43–50.
- Angelier, J., 1994, Fault slip analysis and paleostress reconstruction, *in* Hancock, P.L., ed., Continental Deformation: New York, Pergamon Press, p. 53–100.
- Arehart, G.B., Coolbaugh M.F., and Poulsen, S.R., 2003, Evidence for a magmatic source of heat for the Steamboat Springs geothermal system using trace elements and gas geochemistry, Geothermal Resources Council Transactions, v. 27, p. 269–274.
- Barton, C.A., Zoback, D.M., and Moos, D., 1995, Fluid flow along potentially active faults in crystalline rock: *Geology*, v. 23, p. 683–686.
- Bell, J.W., and Ramelli, A.R., 2007, Active Faults and Neotectonics at Geothermal Sites in the Western Basin and Range: Preliminary Results: Geothermal Resources Council Transactions, v. 31, p. 375–378.
- Bennett, R.A., Wernicke, B.P., Niemi, N.A., Friedrich, A.M., and Davis, J.L., 2003, Contemporary strain rates in the northern Basin and Range province from GPS data: *Tectonics*, v. 22, p. 1–31.
- Berger, B.R., Ridley, W.I., and Tingley, J.V., 1991, Interrelationship of mineralization, volcanism, and tectonism, northern Tuscarora Mountains, Elko County, Nevada, *in* Thorman, C.H., ed., Some current research in eastern Nevada and western Utah: U.S. Geological Survey Open-File Report 91–386, p. 13–19.
- Best, M.G., Christiansen, E.H., Deino, A.L., Grommé, C.S., McKee, E.H., and Noble, D.C., 1989, Eocene through Miocene volcanism in the Great Basin of the western United States, *in* Chapin C.E., and Zidek, J., eds., Field excursions to volcanic terranes in the western United States, Volume II: Cascades and Intermountain West: Socorro, New Mexico, New Mexico Bureau of Mines and Mineral Resources Memoir 47, p. 91–133.
- Blackwell, D.D., 1983, Heat flow in the northern Basin and Range province: Geothermal Resources Council Special Report 13, p.81–93.

- Blackwell, D.D., and Richards, M., 2004, Geothermal map of North America: American Association of Petroleum Geologists, scale 1:6,500,000.
- Blewitt, G., Coolbaugh, M., Sawatzky, D., Holt, W., Davis, J., and Bennett, R., 2003, Targeting of potential geothermal resources in the Great Basin from regional to basin-scale relationships between geodetic strain and geological structures: Geothermal Resources Council Transactions, v. 27, p. 3–7.
- Bowman, J.R., and Cole, D.R., 1982, Hydrogen and oxygen isotope geochemistry of the cold and warm springs from the Tuscarora Nevada thermal area: Department of Energy, Contract No. DE-AC07-80ID 12079, 26 p.
- Brueseke, M.E., Hart, W.K., and Heizler, M.T., 2008, Diverse mid-Miocene silicic volcanism associated with the Yellowstone-Newberry thermal anomaly: Bulletin of Volcanology, v. 70, p. 343–360.
- Caine, J.S., Evans, J.P., and Forster, C.B., 1996, Fault zone architecture and permeability structure: Geology, v. 24, p. 1025–1028.
- Caine, J.S., Bruhn, R.L., and Forster, C.B., 2010, Internal structure, fault rocks, and inferences regarding deformation, fluid flow, and mineralization in the seismogenic Stillwater normal fault, Dixie Valley, Nevada: Journal of Structural Geology, v. 32, p. 1576–1589.
- Castor, S.B., and Henry, C.D., 2000, Geology, geochemistry, and origin of volcanic rock-hosted uranium deposits in northwestern Nevada and southeastern Oregon, USA: Ore Geology Reviews, v. 16, p. 1–40.
- Christiansen, R.L., and Yeats, R.S., 1992, Post-Laramide geology of the U.S. Cordilleran region, *in* Burchfiel, B.C., et al., eds., The Cordilleran orogeny: Conterminous U.S.: Geological Society of America, Geology of North America, v. G-3, p. 261–406.
- Coats, R.R., 1968, Recent fault scarps in Independence Valley near Tuscarora, Elko County, Nevada: U.S. Geological Survey, Professional Paper 600-B, 4 p.
- Coats, R.R., 1987, Geology of Elko County, Nevada: Nevada Bureau of Mines and Geology, Bulletin 101, 112 p.
- Coble, M.A., and Mahood, G.A., 2012, Initial impingement of the Yellowstone plume located by widespread silicic volcanism contemporaneous with Columbia River flood basalts: Geology, v. 40, p. 655–658.

- Colgan, J.P., and Henry, C.D., 2009, Rapid middle Miocene collapse of the Mesozoic orogenic plateau in north-central Nevada, *International Geology Review*, v. 51, p. 920–961.
- Coolbaugh, M.F., Sawatzky, D.L., Opplinger, G.L., Minor, T.B., Raines, G.L., Shevenell, L., and Garg, S.K., 2003, Geothermal GIS coverage of the great basin, USA; defining regional controls and favorable exploration terrains: *Geothermal Resources Council Transactions*, v. 27, p. 9–13.
- Coolbaugh, M., Zehner, R., Kreemer, C., Blackwell, D., Opplinger, G., Sawatzky, D., Blewitt, G., Pancha, A., Richards, M., Helm-Clark, C., Shevenell, L., Raines, G., Johnson, G., Minor, T., and Boyd, T., 2005, Geothermal potential map of the Great Basin, Western United States: Nevada Bureau of Mines and Geology, scale 1:1,000,000.
- Curewitz, D., and Karson, J.A., 1997, Structural settings of hydrothermal outflow: Fracture permeability maintained by fault propagation and interaction: *Journal of Volcanology and Geothermal Research*, v. 79, p. 149–168.
- dePolo, C.M., Smith, K.D., and Henry, C.D., 2011, Summary of the 2008 Wells, Nevada earthquake documentation volume, *in* dePolo, C.M., and LaPointe, D.D., eds., *The 21 February 2008 Mw 6.0 Wells, Nevada Earthquake*: Nevada Bureau of Mines and Geology Special Publication 36, p. 7–13.
- Dohrenwend, J.C., and Moring, B.C., 1991, Reconnaissance photogeologic map of young faults in the McDermitt 1° by 2° Quadrangle, Nevada, Oregon, and Idaho: U.S. Geological Survey Miscellaneous Field Studies Map MF-2177, scale 1:250,000.
- Ehman, K.D., and Clark, T.M., 1986, Geologic map of the Bull Run Mountains, Elko County, Nevada: Nevada Bureau of Mines and Geology, Open-File Report 86-12, scale 1:24000.
- Erwin, J.W., 1988, Discussion of McDermitt gravity sheet: Nevada Bureau of Mines and Geology Open File Report 88-2, 4 p.
- Fagan, J., 1968, Carboniferous cherts, turbidites, and volcanic rocks in northern Independence Range, Nevada: *Geological Society of America Bulletin*, v. 73, p. 595–611.
- Fairley, J.P., and Hinds, J.J., 2004, Rapid transport pathways for geothermal fluids in an active Great Basin fault zone: *Geology*, v. 32, p. 825–828.

- Faulds, J.E., 1996, Geologic map of the Fire Mountain 7.5' quadrangle, Clark County, Nevada and Mohave County, Arizona, Nevada Bureau of Mines and Geology Map 106, scale 1:24,000.
- Faulds, J.E., and Varga, R.J., 1998, The role of accommodation zones and transfer zones in the regional segmentation of extended terranes, *in* Faulds, J. E., and Stewart, J. H., eds., *Accommodation Zones and Transfer Zones: The Regional Segmentation of the Basin and Range Province*: Boulder, Colorado, Geological Society of America Special Paper 323, p. 1–45.
- Faulds, J.E., Coolbaugh, M., Blewitt, G., and Henry, C.D., 2004, Why is Nevada in hot water? Structural controls and tectonic model of geothermal systems in the northwestern great basin: *Geothermal Resources Council Transactions*, v. 28, p. 649–654.
- Faulds, J.E., Coolbaugh, M.F., Vice, G.S., and Edwards, M.L., 2006, Characterizing structural controls of geothermal fields in the northwestern Great Basin: A progress report: *Geothermal Resources Council Transactions*, v. 30, p. 69–76.
- Faulds, J.E., and Henry, C.D., 2008, Tectonic influences on the spatial and temporal evolution of the Walker Lane: An incipient transform fault along the evolving Pacific – North American plate boundary, *in* Spencer, J.E., and Titley, S.R., eds., *Circum-Pacific Tectonics, Geologic Evolution, and Ore Deposits*: Tucson, Arizona Geological Society, Digest 22, p. 437–470.
- Faulds, J.E., Coolbaugh, M.F., Hinz, N.H., Cashman, P.H., and Kratt, C., Dering, G., Edwards, J., Mayhew, B., and McLachlan, H., 2011, Assessment of favorable structural settings of geothermal systems in the Great Basin, western USA: *Geothermal Resources Council Transactions*, v. 35, p. 777–784.
- Faulds, J.E., Hinz, N. H., Kreemer, C., Coolbaugh, M. F., 2012, Regional Patterns of Geothermal Activity in the Great Basin Region, Western USA: Correlation with Strain Rates: *Geothermal Resources Council Transactions*, v. 36, p. 897–902.
- Ferrill, D.A., Morris, A.P., Stamatakos, J.A., and Sims, D.W., 2000, Crossing conjugate normal faults: *American Association of Petroleum Geologists*, v. 84, p. 1543–1559.
- Ferrill, D.A., Morris, A.P., McGinnis, R.N., 2009, Crossing conjugate normal faults in field exposures and seismic data: *American Association of Petroleum Geologists*, v. 93, p. 1471–1488.
- Flannery, J.W., and Rosendahl, B.R., 1990, The seismic stratigraphy of Lake Malawi, Africa: implications for interpreting geological processes in lacustrine rifts: *Journal of African Earth Sciences*, v. 10, p. 519–548.

- Friedrich, A.M., Lee, J., Wernicke, B.P., and Sieh, K., 2004, Geologic context of geodetic data across a Basin and Range normal fault, Crescent Valley, Nevada: *Tectonics*, v. 23, TC2015, doi:10.1029/2003TC001528.
- Glazner, A.F., and Ussler, W., 1989, Crustal extension, crustal density, and the evolution of Cenozoic magmatism in the Basin and Range of the western United States: *Journal of Geophysical Research*, v. 94, p. 7952–7960.
- Goranson, C., 2005, Recent drilling activities at the Earth Power Resources Tuscarora geothermal power project's Hot Sulphur Springs lease area: Sandia National Laboratories Report SAND2005-1395, 48 p.
- Gupta, A., and Scholz, C.H., 2000, A model of normal fault interaction based on observations and theory: *Journal of Structural Geology*, v. 22, p. 865–879.
- Hammond, W.C., and Thatcher, W., 2004, Contemporary tectonic deformation of the Basin and Range province, western United States: 10 years of observation with the Global Positioning System: *Journal of Geophysical Research*, v. 109, B08403, doi:10.1029/2003JB002746.
- Hammond, W.C., Blewitt, G., Kreemer, C., Murray-Moraleda, J.R., and Svarc, J. L., 2011, Global positioning system constraints on crustal deformation before and during the 21 February 2008 Wells, Nevada M 6.0 earthquake, *in* dePolo, C.M., and LaPointe, D.D., eds., *The 21 February 2008 Mw 6.0 Wells, Nevada Earthquake: Nevada Bureau of Mines and Geology Special Publication 36*, p. 181–196.
- Hart, W.K., Aronson, J.L., and Mertzman, S.A., 1984, Areal distribution and age of low-K, high-alumina olivine tholeiite magmatism in the northwestern Great Basin: *Geological Society of America Bulletin*, v. 39, p. 187–195.
- Henry, C.D., Boden, D.R., and Castor, S.B., 1999, *Geologic Map of the Tuscarora Quadrangle, Nevada: Nevada Bureau of Mines and Geology Map 116*, scale 1:24000, 1 sheet, 20 p. text.
- Henry, C.D., McGrew, A.J., Colgan, J.P., Snoke, A.W., and Brueseke, M.E., 2011, Timing, distribution, amount, and style of Cenozoic extension in the northern Great Basin, *in* Lee, J., and Evans, J.P., eds., *Geologic Field Trips to the Basin and Range, Rocky Mountains, Snake River Plain, and Terranes of the U.S. Cordillera: Geological Society of America Field Guide 21*, p. 27–66.
- Henry, C.D., and Colgan, J.P., 2011, The Regional structural setting of the 2008 Wells earthquake and Town Creek Flat Basin — Implications for the Wells earthquake fault and adjacent structures *in* dePolo, C.M., and LaPointe, D.D., eds., *The 21*

February 2008 Mw 6.0 Wells, Nevada Earthquake: Nevada Bureau of Mines and Geology Special Publication 36, p. 53–64.

- Hinz N.H., Faulds, J.E., and Bell, J.W., 2011a, Preliminary geologic map of the Bunejug Mountains 7.5' Quadrangle, Churchill County, Nevada: Nevada Bureau of Mines and Geology Open File Report 11-9, scale 1:24,000.
- Hinz, N.H., Faulds, J.E., and Stroup, C., 2011b, Stratigraphic and structural framework of the Reese River geothermal area, Lander County, Nevada: A new conceptual structural model: *Geothermal Resources Council Transactions*, v. 35, p. 827–832.
- Hoefs, J., 2009, *Stable isotope geochemistry*: Berlin, Springer-Verlag, 285 p.
- Holohan, E.P., Troll, V., van Wyk de Vries, B., Walsh, J., and Walter, T., 2008, Unzipping Long Valley: An explanation for vent migration patterns during an elliptical ring fracture eruption: *Geology*, v. 36, p. 323 – 326.
- Horsfield, W.T., 1980, Contemporaneous movement along crossing conjugate normal faults: *Journal of Structural Geology*, v. 2, p. 305–310.
- John, D.A., 1995, Tilted middle Tertiary ash-flow calderas and subjacent granitic plutons, southern Stillwater Range, Nevada: Cross section of an Oligocene igneous center: *Geological Society of America Bulletin*, v. 107, p. 180-200.
- Johnson J.G., and Pendergast, A., 1981, Timing and mode of emplacement of the Roberts Mountains allochthon, Antler orogeny: *Geological Society of America Bulletin*, v. 92, p. 648–658.
- Koenig, J.B., and McNitt, J.R., 1983, Controls on the location and intensity of magmatic and non-magmatic geothermal systems in the Basin and Range province: *Geothermal Resources Council, Special Report No. 13*, p. 93.
- Kreemer, C., Hammond, W.C., Blewitt, G., Holland, A.A., Bennett, R.A., 2012, A Geodetic strain rate model for the Pacific-North American plate boundary, western United States: Nevada Bureau of Mines and Geology, Map 178, scale 1:1,500,000.
- Larsen, P.H., 1988, Relay structures in a Lower Permian basement-involved extensional system, East Greenland: *Journal of Structural Geology*, v.10, p. 3–8.
- Lipman, P.W., 1976, Caldera-collapse breccias in the western San Juan Mountains, Colorado: *Geological Society of America Bulletin*, v. 87, p. 1397 – 1410.
- Lipman, P.W., 1992, Magmatism in the Cordilleran United States; Progress and problems, *in* Burchfield, B.C., et al., eds., *The Cordilleran Orogen: Conterminous*

- U.S.: Geological Society of America, *Geology of North America*, v. G-3, p. 481–514.
- Marrett, R., and Allmendinger, R.W., 1990, Kinematic analysis of fault-slip data: *Journal of Structural Geology*, v. 12, p. 973–986.
- Micklethwaite, S., and Cox, S., 2004, Fault-segment rupture, aftershock-zone fluid flow, and mineralization: *Geology*, v. 32, p. 813–816.
- Miller, E.L., Holdsworth, B.K., Whiteford, W.B., and Rodgers, D., 1984, Stratigraphy and structure of the Schoonover sequence, northeastern Nevada: Implications for Paleozoic plate-margin tectonics: *Geological Society of America Bulletin*, v. 95, p. 1063–1076.
- Moeck, I., Kwiatek, G., Zimmermann, G., 2009, Slip tendency analysis, fault reactivation potential and induced seismicity in a deep geothermal reservoir: *Journal of Structural Geology*, v. 31, p. 1174–1182.
- Morris, A., Ferrill, D.A., Henderson, D.B., 1996, Slip-tendency analysis and fault reactivation: *Geology*, v. 24, p. 275–278.
- Muntean, J.L., and Henry, C.D., 2006, Preliminary geologic map of the north half of the Jerritt Canyon mining district, Elko County, Nevada: Nevada Bureau of Mines and Geology, Open-File Report 06-17, scale 1:24,000.
- Ortner, H., Reiter, F., and Acs, P., 2002, Easy handling of tectonic data: the programs TectonicVB for Mac and TectonicsFP for Windows: *Computers and Geosciences*, v. 28, p. 1193–1200.
- Personius, S.F., 2002, Fault number 856c, Steens fault zone, Alvord section, Quaternary fault and fold database of the United States:
<http://earthquakes.usgs.gov/hazards/qfaults> (March, 2013)
- Petit, J.P., 1987, Criteria for the sense of movement on fault surfaces in brittle rocks: *Journal of Structural Geology*, v. 9, p. 597–608.
- Pierce, K.L., and Morgan, L.A., 1992, The track of the yellowstone hot spot; volcanism, faulting, and uplift *in* Link, P.K., Kuntz, M.A., and Platt, L.B. eds., *Regional geology of eastern Idaho and western Wyoming*: Geological Society of America Memoir 179, p. 1–53.
- Pilkington, H.D., 1981, Tuscarora area, Nevada geothermal reservoir assessment case history, northern Basin and Range final report: Department of Energy Division of Energy Technology, Contract No. DE-AC08-79ET27011, p. 39.

- Ramelli, A.R., and dePolo, C.M., 2011, Quaternary Faults in the 2008 Wells Earthquake Area, *in* dePolo, C.M., and LaPointe, D.D., eds., The 21 February 2008 Mw 6.0 Wells, Nevada Earthquake: Nevada Bureau of Mines and Geology Special Publication 36, p. 79–88.
- Roche, O., Druitt, T.H., and Merle, O., 2000, Experimental study of caldera formation: *Journal of Geophysical Research*, v. 105, p. 395 – 416.
- Rowan, L.C., and Wetlafer, P.H., 1981, Relation between regional lineament systems and structural zones in Nevada: *American Association of Petroleum Geologists Bulletin*, v. 65, no. 8, p. 1414–1452.
- Russell, L. R., and Snelson, S., 1994, Structure and tectonics of the Albuquerque Basin segment of the Rio Grande rift: Insights from reflection seismic data, *in* Keller, G. R., and Cather, S. M., eds., Basins of the Rio Grande rift: Structure, stratigraphy, and tectonic setting: *Geological Society of America Special Paper 291*, p. 83–112.
- Rytuba, J.J., 1994, Evolution of volcanic and tectonic features in caldera settings and their importance in the localization of ore deposits: *Economic Geology*, v. 89, p. 1687 – 1696.
- Sawyer, T.L., and Anderson, R.E., 1998, Fault number 1355, Kawich-Hot Creek Ranges fault zone, Quaternary fault and fold database of the United States: <http://earthquakes.usgs.gov/hazards/qfaults> (March, 2013)
- Sheppard, S.M., 1986, Characterization and isotopic variations in natural waters: *Reviews in Mineralogy*, v. 16, p. 165–183.
- Shoemaker, K.A., 2004, The tectonomagmatic evolution of the late Cenozoic Owyhee Plateau, northwestern United States [PhD dissertation]: Oxford, Ohio, Miami University, 288 p.
- Sibbett, B.S., 1982, Geology of the Tuscarora geothermal prospect, Elko County, Nevada: *Geological Society of America Bulletin*, v. 93, p. 1264–1272.
- Sibson, R.H., 1996, Structural permeability of fluid-driven fault-fracture meshes: *Journal of Structural Geology*, v. 18, p. 1031–1042.
- Sibson, R.H., 2000, Fluid involvement in normal faulting: *Journal of Geodynamics*, v. 29, p. 469–499.
- Smith, J.F., Jr., and Ketner, K.B., 1976, Stratigraphy of post-Paleozoic rocks and summary of resources in the Carlin–Piñon Range area, Nevada: U.S. Geological Survey Professional Paper 867-B, 48 p.

- Smith, K., Pechmann, J., Meremonte, M., and Pankow, K., 2011, Preliminary analysis of the Mw 6.0 Wells, Nevada, Earthquake Sequence, *in* dePolo, C.M., and LaPointe, D.D., eds., *The 21 February 2008 Mw 6.0 Wells, Nevada Earthquake*: Nevada Bureau of Mines and Geology Special Publication 36, p. 127–145.
- Spang, J.H., 1972, Numerical method for dynamic analysis of calcite twin lamellae: *Geological Society of America Bulletin*, v. 83, p. 467–472.
- Wernicke, B., 1992, Cenozoic extensional tectonics of the U.S. Cordillera, *in* Burchfiel, B.C., et al., eds., *The Cordilleran Orogen: Conterminous U.S.*: Geological Society of America, *Geology of North America*, v. G-3, p. 553–581.
- Wesnousky, S.G. and Willoughby, C.H., 2003, Neotectonic note; the Ruby-East Humboldt Range, northeastern Nevada: *Bulletin of the Seismological Society of America*, v.93, p. 1345–1354.
- Wesnousky, S.G., Barron, A.D., Briggs, R.W., Caskey, S.J., Kumar, S., and Owen, L., 2005, Paleoseismic transect across the northern Great Basin: *Journal of Geophysical Research*, v. 110, B05408, doi:10.1029/2004JB003283.
- Zehner, M., Coolbaugh, M.F., and Shevenell, L., 2009, Preliminary geothermal potential and exploration activity in Nevada: Nevada Bureau of Mines and Geology Open File Report 09-10, scale 1:1,000,000.
- Zoback, M.L., and Thompson, G.A., 1978, Basin and Range rifting in northern Nevada: Clues from a mid-Miocene rift and its subsequent offsets: *Geology*, v. 6, p. 111-116.
- Zoback, M.L., 1989, State of stress and modern deformation of the northern Basin and Range province: *Journal of Geophysical Research*, v. 94, p. 7105-7128.
- Zoback, M.L., McKee, E.H., Blakely, R.J., and Thompson, G.A., 1994, The northern Nevada rift: Regional tectonomagmatic relations and middle Miocene stress direction: *Geological Society of America Bulletin*, v. 106, p. 371–382.

APPENDIX A: DESCRIPTION OF MAP UNITS

Quaternary Deposits

Qa – Active channels and recently active fan alluvium, undivided (Holocene to Pleistocene) Channel and overbank deposits of creeks, annually active washes, and recently to annually active alluvial fans. Generally consists of poorly sorted silt to pebble-cobble gravel up to 5 cm in diameter. Clasts are subrounded to well-rounded. In the southern reaches of the Hot Creek drainage, this unit consists of moderately well sorted pale gray silt and sand. Where incised by streams, Qa is exposed steep-sided gullies up to 5 m deep. Thicknesses are variable and poorly known, but greater than 5 m along Hot Creek.

Qfy – Young fan alluvium (Holocene to Pleistocene) Poorly sorted silt to cobble gravel up to 15 cm in diameter; typically matrix supported; clasts are subangular to well-rounded; clasts are dominantly derived from unit Tdf, rocks of the Tuscarora volcanic field, and reworked older fan deposits. Surfaces are commonly vegetated with variable soil development. Includes recently reworked alluvium deposited in washes incised into older fan deposits of unit Qfo/Qfi. Qfy is less than 7 m thick.

Qfi – Intermediate fan alluvium (Pleistocene) – Poorly sorted silt to pebble gravel up to 6 cm in diameter; typically matrix supported; clasts are subrounded to well-rounded; clasts are dominantly derived from unit Tdf, rocks of the Tuscarora volcanic field, and reworked older fan deposits. Surfaces are commonly vegetated with variable soil development and erosionally rounded near fan edges. Qfi surfaces are distinguished based on their intermediate elevation, relative to units Qfy and Qfo. Thicknesses range from 2 to 10 m.

Qfo – Old alluvial fan (Pleistocene) Poorly sorted sand to cobble gravel up to 15 cm in diameter; typically matrix supported; clasts are subangular to subrounded and consist of Miocene volcanic rocks; surfaces are commonly heavily vegetated with some soil development. Fan edges are erosionally rounded. Fan surfaces are typically dissected by Qfi, Qfy, and/or Qa. Unit Qfo is deposited on the flanks of the northeastern Tuscarora Mountains and the Independence Mountains. Qfo is less than 10 m thick.

Qfi/Qfo – Intermediate and old fan alluvium, undivided (Pleistocene) Poorly to well-sorted sand to pebble-cobble gravel up to 15 cm in diameter. Typically clast-supported with very minor sand matrix; poorly indurated and nonstratified. Clasts are subangular to well-rounded and consist of rocks derived from unit Tdf and rocks of the Tuscarora volcanic field. Fan surfaces are smooth to undulating with little to no soil development. Unit Qfi/Qfo overlies lavas of the Tuscarora volcanic field and unit Tst. Thicknesses are poorly defined but range up to 12 m near fan heads.

Qfqy – Young fan alluvium and recently active alluvium containing > 10% quartzite clasts, undivided (Holocene to late Pleistocene) Poorly sorted silt to cobble gravel up to 20 cm in diameter; typically matrix supported; clasts are subangular to well-rounded and consist of quartzite and Miocene volcanic rocks. Qfqy is derived from older quartzite clast-bearing fan deposits, including Qfqi, Qfqo, Qfqi/Qfqo, and QTq and Miocene volcanic rocks, including units Tdf and Taf. Surfaces are sparsely to non-vegetated with weak to no soil development. Deposit thickness is poorly known, but does not exceed 5 m.

Qfqi – Intermediate fan alluvium containing > 10% quartzite clasts (Pleistocene) Poorly sorted sand to cobble gravel up to 20 cm in diameter with isolated boulders up to 50 cm in diameter; matrix supported; clasts are subangular to well-rounded; surfaces are smooth to moderately dissected. Deposits are mostly derived from older quartzite clast-bearing fan deposits of northern Independence Valley, including Qfqo, Qfqi/Qfqo, and QTq. Locally contains subangular clasts of Miocene volcanic rocks, including units Tdf and Taf. Surfaces are sparsely to non-vegetated. Deposit is distinguished based on the intermediate elevation of the Qfqi surface, relative to units Qfqy and Qfqo. Deposit thickness is generally less than 8 m, but may be much greater along the Independence Mountains range front.

Qfqo – Old alluvial fan containing > 10% quartzite clasts (Pleistocene) Poorly sorted sand to cobble gravel up to 20 cm in diameter with isolated boulders up to 50 cm in diameter. Typically matrix supported with subrounded to well-rounded clasts of quartzite and chert. Clasts are derived from unit QTq and possibly Pleistocene glacial till deposits of the northern Independence Mountains (Sibbett, 1982). Surfaces are broadly rounded to undulating. Soil development is weak and surfaces are sparsely vegetated. Deposits are at least 15 m thick.

Qfqi/Qfqo – Intermediate and old fan alluvium containing > 10% quartzite clasts, undivided (Pleistocene) Poorly sorted sand to cobble gravel with isolated boulders up to 50 cm in diameter; matrix- to clast-supported with subangular to well-rounded clasts. Typically dominated by quartzite pebbles and cobbles, and up to 10% pebbles derived from units Tdf and Taf. Locally contains subangular pebbles of chert, derived from unit QTf. Soil is locally up to 70 cm thick. Vegetation is sparse to dense. Thin deposits (≤ 1.5 m) of Qfqi/Qfqo mantle units Tst, Tdf, and Taf along the northern margin of Independence Valley. Thickness is 1–5 m.

Qgc – Gravel and colluvium, undivided Moderate to well-sorted pebble-cobble gravel up to 10 cm in diameter deposited on gentle slopes. Clast-supported deposits contain

angular to subround pebbles of porphyritic volcanic rocks. Soil is very weakly developed to absent. Deposits up to 1 m thick.

Qls – Landslide deposits Slope-failure-derived deposits of unconsolidated debris. Deposits are typically hummocky and lobate. Curvilinear headwall scarps are recognizable, though commonly rounded by erosion. Landslide deposits are moderately to densely vegetated. Estimated maximum thickness is ~10 m.

Qc – Colluvium and talus, undivided Deposits of colluvium and talus on, and at the base of steep slopes. Deposits are typically poorly sorted, clast-supported with angular to subangular pebbles to boulders up to 40 cm long. Deposits are generally less than 4 m thick.

Geothermal Deposits

Qss – Siliceous sinter, undivided (late Holocene to late Pleistocene) Undivided chalcedonic and opaline sinter terraces, mounds, and aprons precipitated at active and ancient hot springs; restricted to the northeast-trending zone of hydrothermal alteration and geothermal activity along the margins of Hot Creek. Locally, deposits of Qfy mantle unit Qss. Unit crops out in T41N R52E Sections 5 and 8. Estimated maximum thickness is ~ 10 m.

Qfs – Silica-cemented alluvium (Holocene to late Pleistocene) Poorly to moderately-sorted coarse sand to cobble-gravel up to 15 cm in diameter cemented by silica; well-indurated deposits, locally forming erosionally resistant ledges; mainly mapped to the south and southeast of the large sinter terrace (unit Qss). Deposits from 0.5 – 1.5 m thick. Unit crops out in T41N R52E Sections 5, 8, and 17.

Qfsq – Silica-cemented alluvium containing >10% quartzite clasts (Pleistocene?) Poorly sorted coarse sand to cobble-gravel up to 25 cm in diameter cemented by silica. Unaltered quartzite clasts are cemented by silicified sand matrix; well indurated; clast-supported, consisting of >10% rounded quartzite cobbles, as well as subangular to subrounded volcanic clasts. Silica induration is of the same style as unit Qfs. Less than 1 m thick. Unit crops out in T41N R52E Section 17 (NE ¼). Unit is up to 1.5 m thick.

Qbh – Silicified fault breccia Silica-cemented breccia. Qbh contains angular clasts of tuffaceous siltstone of unit Tst and porphyritic dacite of unit Ti up to 15 cm long. Clasts are argillically altered, though phenocryst composition in dacite clasts remain discernible. Siltstone clasts are pitted and partially flooded with silica. The matrix consists of coarse cataclasite flooded with opalized silica. Locally, silica cement is finely banded. Dark

orange to dark red exotic iron oxide coats the weathered outcrop surface. Qbh lies in the footwall of a west-dipping fault zone that bounds the large sinter terrace (Qss) to the east. Unit crops out in T41N R52E Section 8 (NE ¼).

Quaternary and Tertiary deposits

QTbf – Silicified cataclasite Well-indurated silicified fault zone breccia. Composed of ~70% finely milled matrix, quartz stringers (1–5 mm wide), quartz vein fragments (≤ 15 cm long), and angular lithic clasts of tuff (≤ 5 mm long). Unit QTbf is exposed along the Cottonwood Peak fault in tabular, steeply dipping, fin-shaped outcrops with up to 5 m of vertical relief. The age of faulting and hydrothermal alteration along the fault zone is constrained to between ~16 Ma and Holocene. The age of the youngest clearly faulted unit (Tdf) is ~16 Ma. Locally, silicified cataclasite of the Cottonwood Peak fault forms a buttress unconformity with Quaternary fan deposits in the hanging wall. Quaternary units contacting the fault zone rocks are not offset by faulting. Rather, the fan deposits accumulated at the break in slope formed between the silicified fault zone rock and less resistant tuffaceous sedimentary rock (unit Tst) in the hanging wall. Unit crops out in T41N R52E Section 6 (NW ¼). Perpendicular to fault strike, QTbf ranges in thickness from ~1–8 m.

QTq – Quartzite-bearing coarse gravel Moderate to well-sorted, well-rounded coarse pebble- to boulder-sized quartzite gravel mostly less than 40 cm in diameter with sparse boulders up to 1.2 meters in diameter. Clasts are possibly derived from Ordovician McAfee Quartzite of the Independence Mountains, described by Miller et al. (1981) and Muntean and Henry (2006). Quartzite boulders are up to 1.3 m in diameter. Deposits are non-stratified. Matrix was not exposed. Surfaces are typically smoothed and non-vegetated. Most QTq deposits are gently tilted (4° to 10°) and not associated with the present drainage pattern. Margins of deposits commonly bleed out into younger fan surfaces. A QTq surface is gently deformed in part by drag in the hanging wall of the Independence Mountains fault zone (T41N R52E Sections 3 and 10). Erosional remnants of QTq are commonly only 1–2 m thick with a maximum observed thickness of ~6 m. This unit may be thicker along the Independence Mountains range front, where it is mostly concealed beneath younger fan deposits.

QTf – Old fan alluvium (Pleistocene to late Tertiary) Poorly to moderately sorted sand to cobble gravel up to 20 cm in diameter; clast-supported; clasts are subrounded to well rounded. Dominated by chert with lesser quartzite and siltstone clasts. Deposit lies beneath unit QTq and is exposed in a single locality (T41N R52E Section 9). Thickness is approximately 3 m.

TERTIARY ROCKS

Miocene Lavas

Taf – Porphyritic dacite (middle Miocene) Dacite flows, typically glassy, locally spherulitic, with poorly developed columnar joints perpendicular to the base of flows. Flows contain 4-11% phenocrysts. Phenocrysts include 3-10% euhedral to subhedral plagioclase (0.5-4 mm long), 1% subhedral clinopyroxene (0.2-2 mm long), and <1% anhedral quartz (≤ 2 mm long). These flows are mainly preserved as erosional remnants atop more resistant Tdf flows. Thickness – 190 m.

Tvt – Glassy dacite flow (middle Miocene) Dacite flow distinguished by very fine flow banding. Flow-parallel foliation is readily observed in outcrop where weathering accentuates finely banded groundmass. Tvt is relatively porous, and soft, though discrete vesicles are not evident in hand sample. This unit weathers easily and is preserved either atop, or as a distinctive flow within, the uppermost portion of unit Tdf. The lateral extent of Tvt is limited. Phenocrysts include 2-3% subhedral embayed sanidine (0.5–1 mm long), 1% plagioclase (2-3 mm long) with sharp normal zoning, and 1% anhedral quartz (≤ 0.5 mm long). Thickness – 40 m.

Tdf – Porphyritic rhyolite (middle Miocene) Laterally extensive package of grayish-pink porphyritic rhyolite flows. Distinctive flow-parallel platy partings spaced 1-3 cm apart characterize the middle of this unit. Dips of platy partings steepen near flow tops. Elliptical (flattened) vesicles are locally present at flow tops. Also contains sparse glass-dominant layers up to several meters thick and pods of flow breccia. Coarsely porphyritic unit with 12-20% phenocrysts, including 4-15% subhedral to euhedral plagioclase (0.5-3 mm long), 2-12% anhedral quartz (0.5-3 mm long), 2-3% euhedral sanidine (3-5 mm long with sparse cumulophyric aggregates up to 8 mm long), <1% magnetite (0.5 mm long). Groundmass ranges from entirely glass to 90% microcrystalline feldspar microlites with minor glass stringers. Thickness – 120 m.

Oligocene (?) Sedimentary Rocks

Tst – Tuffaceous sedimentary rocks of Chicken Creek (middle Eocene to middle Miocene) White to light-tan tuffaceous siltstone and sandstone with sparse conglomerate lenses up to 5 m thick. This unit encompasses the undivided package of sedimentary rocks that lie beneath unit Tdf and above the igneous rocks of the Tuscarora volcanic field. Tst is dominated by poorly-indurated massive siltstone composed of subrounded

grains of devitrified tuff, angular grains of plagioclase (2–20%), quartz grains (<1%), and rare broken biotite grains (<1%). Sandstone is moderately indurated, thinly bedded, locally cross-bedded. The sandstone is a moderately sorted litharenite, consisting of coarse sand to coarse silt with subangular grains of feldspar, biotite, quartz, and well-rounded grains of pumice. Conglomerate lenses between 0.5 and 5 m thick occur throughout the section. These conglomerates are well indurated and consequently relatively resistant within the Tst section. Conglomerate lenses are clast-supported, moderately to poorly-sorted with subrounded to subangular clasts of porphyritic andesite, porphyritic dacite, argillite, quartzite, and siltstone of units Ms and Pu up to 10 cm long. Unit Tst is pervasively silicified adjacent to the Cottonwood Peak fault (T41N R52E Section 6) and within the geothermal area. Total thickness is ~300 m.

Eocene Rocks – Tuscarora Volcanic Field

Te – Andesite and dacite undivided Poorly exposed porphyritic flows, domes, and intrusive rocks of andesitic to dacitic composition associated with the Tuscarora volcanic field. Unit Te encompasses units Tsa, Tsd, Tn, and Tao, where weathering and/or poor exposure prevents further distinction of these rocks. Phenocryst abundance ranges from 5–40% and consists of some combination of the following minerals: plagioclase (3–40% of rock volume), clinopyroxene ($\leq 2\%$), orthopyroxene ($\leq 2\%$), biotite ($\leq 3\%$), and hornblende ($\leq 1\%$). Unit Te includes all rocks of Tuscarora volcanic field that intrude and overlie intracaldera deposits of unit Tct. The estimated thickness of Te, constrained by drilling within the geothermal field, is ~250 m.

Ti – Porphyritic dacite Medium gray porphyritic (~17% phenocrysts) dacite domes and possibly flows. Weathers distinctly as platy talus (2–6 cm thick) which accumulates at the base of outcrops. Groundmass composed of pilotaxitic plagioclase microcrysts. Phenocrysts consist of 15% euhedral to subhedral plagioclase (0.3–4 mm long) are commonly embayed; 2–3% biotite (0.3–2 mm long), commonly partially replaced by magnetite. Weak hydrothermal alteration and secondary mineralization is present near the Cottonwood Peak fault and adjacent to the geothermal field. Secondary mineralization includes interstitial chalcedony in groundmass ($\leq 3\%$ of rock volume) and rare replacement of biotite by epidote. Unit Ti is nonconformably overlain by unit Tst. Thickness probably varies and is estimated to be less than 250 m.

Tsa – Densely porphyritic andesite Dark gray andesite flows locally exhibit flow-parallel planar partings spaced 5–20 cm apart. Tsa locally contains pods of flow breccia. Columnar jointing is well developed at the base of some flows within unit Tsa. Groundmass ranges from glass-dominant to felty, with plagioclase microlites. Phenocryst

assemblage consists of 15–30% subhedral to euhedral plagioclase, commonly embayed (1–4 mm long) and 2% equant subhedral grains of clinopyroxene (0.2– 1 mm long).

Ts – Tuffaceous sandstone, undivided Moderately sorted, coarse-grained tuffaceous sandstone intercalated between lava flows of unit Tsa. Unit Ts is thin bedded and well indurated, consisting mainly of sand-sized particles of devitrified pumice with grains of rounded quartz, feldspar, and broken biotite. Thickness is less than 10 m.

Tsd – Porphyritic andesite Pale gray hornblende-bearing andesite. The phenocryst assemblage consists of 15% euhedral plagioclase (0.8–3 mm long) commonly in cumulophyric aggregates up to 5 mm in diameter; 2% subhedral biotite (0.3–1 mm long); <1% euhedral to subhedral hornblende (0.4–0.8 mm), with partially resorbed rims. Groundmass is cryptocrystalline with microphenocrysts of plagioclase, lesser pyroxene, glass, and sparse magnetite. Thickness is poorly known but probably less than 300 m.

Tn – Porphyritic andesite Medium-gray porphyritic andesite flow breccia poorly exposed beneath colluvium and alluvial fans along the north bank of the Owyhee River. Trachytic groundmass is composed of plagioclase laths and sparse pyroxene. Phenocryst assemblage consists of 7% subhedral to euhedral plagioclase (0.4–3 mm long); 2% subhedral to euhedral orthopyroxene (0.2– 0.8 mm) occurs in cumulophyric aggregates up to 3 mm in diameter; <1% clinopyroxene (0.2– 0.5 mm); and <1% subhedral biotite (0.5–0.8 mm long). Thickness is poorly known but probably less than 100 m.

Tao – Porphyritic andesite Dark gray andesite with closely spaced (1–3 cm) planar partings, which are interpreted to be flow-parallel. Groundmass is commonly glassy and dark green. Phenocrysts (<9%) consist of ~5% euhedral plagioclase laths, 2% euhedral augite (\leq 5 mm long), and <1% biotite (\leq 1 mm long). Where present, this unit directly overlies Tct. Thickness is poorly known but probably less than 300 m.

Tct – Tuff of Big Cottonwood Canyon Light gray to tan, moderately to densely welded, porphyritic (2–6% phenocrysts) intracaldera tuff, containing fine-grained phenocrysts of quartz, sanidine, plagioclase, and biotite. The tuff is abundantly lithic, containing up to ~15% subangular to angular clasts of bluish-gray argillite, quartzite, and siltstone derived from units Ms and Pu, as well as porphyritic dacite and andesite derived from the Tuscarora volcanic field. Lithic clasts are mostly less than 3 cm in length with the exception of a siltstone block ~1.5 m in diameter (T41N R51E Section 1 SW $\frac{1}{4}$). Unit Tct locally contains up to ~20% pale tan fiamme (1–5 cm long). Tuff is crystal poor and contains quartz (2–4%; 0.6–1.2 mm long), sanidine (1–3%; 0.6–1 mm long), plagioclase (<1–2%; ~1 mm long), and biotite (~1%; \leq 1 mm long). Phenocryst assemblage, abundant lithics, and overall thickness distinguish tuff of the Big Cottonwood Canyon caldera from ash-flow tuffs elsewhere in the Tuscarora volcanic field (Henry et al., 1999). The tuff is

non-stratified, though locally, fiamme define a prominent compaction foliation. Tuff is at least 2.5 km thick, based on the 30°–60° northeast dips across a 4 km-wide area of continuous exposure west of the geothermal area. Tct thins eastward to ~700 m within the geothermal area.

Tr – Dacite intrusion Porphyritic dacite intrusion with distinctive pale pink to light gray crystalline groundmass. Felty groundmass is mainly composed of plagioclase microlites. Phenocrysts consist of 15% euhedral to subhedral plagioclase (0.5–3 mm long) and 2–3% euhedral to subhedral biotite (≤ 1.5 mm long). Relatively abundant biotite phenocrysts against pale groundmass pink distinguish this unit from other andesite and dacite of the Tuscarora volcanic field.

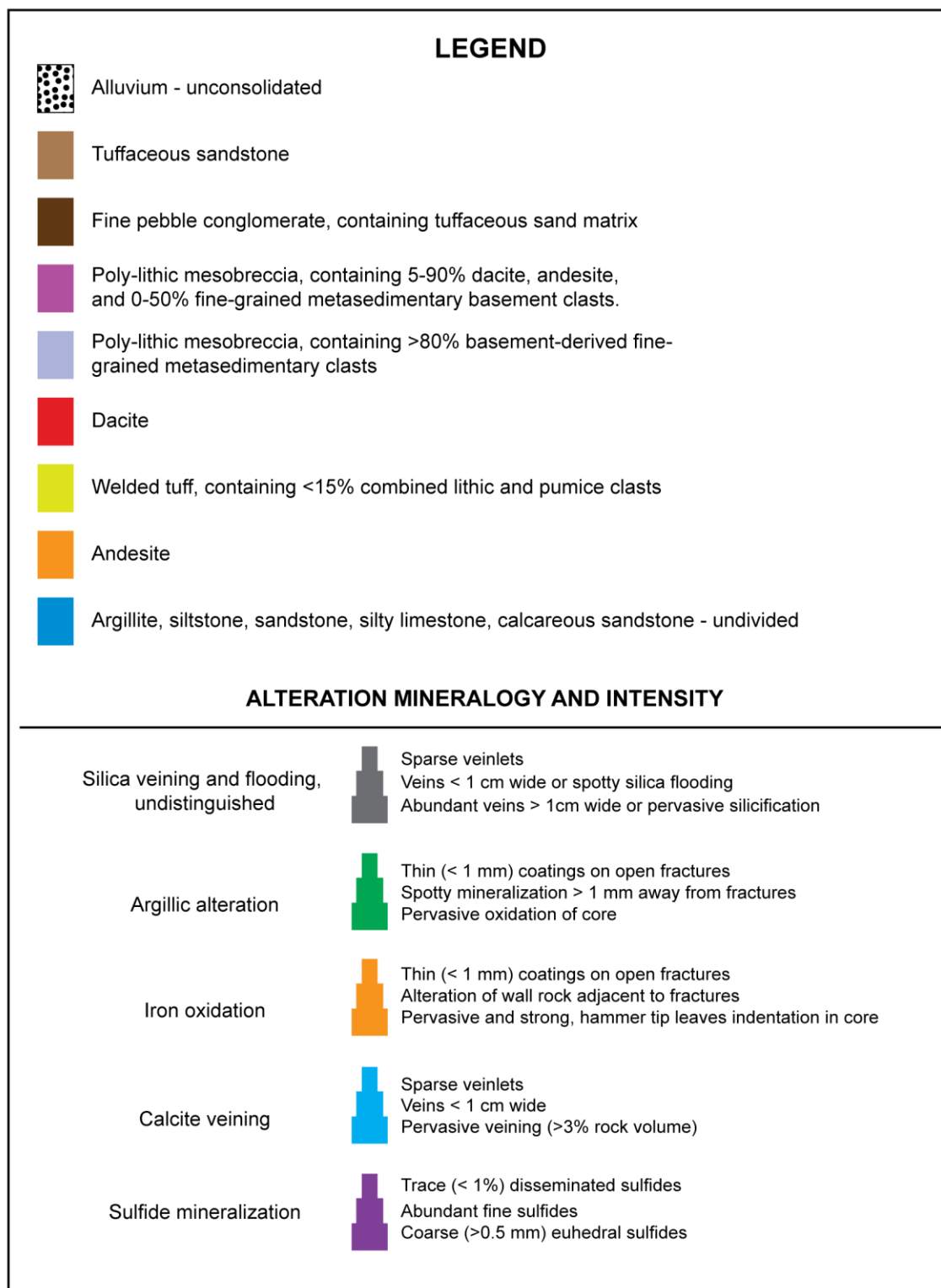
Tbr – Intracaldera megabreccia and mesobreccia deposits, undivided Volcanogenic breccia deposits near the inner walls and floor of the Big Cottonwood Canyon. Unit Tbr contains two main breccia subtypes: 1) Heterolithic mesobreccia that is variably matrix and clast-supported. The breccia matrix is quartz-rich and composed mainly of sand-sized dark gray clastic material. Clasts are angular to subrounded and range from 5 mm to ~1.2 m in diameter. Clasts of both Paleozoic metasedimentary rocks and Eocene volcanic rocks are present, with the ratio of Paleozoic to Eocene clasts ranging from 10:1 to 1:10. No gradation of rock type or clast size is apparent in the mesobreccia. These caldera-related mesobreccia deposits are further distinguished from tectonic breccias by their vertical thickness (up to 250 m). 2) Blocks of basement-derived megabreccia that range from 2 to 73 m in diameter, composed mainly of argillite and siltstone with lesser calcareous sandstone and sandy limestone. Unit Tbr does not crop out in the study but is encountered in drill holes within the geothermal field.

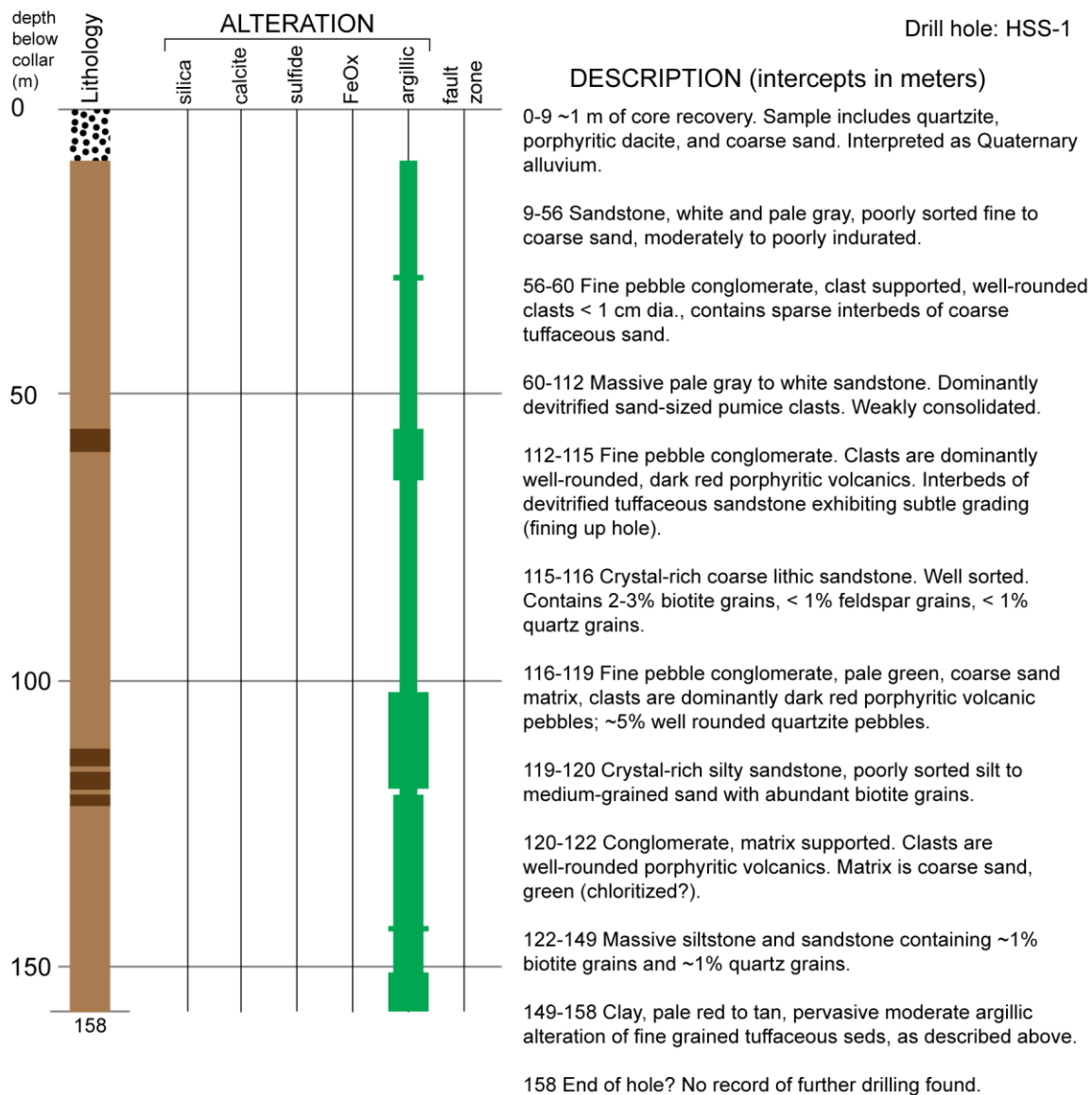
PALEOZOIC BASEMENT

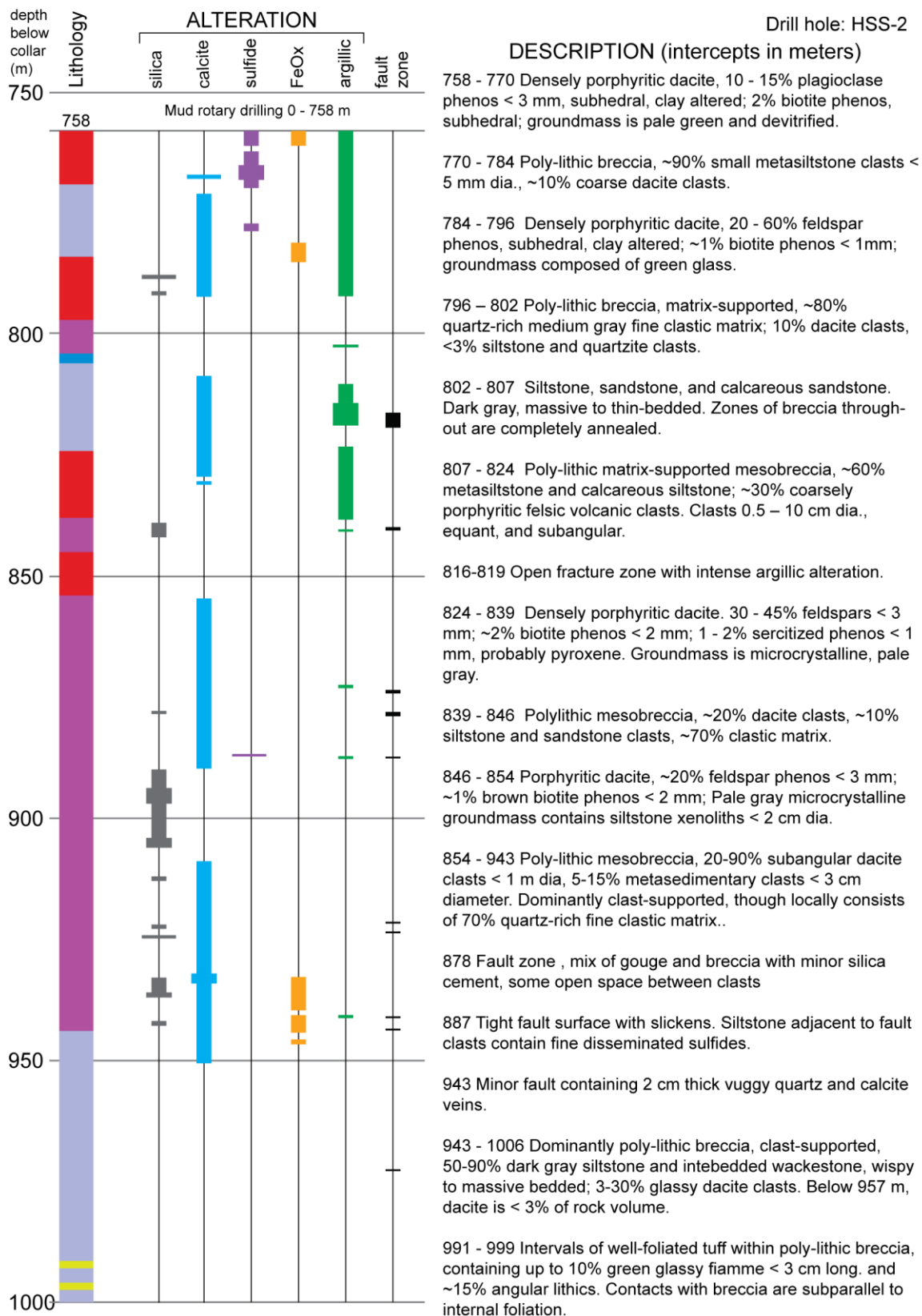
Ms – Siltstone, shale, and silty limestone Poorly exposed siltstone, identified and described in detail by Fagan (1962) and Miller et al. (1984), belonging to the Mississippian-Devonian Schoonover Formation. Unit Ms weathers to reddish brown, tan, and blue-gray siltstone chips. Silty limestone turbidite sequences, interbedded with dark gray siltstone and metavolcanic rocks, of the Schoonover Formation are intercepted in geothermal drill holes but do not crop out in the study area.

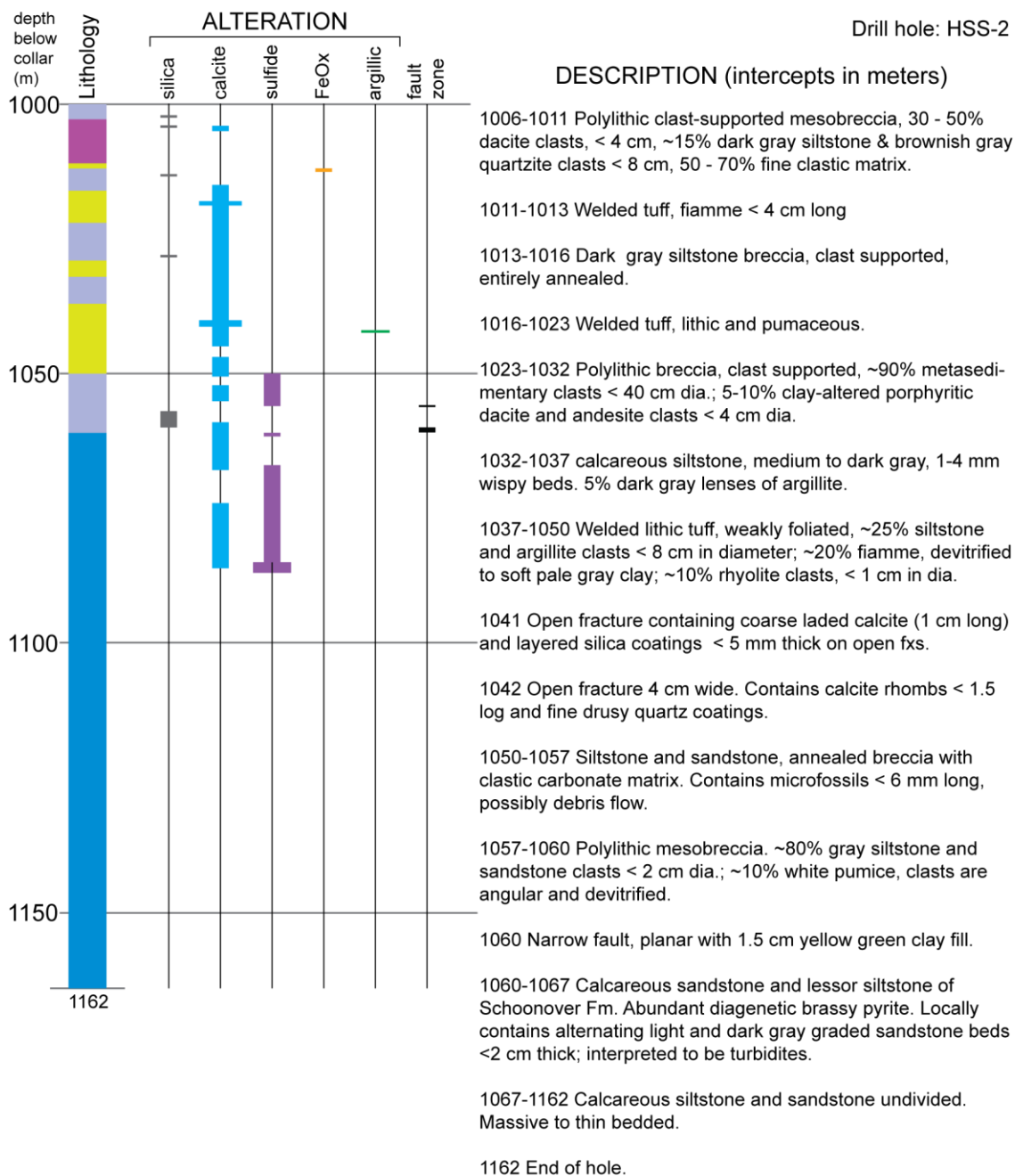
Pu – Paleozoic metasedimentary rocks, undivided Chert, argillite, shale, and quartzite of the Roberts Mountains allochthon, regionally correlated with the Ordovician Valmy Formation (Henry et. al, 1999; Miller, 1984); described in detail by Coats (1987) and Muntean and Henry (2006).

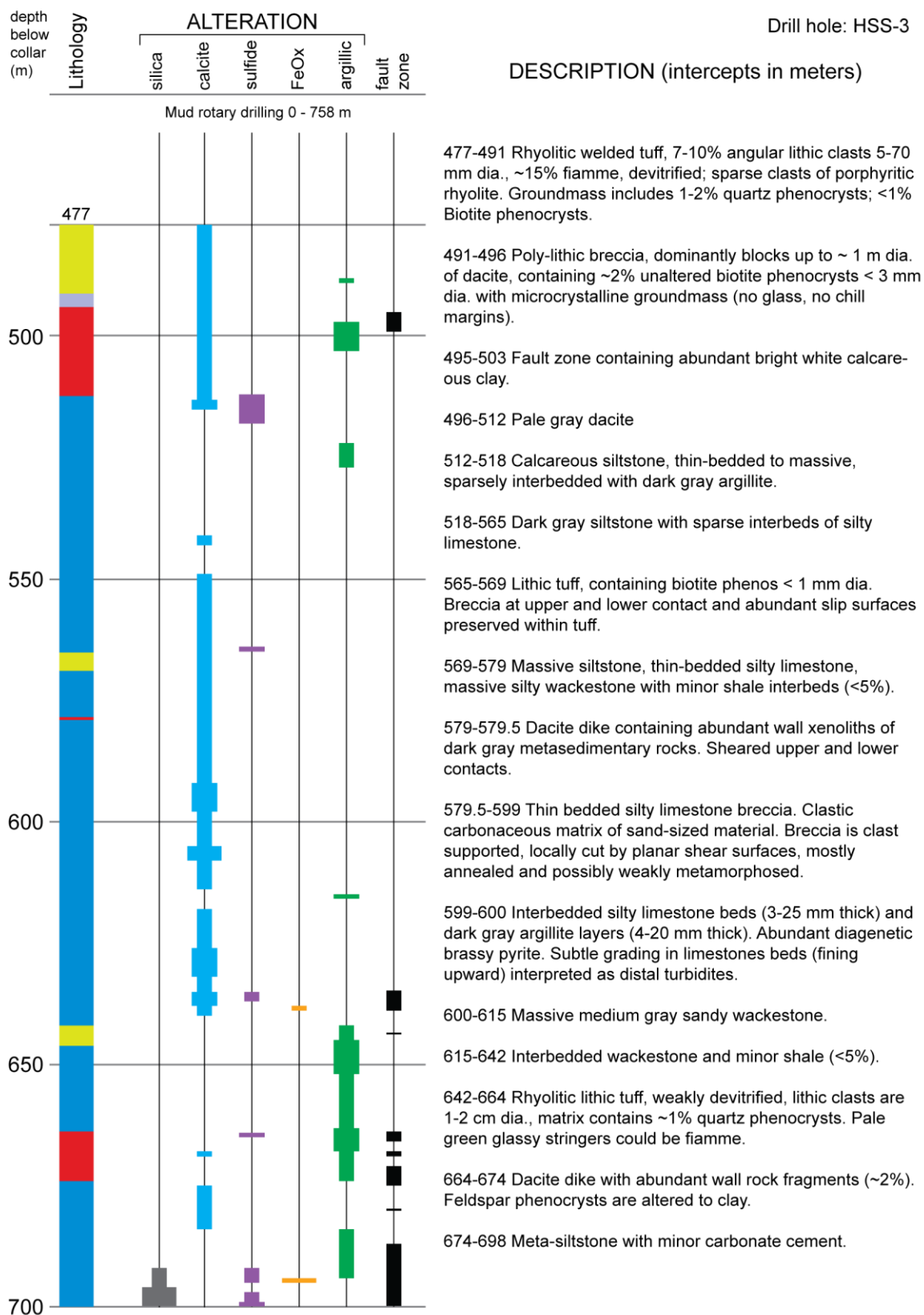
Appendix B: Geologic logs of drill core











MAP EXPLANATION

Symbology (per FGDC-STD-013-2006)

QUATERNARY DEPOSITS

- Alluvium, fluvial deposits, and colluvium
- Qa Active stream channels and Pleistocene (?) channel deposits
- Qfy Youngest alluvial fan
- Qfi Intermediate age alluvial fan
- Qfo Oldest alluvial fan
- Qfi/Qfo Oldest and intermediate age alluvial fan undivided
- Qfyy Youngest alluvial fan containing > 10% quartzite cobbles
- Qfij Intermediate age alluvial fan containing > 10% quartzite cobbles
- Qfjo Oldest alluvial fan containing > 10% quartzite cobbles
- Qfi/Qfjo Oldest and intermediate age alluvial fan containing > 10% quartzite cobbles, undivided
- Qgc Unconsolidated gravel and colluvium on low angle slopes
- Qls Landslide deposit
- Qc Colluvium

Geothermal deposits

- Qss Sinter deposit
- Qfs Silica cemented alluvium
- Qfsq Quartzite clast-bearing silica cemented alluvium
- Qbh Breccia, dominantly hydrothermal silica

QUATERNARY AND TERTIARY DEPOSITS

- QTbf Fault breccia, silicified
- QTq Unconsolidated quartzite cobbles and boulders
- QTI Alluvial fan-early Quaternary or late Tertiary age

MIOCENE LAVAS

- Taf Dacite flows
- Tvt Dacite flow
- Tdf Rhyolite flows - Jarbridge Rhyolite

OLIGOCENE (?) ROCKS - SEDIMENTS OF CHICKEN CREEK

- Tst Tuffaceous sandstone, siltstone, and conglomerate

Eocene rocks - TUSCARORA VOLCANIC FIELD

- Te Andesite and dacite flows, domes, and plugs undivided
- Ti Andesite flows
- Tsa Andesite flows
- Ts Siltstone intercalations
- Tsd Dacite flows
- Tn Andesite flow
- Tao Andesite flows
- Tct Lithic welded intracaldera tuff
- Tr Rhyolite and dacite intrusions, undivided
- Tbr Intracaldera megabreccia and mesobreccia deposits, undivided

PRE-TERTIARY ROCKS

- Ms Mississippian siltstone - Schoonover Formation
- Pu Undivided Paleozoic quartzite, siltstone, and argillite

Contact Solid where certain and location accurate, long-dashed where approximate, short-dashed where inferred, dotted where concealed.

Normal fault Show dip of fault (tick) and trend of striae on fault surface (arrow); ball on downthrown side; solid where certain and location accurate, long-dashed where approximate, dotted where concealed, queried if identity or existence uncertain.

Mainly strike-slip fault Solid where certain and location accurate, long-dashed where approximate, dotted where concealed; queried if identity or existence uncertain. Arrows show relative motion.

Anticline Long-dashed where approximate, dotted where concealed.

Syncline Long-dashed where approximate, dotted where concealed.

Head or main scarp of landslide Hachures point downslope.

Strike and dip of bedding

Inclined

Strike and dip of compaction foliation in tuff

Inclined

Strike and dip of flow parting or flow foliation in volcanic rocks

Inclined

Geochronology sample locality

Surface sample Sample from drill core, showing depth below surface

Geothermal well

Injection well Production well Monitoring well

Hot spring **Strike and dip of silica vein** **Silicified bedrock**

Line of cross section

Scale 1:24,000

0 0.5 1 kilometer

0 1000 2000 3000 4000 5000 feet

CONTOUR INTERVAL 40 FEET

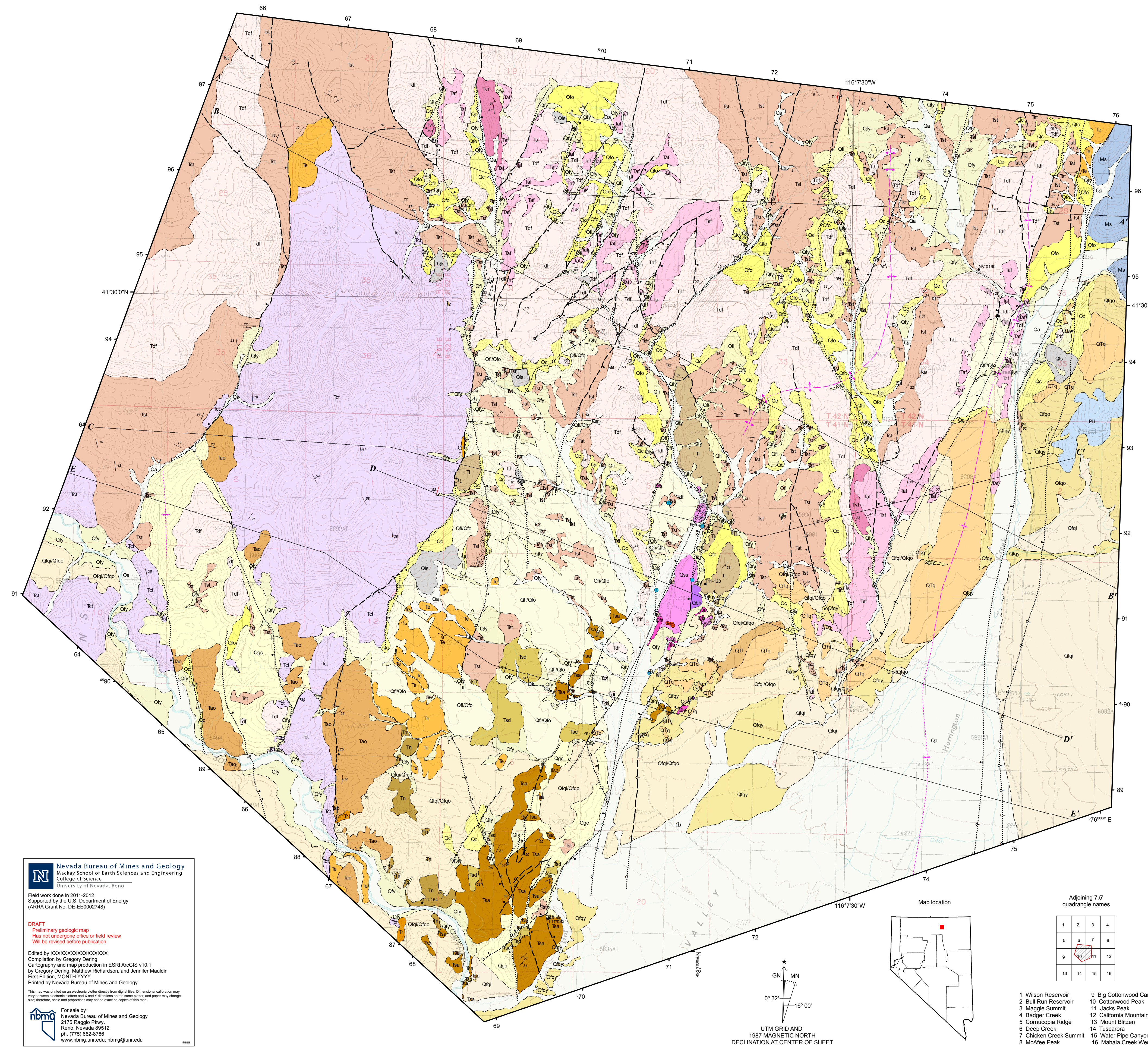
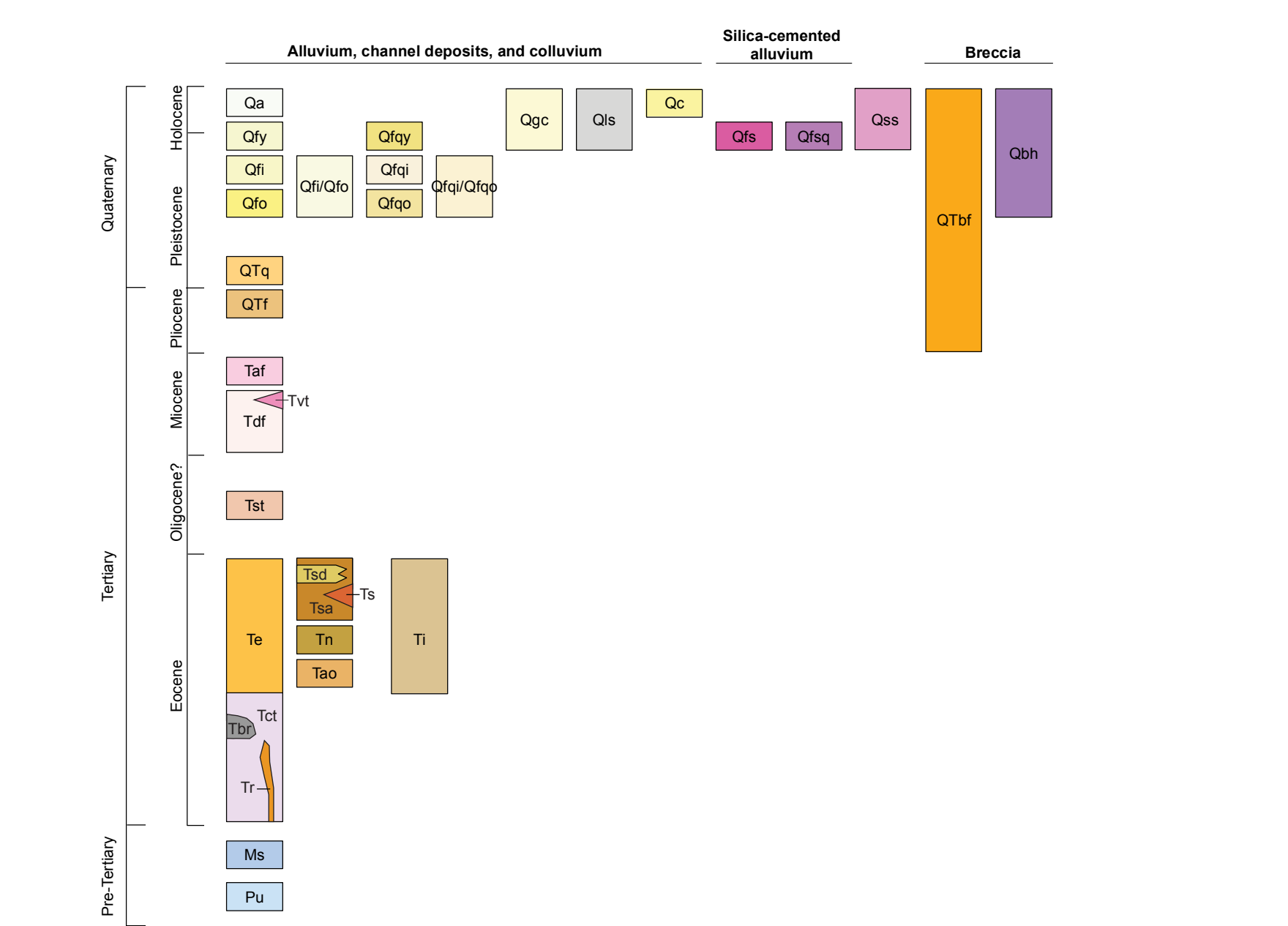
Projection: Universal Transverse Mercator, Zone 11, North American Datum 1927 (m)

Base map: U.S. Geological Survey Deep Creek 7.5' quadrangle (1996)

Base map: U.S. Geological Survey Chicken Creek Summit 7.5' quadrangle (1996)

Base map: U.S. Geological Survey Cottonwood Peak 7.5' quadrangle (1996)

Base map: U.S. Geological Survey Jacks Peak 7.5' quadrangle (1996)



Adjoining 7.5' quadrangle names

1	2	3	4
5	6	7	8
9	10	11	12
13	14	15	16

- Wilson Reservoir
- Bull Run Reservoir
- Maggie Summit
- Badger Creek
- Cornucopia Ridge
- Deep Creek
- Chicken Creek Summit
- McAfee Peak
- Big Cottonwood Canyon
- Cottonwood Peak
- Jacks Peak
- California Mountain
- Mount Blitzen
- Tuscarora
- Walter Pipe Canyon
- Mahala Creek West

N Nevada Bureau of Mines and Geology
Mackay School of Earth Sciences and Engineering
College of Science
University of Nevada, Reno

Field work done in 2011-2012
Supported by the U.S. Department of Energy
(ARPA Grant No. DE-EE0002748)

DRAFT
Preliminary geologic map
Has not undergone office or field review
Will be revised before publication

Edited by XXXXXXXXXXXXXXXXXXXX
Compilation by Gregory Dering
Cartography and map production in ESRI ArcGIS v10.1
by Gregory Dering, Matthew Richardson, and Jennifer Maudin
First Edition, MONTH YYYY
Printed by Nevada Bureau of Mines and Geology

This map was generated on an electronic plotter directly from digital files. Dimensional calibration may vary between electronic plotters and X and Y directions on the same plotter, and paper may change with time; therefore, scale and proportions may not be based on copies of this map.

For sale by:
Nevada Bureau of Mines and Geology
2175 Raggio Parkway
Reno, Nevada 89512
ph. (775) 682-8766
www.nbmg.unr.edu; nbmg@unr.edu

PRELIMINARY GEOLOGIC MAP OF THE TUSCARORA GEOTHERMAL AREA, ELKO COUNTY, NEVADA PLATE 2: CROSS SECTIONS

